



**Politecnico
di Torino**

Politecnico di Torino

Master's Degree Thesis in Course Aerospace Engineering

Academic Year 2020/2021

July 2021

Performance Requirements for a Descent and an Ascent Lunar Engine

Supervisors:

Candidate:

Prof. Lorenzo CASALINO

Francesco MORMILE

Ing. Mario PESSANA

Index

1	Abstract.....	21.
2	Introduction.....	22.
3	Fundamentals of liquid rocket engine.....	25.
3.1	Propellant.....	25.
3.2	Performance parameters.....	26.
3.3	Fundamentals of chemical reactions.....	35.
3.4	Software-assisted analysis.....	40.
4	Preliminary mass estimation.....	60.
4.1	Selection of input parameters.....	60.
4.2	Preliminary mass budget.....	64.
4.2.1	Scaling relationship method.....	70.
5	Feed system and tank sizing.....	79.
5.1	High-pressure gas feed system overview.....	79.
5.2	Reservoir sizing	85.
5.2.1	Spherical reservoirs.....	85.
5.2.2	Cylindrical reservoir.....	96.
6	Propulsion system architecture.....	102.
6.1	Space market: pressure vessels and propellant tanks.....	102.
6.2	Descender architecture.....	117.
6.3	Ascender architecture.....	118.
6.3.1	Ascender pressurization system.....	119.

6.3.2	Ascender propellant storage and feed system.....	120.
6.3.3	Ascender engine assembly.....	121.
6.4	Reaction control system architecture.....	122.
6.4.1	Reaction control system pressurization system.....	123.
6.4.2	Reaction control system propellant storage and feed system.....	124.
6.4.3	Reaction control system engine assembly.....	125.
6.5	Space market: valves.....	126.
7	Thrust chamber.....	134.
7.1	Thrust chamber fundamentals.....	134.
7.1.1	Thrust chamber body.....	137.
7.1.2	Injector.....	142.
7.2	Thrust chamber preliminary design.....	145.
7.2.1	Descender thrust chamber.....	145.
7.2.2	Throttling.....	158.
7.2.3	Descender pintle injector.....	161.
7.2.4	Descender cavitating venturi flow control valves.....	166.
7.2.5	Ascender thrust chamber.....	175.
7.2.6	Ascender injector.....	179.
7.2.7	Reaction control system thrust chamber.....	181.
7.2.8	Reaction control system injector.....	185.
8	Conclusions and future works.....	187.
	Bibliography.....	188.

List of Figures

Figure 3.1 Pressure distribution in a thrust chamber

Figure 3.2 Nozzle expansion conditions

Figure 3.3 Variation in thrust coefficient as altitude, specific heat ratio, and expansion ratio change

Figure 3.4 Thermochemical properties of various species

Figure 3.5 Variation of MMH density as a function of temperature

Figure 3.6 Variation of MMH specific heat as a function of temperature

Figure 3.7 Variation of MON-x freezing point as a function of NO%

Figure 3.8 Variation of MON-x vapor pressure as a function of temperature and NO%

Figure 3.9 Variation of specific impulse as a function of mixture ratio and NO%

Figure 3.10 Variation of characteristic velocity as a function of mixture ratio and NO%

Figure 3.11 Variation of specific impulse as a function of mixture ratio for the MON3-MMH pair

Figure 3.12 Variation of temperatures as a function of mixture ratio

Figure 3.13 Shifting equilibrium performances of the MON3-MMH pair

Figure 3.14 Variation of specific heat as a function of the mixture ratio

Figure 3.15 Variation of several parameters as a function of mixture ratio for MON3-MMH pair

Figure 3.16 Frozen equilibrium performances for the MON3-MMH pair

Figure 3.17 Variation of temperatures as a function of mixture ratio

Figure 3.18 Variation of several parameters as a function of mixture ratio

Figure 3.19 Variation of characteristic velocity as a function of mixture ratio and chamber pressure

Figure 3.20 Variation of specific impulse as a function of mixture ratio and chamber pressure

Figure 3.21 Variation of specific impulse as a function of mixture ratio and expansion area ratio

Figure 3.22 Variation of specific impulse as a function of mixture ratio and chamber pressure

Figure 3.23 Variation of specific impulse as a function of mixture ratio and expansion area ratio

Figure 3.24 Comparison of computed specific impulse with CEA and RPA

Figure 3.25 Comparison of computed characteristic velocity with CEA and RPA

Figure 3.26 Comparison of computed thrust coefficient with CEA and RPA

Figure 3.27 Comparison of computed chamber temperature with CEA and RPA

Figure 4.1 Properties of several propellant combination

Figure 4.2 Variation of specific impulse as a function of mixture ratio for MON3-MMH pair

Figure 4.3 Rocket engine schematic

Figure 4.4 Comparison of lander gross-to-dry mass ratio as a function of lander gross mass for several estimations

Figure 4.5 Comparison of lander gross-to-dry mass ratio as a function of lander gross mass for several estimations

Figure 5.1 Typical high-pressure gas feed system

Figure 5.2 Typical blow-down feed system

Figure 5.3 Comparison of high-pressure gas and blow-down feed systems

Figure 5.4 Torayca composite properties

Figure 5.5 Section of spherical tank

Figure 5.6 Section of cylindrical tank

Figure 5.7 Typical tank head shapes

Figure 6.1 Cobham composite pressure vessels

Figure 6.2 IHI AeroSpace pressure vessels

Figure 6.3 MT Aerospace composite pressure vessel

Figure 6.4 InfiniteComposite pressure vessels

Figure 6.5 ArianeGroup propellant tank

Figure 6.6 Properties of P/N 80507 propellant tank

Figure 6.7 ArianeGroup propellant tank

Figure 6.8 ArianeGroup propellant tank

Figure 6.9 ArianeGroup propellant tank

Figure 6.10 NuSpace propellant tank

Figure 6.11 Ascender valve legend for current architecture

Figure 6.12 Ascender pressurization section

Figure 6.13 Ascender propellant storage and feed system

Figure 6.14 Ascender engine assembly

Figure 6.15 RCS valve legend for current architecture

Figure 6.16 RCS pressurization system

Figure 6.17 RCS propellant storage and feed system

Figure 6.18 RCS engine assembly

Figure 6.19 ArianeGroup pyro valve

Figure 6.20 Omnidea-RTG pressurant filter

Figure 6.21 ArianeGroup ground half coupling

Figure 6.22 fill & drain valve

Figure 6.23 MAROTTA relief valve

Figure 6.24 BRADFORD SPACE pressure transducer

Figure 6.25 MAROTTA pressure regulator

Figure 6.26 VACCO check valve

Figure 6.27 Omnidea-RTG ball valve

Figure 6.28 ArianeGroup solenoid valve

Figure 7.1 Rocket engine main sections

Figure 7.2 Variation of injector-to-nozzle inlet pressure ratio as a function of contraction area ratio

Figure 7.3 Variation of injector-to-nozzle inlet pressure ratio and approximate equation as a function of contraction area ratio

Figure 7.4 Characteristic length values for several propellant combination

Figure 7.5 Several combustion chamber shapes

Figure 7.6 Variation of contraction area ratio as a function of throat chamber diameter

Figure 7.8 Rao nozzle section approximation

Figure 7.9 Nozzle angle variation as a function of expansion area ratio and bell nozzle

Figure 7.10 Injection design using holes

Figure 7.11 Spray Injection elements

Figure 7.12 Combustion chamber section

Figure 7.13 Nozzle section

Figure 7.14 Descent engine sketch

Figure 7.15 Thrust variation as a function of throttling ratio

Figure 7.16 Chamber pressure variation as a function of throttling ratio

Figure 7.16 Specific impulse variation as a function of throttling ratio

Figure 7.17 Flow rate variation as a function of throttling ratio

Figure 7.18 Pintle injector section

Figure 7.19 Pintle injector slotted orifice section

Figure 7.20 Pintle injector main design parameters

Figure 7.21 Pintle section with primary and secondary circular orifices

Figure 7.22 Cavitating venturi flow control valve section

Figure 7.23 Variation of pressure drop across venturi valve as a function of thrust level

Figure 7.24 Pressure evolution inside the valve

Figure 7.25 Apollo oxidizer evolution as a function of pintle stroke

Figure 7.26 Apollo fuel evolution as a function of pintle stroke

Figure 7.27 Conical-shaped cavitating venturi flow control valve

Figure 7.28 MON3 flow rate distribution as a function of pintle stroke

Figure 7.29 MMH flow rate distribution as a function of pintle stroke

Figure 7.30 MON3 flow rate distribution as a function of pintle stroke and pintle half-angle

Figure 7.31 MMH flow rate distribution as a function of pintle stroke and pintle half-angle

Figure 7.32 Ascent engine sketch

Figure 7.33 Several attitude and control engines

Figure 7.34 RCS engine sketch

List of Tables

Table 3.1 Mission requirements

Table 3.2 Monomethylhydrazine main properties

Table 3.3 Mixed oxides of nitrogen main properties

Table 3.4 Shifting equilibrium performance for the MON3-MMH pair

Table 3.5 Frozen equilibrium performance for the MON3-MMH pair

Table 3.3 Mixed oxides of nitrogen main properties

Table 3.4 Shifting equilibrium performance for the MON3-MMH pair

Table 3.5 Frozen equilibrium performance for the MON3-MMH pair

Table 4.1 Several upper stage engine

Table 4.2 Apollo masses from Ref. [8]

Table 4.3 Apollo masses from Ref. [9]

Table 4.4 Apollo masses from Ref. [10]

Table 4.5 Apollo masses from Ref. [11]

Table 4.6 Apollo masses from Ref. [11]

Table 4.7 Apollo propellant-to-dry mass ratios

Table 4.8 Apollo masses estimation

Table 4.9 Propellant input parameter for scaling relationship

Table 4.10 Scaling relationship coefficient for a specified propellant

Table 4.12 Input data from Ref. [12]

Table 4.11 Velocity change estimation for the listed manoeuvres

Table 4.13 Results from Ref.[12]

Table 4.14 Current mission parameters

Table 4.15 Current mission input data

Table 4.16 Current mission propellant specifications

Table 4.17 Current mission estimated results

Table 4.18 Mass-ratio summary for several estimation

Table 4.19 Current mission preliminary mass breakdown

Table 5.1 Gas properties

Table 5.2 Summary of propellant mass required

Table 5.3 Descender tank requirements

Table 5.4 Ascender propellant tank requirements

Table 5.5 Pressure losses through engine

Table 5.6 Descender regulating pressure requirements

Table 5.7 Ascender regulating pressure requirements

Table 5.8 Descender pressure vessel requirements

Table 5.9 Ascender pressure vessel requirements

Table 5.10 Propellant tank material and tensile strength

Table 5.11 Pressure vessel material and tensile strength

Table 5.12 Descender spherical pressure vessel requirements

Table 5.13 Ascender spherical pressure vessel requirements

Table 5.14 Descender spherical propellant tank requirements

Table 5.15 Ascender spherical propellant tank requirements

Table 5.16 Descender cylindrical pressure vessel with hemispherical dome requirements

Table 5.17 Ascender cylindrical pressure vessel with hemispherical dome requirements

Table 5.18 Descender cylindrical propellant tank with hemispherical dome requirements

Table 5.19 Ascender cylindrical propellant tank with hemispherical dome requirements

Table 6.1 Descender pressure vessel requirements with COBHAM's reservoirs

Table 6.2 Ascender pressure vessel requirements with COBHAM's reservoirs

Table 6.4 Ascender pressure vessel requirements with different MEOP

Table 6.5 Descender pressure vessel requirement with COBHAM's reservoirs and vessel design MEOP

Table 6.6 Ascender pressure vessel requirement with COBHAM's reservoirs and vessel design MEOP

Table 6.7 Descender pressure vessel requirements with MT AeroSpace's reservoirs

Table 6.8 Ascender pressure vessel requirements with MT AeroSpace's reservoirs

Table 6.9 Descender pressure vessel requirements with IC's reservoirs

Table 6.10 Ascender pressure vessel requirements with IC's reservoirs

Table 6.11 Descender vessel requirements with different MEOP

Table 6.12 Ascender vessel requirements with different MEOP

Table 6.12 Descender pressure vessel requirements with IC's reservoirs and vessel design MEOP

Table 6.13 Ascender pressure vessel requirements with IC's reservoirs and vessel design MEOP

Table 6.14 Descender propellant tank requirements with ArianeGroup's reservoirs

Table 6.15 Descender oxidizer tank requirements with Northrop Grumman's reservoirs

Table 6.16 Descender fuel tank with ArianeGroup's reservoirs

Table 6.17 Ascender propellant tank requirements with ArianeGroup's reservoirs

Table 6.18 Ascender propellant tank requirements with ArianeGroup's reservoirs

Table 6.19 Ascender propellant tank requirements with ArianeGroup's reservoirs

Table 6.20 Ascender propellant tank requirements with NuSpace's reservoirs Ref. [23]

Table 6.21 ArianeGroup's pyro valve Ref. [25]

Table 6.22 Omnidea-RTG's pressurant filter Ref. [26]

Table 6.23 ArianeGroup's fill & drain valves

Table 6.24 MAROTTA's relief valve Ref. [27]

Table 6.25 Bradford Space's pressure transducer Ref. [28]

Table 6.26 MAROTTA's pressure regulator Ref. [29]

Table 6.27 VACCO's check valve Ref. [30]

Table 6.28 VACCO's propellant filter Ref. [31]

Table 6.29 VACCO's propellant filter

Table 6.30 Omnidea-RTG ball valve

Table 6.31 ArianeGroup's solenoid valve

Table 7.1 Gravitational acceleration parameters

Table 7.2 Descender engine preliminary requirements

Table 7.3 Descender throat and outlet section engine requirements

Table 7.4 Descender RPA input parameters

Table 7.5 Descender combustion chamber main design parameters

Table 7.6 Descender nozzle section main design parameters

Table 7.7 Descender thermodynamic properties

Table 7.8 Descender RPA theoretical performance

Table 7.9 Descender RPA estimated performance

Table 7.10 Descender estimated efficiencies

Table 7.11 Descender pintle injector preliminary design

Table 7.12 Descender cavitating venturi preliminary design

Table 7.13 Ascender engine preliminary requirements

Table 7.14 Ascender RPA input parameters

Table 7.15 Ascender combustion chamber main design parameters

Table 7.16 Ascender nozzle section main design parameters

Table 7.17 Ascender thermodynamic properties

Table 7.18 Ascender RPA theoretical performance

Table 7.19 Ascender RPA estimated performance

Table 7.20 Ascender estimated efficiencies

Table 7.21 Ascender unlike doublet injector preliminary design

Table 7.22 RCS preliminary requirements

Table 7.23 RCS combustion chamber main design parameters

Table 7.24 RCS nozzle section main design parameters

Table 7.25 RCS thermodynamic properties

Table 7.26 RCS RPA theoretical performance

Table 7.27 RCS RPA estimated performance

Table 7.28 RCS estimated efficiencies

Table 7.29 RCS unlike doublet injector preliminary design

Nomenclature

T Thrust [kN]

\dot{m} Flow rate [kg/s]

v_e Exhaust velocity [m/s]

A_e Exit area [m²]

A_t Throat area [m²]

ε_e Expansion area ratio

P_e Exit pressure [MPa]

P_a Ambient pressure [MPa]

I_t Total impulse [kN s]

I_{sp} Specific impulse [s]

c Effective exhaust velocity [m/s]

MR Mixture ratio

m_p Propellant mass [kg]

m_{fu} Fuel mass [kg]

m_{ox} Oxidizer mass [kg]

c^* Characteristic velocity [m/s]

P_c Chamber pressure [MPa]

C_F Thrust coefficient

Γ Vandenkerckhove function

T_c Chamber temperature [K]

T_e Exit temperature [K]

\mathcal{R} Universal gas constant [J/mol K]

\mathfrak{M} Molar mass [g/mol]

γ Specific heat ratio

c_p Specific heat at constant pressure [J/mol K]

c_v Specific heat at constant volume [J/mol K]

v_c Chamber velocity [m/s]

M Mach number

a Speed of sound [m/s]

X_j Mol fraction

n Molar concentration [mol]

$\Delta_r H^0$ Heat of reaction [kJ/mol]

ΔG Free energy variation [kJ/mol]

S Entropy [J/mol K]

η_T Thrust correction factor

η_d Discharge factor

η_* Characteristic velocity efficiency

η_v Effective exhaust velocity efficiency

η_{CF} Thrust coefficient correction factor

η_n Nozzle efficiency

ΔV Velocity change [m/s]

m_{dry} Dry mass [kg]

m_{gross} Total mass [kg]

m_{cabin} Crew cabin mass [kg]

$m_{consumables}$ Consumable mass [kg]

n_{crew} Number of crew

$t_{support}$ Number of days for life support [days]

A_i Mass estimation coefficient

B_i Mass estimation coefficient

C_i Mass estimation coefficient [kg]

ρ_{Bulk} Mean propellant density [kg/m³]

$\rho_{Oxidizer}$ Oxidizer density [kg/m³]

ρ_{Fuel} Fuel density [kg/m³]

E_i Dry-to-total mass ratio

V volume [m³]

m_0 Pressurizing gas mass [kg]

V_{tank} Propellant volume [m³]

V_0 Pressurizing gas volume [m³]

P_p Regulating pressure [MPa]

P_0 Vessel pressure [MPa]

ΔP_{dyn} Dynamic pressure loss [MPa]

ΔP_{inj} Pressure loss through injector [MPa]

ΔP_{cool} Pressure loss through cooling system [MPa]

ΔP_{feed} Pressure loss through feed lines [MPa]

$\sigma_{allowable}$ Allowable stress inside the reservoir [MPa]

k Safety factor

r Reservoir's radius [m]

t Reservoir's thickness [m]

N_i Number of reservoirs/injector orifices

σ_{hoop} Circumferential stress [MPa]

σ_{long} Longitudinal stress [MPa]

$P_{c_{inj}}$ Pressure at injector face-end [MPa]

ε_c Contraction ratio

t_s Stay time [s]

L^* Characteristic length [m]

V_c Chamber volume [m³]

$L_{n_{conical}}$ Conical engine length [m]

α Nozzle convergent half-angle [deg]

D_i Engine diameter [m]

L_c Chamber length [m]

R_1 Chamber curvature radius [m]

R_2 Nozzle section curvature radius [m]

L_f Bell nozzle percentage [%]

L_n Nozzle section length [m]

θ_n Parabola initial wall angle [deg]

θ_e Nozzle-exit wall angle [deg]

C_d Flow rate discharge coefficient

ΔP Pressure drops [MPa]

W Weight [kN]

TR Throttling ratio

K Sliding parameter

v_i Fluid velocity [m/s]

TMR Total momentum ratio

W Slot width [m]

L Slot height [m]

C cross influence term

d Orifice diameter [m]

d_p Pintle diameter [m]

t_f Annular propellant sheet thickness [m]

h Pintle stroke [m]

θ Pintle half-angle [deg]

1. ABSTRACT

The renewed interest in lunar exploration and the need to extend the crew's time on the Moon, has led to the conceptual development of several manned landing systems, characterized by numerous architectures that differ mainly in the number of stages and the peculiarity to be re-used or not. Each architecture will depend on the type of assumptions made, the manoeuvres performed by the landing system and the type of orbit used. Generally, the tendency is to choose as an outpost a near-rectilinear halo orbit (NRHO) that serves as a reusable command and service module in lunar space. The purpose of the following discussion is to preliminarily define the requirements for lunar descent and ascent propulsion systems based on data associated with previous Apollo missions. After an introduction on the main parameters of a rocket engine and the major influencing factors, the oxidizer and fuel pair used in the current mission and the performance provided by that propellant will be analysed. Choosing the design parameters appropriately, the masses of the individual stages will then be calculated. These values will be compared with approximate models and with known data from the Apollo lunar descent and ascent modules, to obtain reasonable estimates to be used in subsequent sizing of pressurizing gas systems. In addition to the required masses, the most common tank geometries and the stresses to which they are subjected, generated by the high storage pressures of the fluids in question, will be analysed. Then, the solutions provided by the space market will be evaluated and compared with those previously calculated. Once the particular geometry and the number of tanks has been chosen, the architecture of the descent, ascent and attitude control systems will be realized, whose fundamental requirement is the redundancy of the single components. The valves used by the systems will then be selected appropriately. Finally, once the fundamental principles associated with the geometry of a rocket engine have been analysed, the thrust chambers will be sized and the substantial differences between the main stages evaluated.

2. INTRODUCTION

A lunar lander is a spacecraft designed to land on the Moon. If manned, it is generally required that the lander return astronauts from the lunar surface to a predefined location, such as a command and service module. To perform these manoeuvres, a two-stage lander must be equipped with a descent and ascent engine, as well as an attitude control system. These engines operate in totally different ways, as different are the manoeuvres and the problems associated with them, related to the lack of atmosphere, the relatively high gravity, and the thermal environment. A lack of atmosphere does not allow a parachute to be exploited, which is useful both to slow the lander down during descent and to size a lighter net structure. A relatively high gravity dictates that lander must be decelerated considerably, to perform a soft landing. Finally, lunar temperatures can swing between -250 to 120 °C, so thermal control systems must be designed to handle long periods of extreme cold and heat. Generally, the descent engine is a variable-thrust gimbaled rocket. Apollo descent propulsion system (DPS) is a pressure-fed ablative cooled throttle-engine which employs hypergolic propellant, a combination of oxidizer and fuel chosen for their storage capability and rapid combustion, as they do not require an igniter. The current mission will use a family of storable bipropellants, with performance similar to that of the Apollo propulsion systems. Generally, a powered descent manoeuvre is divided into the main following sub-phases:

- Initial fuel-optimum phase
- Landing-approach transition phase
- Final translation and touchdown

A schematic of the apollo powered descent is presented below:

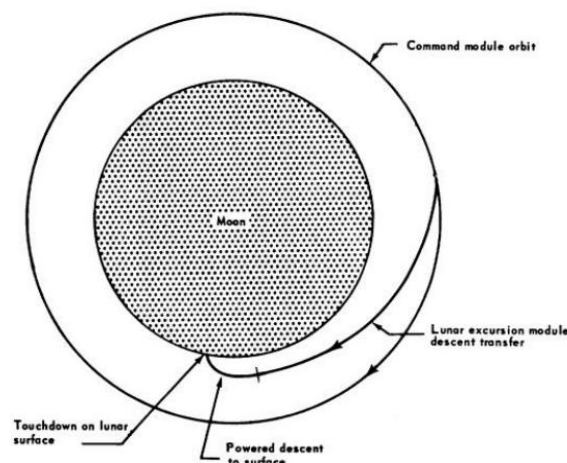


Figure 2.1 Apollo descent manoeuvre

The powered descent is a manoeuvre initially with continuous thrust, of some minutes, performed near the perilunium of the transfer orbit. In the initial phase, away from the landing site, the tendency is to optimize propellant performance in terms of consumption. This means that the descent phase of the fuel-optimum type continues until trajectory changes are necessary to allow the landing site to be viewed correctly (landing-approach transition). Finally, the last phase is the final translation and touchdown in which low speeds and small changes in attitude are required to translate and descend softly to the point of contact with the lunar soil. The ascent manoeuvre is shown in the following figure:

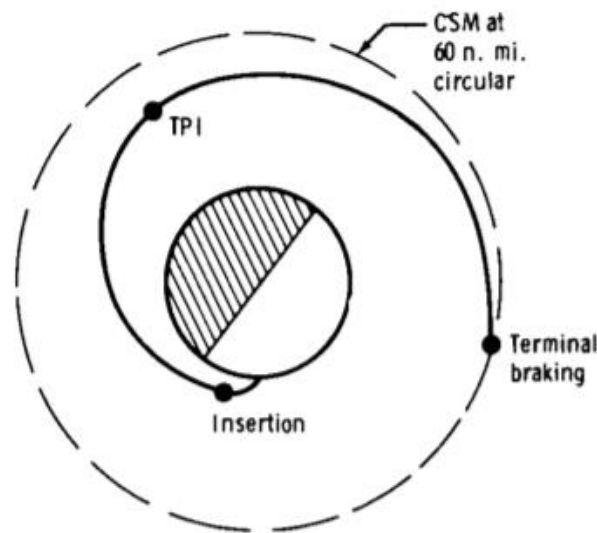


Figure 2.2 Apollo ascent manoeuvre

and mainly consists of a launch from the lunar surface to a middle orbit, a Terminal Phase Initiation (TPI) used to intercept the command module and a Terminal Phase Final (TPF) in which a manual braking is performed, to then proceed with docking and rendezvous. Apollo ascent propulsion system (APS) is a hypergolic rocket characterized by fixed-thrust. The substantial difference from the descent engine is in fact that it does not require a continuous engine-throttling, implying a diversification of the architecture in the engine assembly. In addition, the ascent engine feed system is continuously connected to the reaction control system (RCS), acting as a propellant reserve for the thrusters in case of need. The current mission is based on the same principles as the Apollo propulsion systems, but with different mission planning. In fact, the renewed interest in lunar exploration and the goal of establishing a constant human presence on the Moon, has led to the development of landing systems that take the crew, starting from a lunar outpost (Gateway) to the lunar surface and back, increasing the crew's residence time. This Gateway follows a near-rectilinear halo orbit (NRHO), a type of halo orbit that has slightly curved, so near straight sides, between close passes with an orbiting body. A halo orbit is a three-dimensional periodic orbit traversable by a third body in vicinity

of Lagrange points of two other bodies. It constitutes a solution of the three-body problem in the simplified case where the third body has negligible mass relative to the other two. A body placed on a halo orbit is not physically orbiting around the Lagrange point (since this is only a massless equilibrium point), but it follows a closed trajectory placed near it and the trajectory is the result of an interaction between the gravitational attraction exerted by the two main bodies of the system and the centripetal force to which is subjected the third body. In these regions the gravitational pull between the Earth and the Moon is balanced. Placing a Gateway farther from the Moon in halo orbit relative to its position on the line of the Moon-Earth, known as the L_2 Lagrange point, is a suitable area, because the force balance allows to park the structure for the accomplishment of various purposes. However, even if there is a gain in velocity increment, the remoteness of this orbit from the surface of the Moon is its disadvantage, since it will take a lot of time to fly from this orbit on the surface of the Moon. The subset of the halo orbit family, NRHO, is attractive as intermediate orbits for several reasons, including advantageous movements from the Earth and to destinations beyond the Earth's proximity, communication lines, the possibility of limiting eclipse time and favourable access to the lunar surface. Because of its close position to the moon, flight time is reduced accordingly, but its configuration makes it necessary to constantly recalculate the position of the spacecraft in orbit, due to its slight instability. In any case, the purpose of the following discussion is not focused on mission analysis related to this type of orbits, but on the study of the preliminary requirements that a landing propulsion system must have to perform the desired manoeuvres, starting with the evaluation of propellant performance and concluding with the analysis of the thrust chambers.

3. Fundamentals of liquid rocket engines

3.1 Propellant

The propellant furnishes the energy and the working fluid for the rocket engines [1]. The expression “liquid propellant” embraces all the various propellants stored as liquids and may be one of the following [Refs. Sutton]:

- Oxidizer
- Fuel
- Chemical compound capable of self-decomposition (i.e., Hydrazine)
- Any of the above, with a gelling agent

The term bipropellant identifies the family of propellants characterized by two liquids, stored separately, and mixed inside the combustion chamber. When selecting a propellant or a combination of these, it is clear to realize that most propellants, in addition to their advantages, may have certain disadvantages. Therefore, the correct selection will be characterized by trade-offs. The more important and desirable features from [1] are listed below:

- High energy release per unit of propellant mass, combined with low molecular weight of the combustion product for high specific impulse.
- Ease of ignition.
- Stable combustion.
- High density or high-density impulse to minimize the size and weight of propellant tanks and feed systems.
- Ability to serve as coolant for the thrust chamber.
- Low freezing point (preferably less than 219 K) to facilitate engine operation at low temperature.
- Absence of corrosive effects and compatibility with engine construction materials.
- Good storability (for storable propellant) as assisted by high boiling point (preferably above 344 K) and by the resistance to deterioration during storage.
- Low viscosity to minimize pressure drops through feed system and injector.
- High thermal and shock stability to minimize explosion and fire hazard.
- Low toxicity of raw propellants, their fumes, and their combustion products.
- Low cost.
- Availability.

For the mission analysed, MON-x/MMH was chosen as propellant. This oxidizer-fuel pair belongs to the family of storable hypergolic, or self-ignited, bipropellant. These types of propellants, by definition of “storable” are generally stable over a reasonable range of temperature and pressure and are sufficiently non-reactive with construction materials to permit storage in closed container for a long period. They also permit almost instant readiness of the rocket engine and may result in greater reliability due to the absence of extremely low temperatures. The Mixed Oxides of Nitrogen (MON) is a derivative of N_2O_4 , the ‘dinitrogen tetroxide’ or simply NTO (nitrogen tetroxide). It is a high-density liquid, hypergolic with hydrazine, monomethylhydrazine (MMH) and unsymmetrical dimethylhydrazine (UDMH) and is classified as the most common storable oxidizer employed today [Sutton]. Its liquid phase is characterized by a narrow temperature range and therefore can be easily frozen or vaporized. In addition, NTO is only averagely corrosive when pure but forms strong acids when moist or allowed to mix with water and due to its high vapor pressure, it must be kept sealed in relatively heavy tanks. To lower the freezing point, a certain amount of nitric oxide or simply NO is added, ranging from 2% to 30%, which leads to an increase in vapor pressure and a slight reduction in performance. The mixture of N_2O_4 with a certain percentage of NO is commonly called MON-x, where x is the amount of nitric oxide used. Monomethylhydrazine or simply MMH is being used extensively in spacecraft rocket engine with N_2O_4 as oxidizer. It has a better liquid temperature range than pure hydrazine and a better shock resistance to blast waves. If MMH decomposes at 491 K, pure hydrazine can explode at 369 K when subjected to certain pressure shock. In addition, MMH have slightly lower specific impulses with storable oxidizer than pure Hydrazine and its vapours are easily ignited in air. In any case, all materials compatible with Hydrazine are also compatible with MMH.

3.2 Performance parameters

This discussion summarizes the fundamental principles of the rocket and the related equations used to calculate theoretical performance. Thrust is defined as the force produced by rocket propulsion system acting at the vehicle’s centre of mass. It is a reaction force experienced by vehicle’s structure from the ejection of propellant at high velocities [2]. Momentum is a vector quantity defined as the product of mass times its vector velocity. In rocket propulsion, relatively small amounts of propellant carried within the vehicle are ejected at high velocities. It is possible to define the thrust contribution related to the momentum variation (momentum thrust) as:

$$T = \frac{d(mv_e)}{dt} = \dot{m}v_e = \frac{\dot{W}}{g_0}v_e \text{ at sea level} \quad (3.1)$$

where \dot{m} is the flow rate, v_e the exhaust velocity and g_0 the Earth's gravitational acceleration. This force represents the total propulsive force only when the nozzle exit pressure equals the ambient pressure. In accordance with the following schematization:

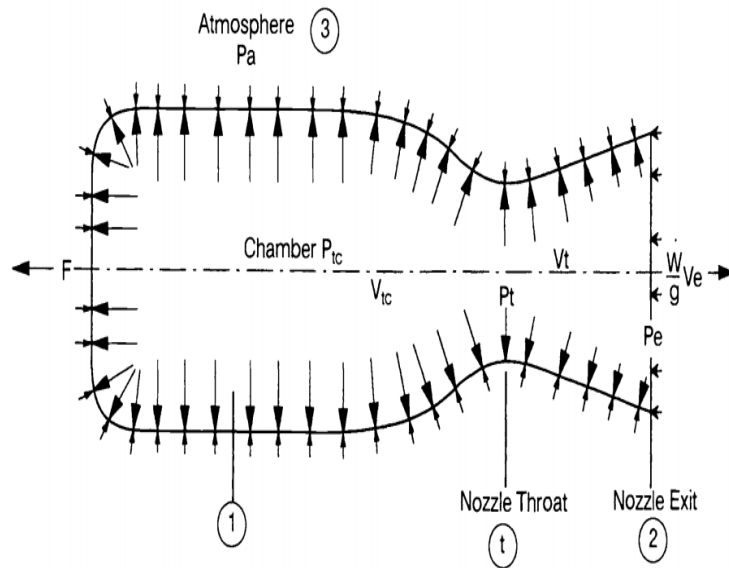


Figure 3.1 Pressure distribution in a thrust chamber

an external pressure acts uniformly on the outer surface of a rocket chamber as well as the changing gas pressure on the inner wall, with the direction and length of the arrows that indicate the magnitude of the relative forces. Axial thrust can be determined by the integration of all pressures acting on areas that have a projection on the plane normal to the nozzle axis, and the pressure of the surrounding fluid (i.e., the local atmosphere) brings a further increase of the thrust component, commonly defined as pressure thrust. For a fixed nozzle geometry, changes in ambient pressure due to variations in altitude during flight results in imbalances between the exit and ambient pressure, denoted respectively as P_e and P_a . The total thrust equation can be written as:

$$T = \dot{m}v_e + A_e(P_e - P_a) \quad (3.2)$$

where A_e is the nozzle exit area. If P_e is less than P_a , the rocket propulsion system is over-expanded and there is a decrease in overall thrust. In the opposite case, under-expansion conditions are noted with a corresponding increase in thrust. Both cases are associated with problems of various nature that are not

pertinent to this preliminary study. It is preferable to operate in adaptive conditions, where P_e is equal to P_a . Most nozzles have a designed expansion ratio, defined as:

$$\varepsilon_e = \frac{A_e}{A_t} \quad (3.3)$$

with A_t the nozzle throat area, such that the pressure at the outlet equals the ambient pressure somewhere at or above sea level. If the geometry is fixed, this phenomenon can only occur at a certain altitude, and this location is referred to as a nozzle operation at its optimum expansion ratio. In the vacuum of space:

$$P_a = 0$$

$$T = \dot{m}v_e + A_e P_e \quad (3.4)$$

Other fundamental parameters are highlighted below. The effective exhaust velocity is defined as the ratio between the total thrust and the flow rate and represents an average velocity at which propellant is being ejected from rocket:

$$c = \frac{T}{\dot{m}} = v_e + \frac{A_e}{\dot{m}}(P_e - P_a) \quad (3.5)$$

The total impulse is the integration of thrust force over its application time:

$$I_t = \int_0^t T dt \quad (3.6)$$

The specific impulse is related to the total impulse and the effective exhaust velocity. It is defined as the thrust per unit propellant “weight” flow rate [Sutton] and is equal to:

$$I_{sp} = \frac{\int_0^t T dt}{g_0 \int_0^t \dot{m} dt} \quad (3.7)$$

This equation furnishes a time-averaged specific impulse in seconds for any type of rocket propulsion system.

For short time intervals this can be rewritten as:

$$I_{sp} = \frac{I_t}{g_0 m_p} = \frac{T}{g_0 \dot{m}} = \frac{c}{g_0} \quad (3.8)$$

where m_p is the total effective propellant mass expelled. The latter is equal to:

$$m_p = m_{ox} + m_{fu} \quad (3.9)$$

with m_{ox} the oxidizer mass and m_{fu} the fuel mass. It is possible to define the mixture ratio (MR) as:

$$MR = \frac{m_{ox}}{m_{fu}} = \frac{\dot{m}_{ox}}{\dot{m}_{fu}} \quad (3.10)$$

and associate it with the total propellant mass:

$$m_{fu} = \frac{m_p}{1 + MR} \quad (3.11)$$

$$m_{ox} = \frac{m_p}{1 + \frac{1}{MR}} \quad (3.12)$$

The above equations are useful for preliminary sizing of the propulsion system. Another fundamental parameter for evaluating rocket performance is the characteristic velocity, defined as:

$$c^* = \frac{P_c A_t}{\dot{m}} \quad (3.13)$$

where P_c is the chamber pressure. This velocity may be related to the efficiency of the combustion process and is used for comparing the relative performance of different chemical rocket and propellants. Finally, the thrust coefficient is defined as:

$$C_F = \frac{T}{P_c A_t} \quad (3.14)$$

This quantity reflects the product-gas expansion properties and design quality of the nozzle. The effective exhaust velocity is related to the thrust coefficient and the characteristic velocity by the following relationship:

$$c = c^* C_F \quad (3.15)$$

For an ideal rocket propulsion unit, the following assumptions are valid:

- Homogeneous gas composition
- Perfect gas
- No heat transfer through the motor wall in either direction (i.e., adiabatic process)
- No friction
- Steady flow rate
- One-dimensional flow
- Velocity uniformity across any section normal to chamber axis
- Chemical equilibrium established within the combustion chamber and remaining constant in the nozzle (frozen composition)

In the actual design of a rocket and for the prediction of its behaviour, certain correction factors, usually empirically obtained, will be applied to the results derived from these ideal assumptions. In first approximation, however, it is supposed an ideal rocket. Substituting the equation (3.4) into (3.14) it is possible to rewrite the thrust coefficient as follows:

$$C_F = \frac{\dot{m} v_e + A_e P_e}{P_c A_t} \quad (3.16)$$

From the well-known principles of thermodynamics and fluid dynamics for isentropic flows, it is possible to write the flow rate as follows:

$$\dot{m} = \frac{P_c A_t}{\sqrt{RT_c}} \Gamma \quad (3.17)$$

where R and Γ are respectively the universal gas constant divided by the molar mass of the fluid considered, and the Vandekerckhove function defined as:

$$R = \frac{\mathcal{R}}{\mathfrak{M}} \text{ with } \mathcal{R} = 8.314462 \left[\frac{J}{mol \cdot K} \right] \quad (3.18)$$

$$\Gamma = \sqrt{\gamma \left(\frac{2}{\gamma + 1} \right)^{\frac{\gamma+1}{\gamma-1}}} \quad (3.19)$$

The specific heat ratio γ is defined as:

$$\gamma = \frac{c_p}{c_v} \quad (3.20)$$

where c_p and c_v are respectively the specific heat at constant pressure and volume. Using the conservation of energy applied between the chamber section and the nozzle outlet, it is possible to define the exhaust velocity as:

$$v_e = \sqrt{2c_p(T_c - T_e) + v_c^2} \quad (3.21)$$

The transformation of the reactants into combustion products take place in the chamber section but the flow is not yet expanded. Therefore, the Mach number defined as:

$$M = \frac{v_i}{a_i} \quad (3.22)$$

$$a_i = \sqrt{\gamma_i R T_i} \quad (3.23)$$

where v_i , a_i are the velocity and the speed of sound in a generic section, is equal to or about zero. It is reasonable to assume that v_c^2 is a negligible term:

$$v_e = \sqrt{2c_p(T_c - T_e)} = \sqrt{2 \frac{\gamma R}{\gamma - 1} T_c \left[1 - \left(\frac{P_e}{P_c} \right)^{\frac{\gamma-1}{\gamma}} \right]} \quad (3.24)$$

Substituting the equation [] into the thrust coefficient:

$$C_F = \Gamma \sqrt{2 \frac{\gamma}{\gamma - 1} \left[1 - \left(\frac{P_e}{P_c} \right)^{\frac{\gamma-1}{\gamma}} \right]} + \varepsilon_e \left(\frac{P_e}{P_c} - \frac{P_a}{P_c} \right) \quad (3.25)$$

$$C_F = C_{F_{vacuum}} - \varepsilon_e \frac{P_a}{P_c} \quad (3.26)$$

and rewriting the characteristic velocity as follows:

$$c^* = \frac{P_c A_t}{\dot{m}} = \frac{I_{sp} g_0}{C_F} = \frac{c}{C_F} = \frac{\sqrt{\gamma R T_c}}{\gamma \sqrt{\left(\frac{2}{\gamma + 1} \right)^{\frac{(\gamma+1)}{\gamma-1}}}} \quad (3.27)$$

it is possible to notice, in accordance with [1], that:

- An ambient pressure P_a reduces the vacuum thrust T of an engine by the amount $P_a A_e$; C_F will be similarly affected by the amount $\varepsilon_e \frac{P_a}{P_c}$ as shown in eq.(3.25). The lower the ambient pressure, the higher will be thrust and performance, with maximum values obtained in vacuum.
- Optimum thrust for a given ambient pressure is obtained when the nozzle expansion ratio ε_e is such that $P_e = P_a$. This can be seen in the following figure:

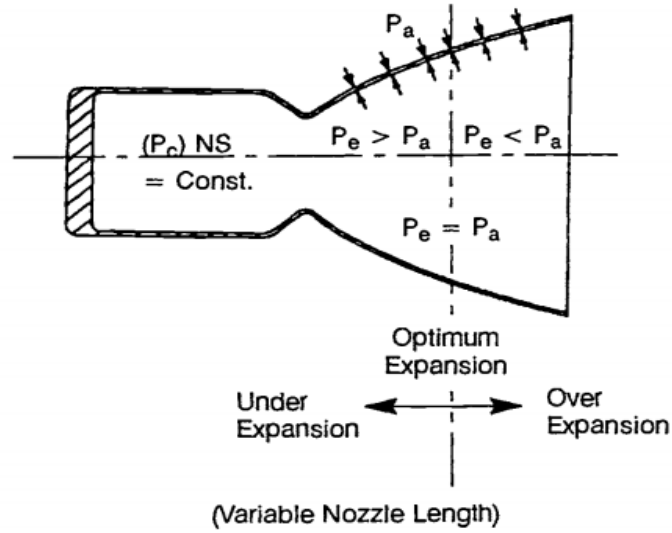


Figure 3.2 Nozzle expansion conditions

as previously mentioned, if the divergent nozzle section is extended in the region where $P_e > P_a$ thrust will increase; however, where $P_e < P_a$ lengthening the nozzle will decrease thrust. Therefore, it would be beneficial to design the nozzle such that $P_e = P_a$ (optimum nozzle expansion ratio). Unfortunately, because of changing ambient pressure during flight, no one ϵ_e is optimum. Trajectory and payload optimization studies usually determine the best compromise. Such a study is not required, except for weight and size considerations, for rockets that generally operate in vacuum, where the ambient pressure is zero or near zero. In this case ϵ_e would become infinity to satisfy the ideal expansion. An increase in nozzle expansion ratio increases specific impulse, as can be seen by substituting eq. (3.8) and (3.13) in (3.2):

$$I_{sp} = \frac{v_e}{g_0} + \frac{\epsilon_e c^*}{P_c} (P_e - P_a) = I_{sp_{opt}} + \frac{\epsilon_e c^*}{P_c} (P_e - P_a) \quad (3.28)$$

At the same time this leads to an increase in weight, so the choice of ϵ_e is related to a tradeoff. For a space engine generally the expansion ratio does not exceed 400.

- The specific heat ratio γ indicates the energy-storing capacity of the gas molecule, i.e., its degrees of freedom. A smaller value of γ indicates a higher energy storing capability, and in turn provides a higher engine performance. This can be observed in the equation (3.25) and (3.27) or simply by imposing the vacuum and nozzle adaptive condition. With these assumptions, the thrust coefficient is:

$$C_{F_{MAX}} = \Gamma \sqrt{2 \frac{\gamma}{\gamma - 1}} \quad (3.29)$$

It is possible to observe the trend of C_F as function of altitude, γ and ϵ_e :

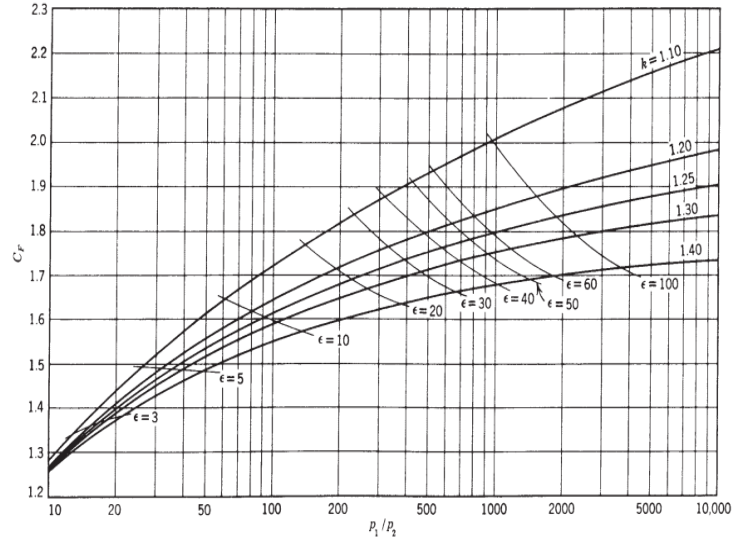


Figure 3.3 Variation in thrust coefficient as altitude, specific heat ratio, and expansion ratio change

- For a constant chamber temperature, the equation (3.27) shows that c^* will increase if R increases, i.e., if the molecular weight \mathfrak{M} decreases. This results in better engine performance.
- The effective chamber pressure affects overall engine performance. This can be observed in eq. (3.25) where C_F is affected by $\frac{P_e}{P_c}$ and $\frac{P_a}{P_c}$. An increase in P_c results in decrease of the negative term and hence increases C_F . Since the thrust is proportional to both C_F and P_c , an increase in P_c will bring a gain in thrust. The chamber pressure also has some effect on the combustion process. Increasing P_c tends to increase T_c and to reduce γ and R . The overall result is usually an increase in c^* .

The assumptions listed above are approximations that allow relatively simple mathematical relations for the analysis of real rocket nozzles. The latter have losses and some of the flow internal energy is unavailable for conversion into kinetic energy of the exhaust. Principal losses are mentioned below:

- The divergence of the flow in the nozzle outlet is a loss that varies as a function of the cosine of the divergence angle for conical nozzles. These losses can be reduced with bell-shaped nozzle contours.

- Small chamber cross sections relative to the throat area (contraction ratio) cause pressure losses in the chamber and slightly reduce the thrust and exhaust velocity.
- The lower velocities at the wall boundary layers reduce the effective average exhaust velocity by 0.5 to 1.5%.
- Solid particles and/or liquid droplets in the gas may cause losses of perhaps up to 5%, depending on particle size, shape, and percent solids.
- Unsteady combustion and/or flow oscillations may result in small losses.
- Chemical reactions within nozzle flows change gas composition, gas properties and temperatures, amounting to typically a 0.5% loss.
- Chamber pressures and overall performance are lower during transient operations.
- Any gradual throat erosion increases its diameter by perhaps 1 to 6% during operation with uncooled nozzle materials. In turn, this will reduce the chamber pressure and thrust by about 1 to 6%. Such throat area enlargements cause a slight reduction in specific impulse, usually less than 0.7%.
- Nonuniform gas compositions may reduce performance, due to incomplete mixing or combustion.
- Real gas properties may noticeably modify gas composition, that is, actual values of γ and M cause a small loss in performance, about 0.2 to 0.7%.

3.3 Fundamentals of chemical reactions

To properly size the propulsion system associated with the current mission, it is appropriate to evaluate rocket performance with the mixture ratio. As noted above, gas composition may change somewhat in the nozzle when chemical reactions are occurring in the flowing gas, and the assumption of uniform or “chemically frozen-composition” gas flow may not be fully valid for all chemical systems. A more sophisticated approach allows the problem to be broken down and studied as follows:

- The combustion process is the first part and normally occurs at essentially constant pressure (isobaric) in the combustion chamber. Chemical reactions do occur very rapidly during propellant combustion. The chamber volume is assumed to be large enough and the residence time long enough for attaining chemical equilibrium within chamber.
- The nozzle gas expansion process constitutes the second set of calculations. The equilibrated gas combustion products from the chamber then enter a supersonic nozzle where they undergo an adiabatic expansion without further chemical reactions. The gas entropy is assumed constant during reversible nozzle gas expansions, although in real nozzles it increases slightly.

The chemical rocket combustion analysis is based on chemical reactions between oxidizer and fuel. The heat released by these reactions transforms the propellant into hot gases that are expanded inside the nozzle in order to generate thrust. Therefore, it is necessary to accurately know the chemical composition of the propellant used, which in liquid propulsion system translates into the knowledge of the mixture ratio. The mixture of resulting gases at equilibrium exerts a pressure that is the sum of all the partial pressures of its individual constituents, each acting at a common total chamber volume and temperature (Dalton's law):

$$P = P_a + P_b + P_c + \dots$$

$$T = T_a = T_b = T_c = \dots$$

where a,b,c are the individual gas constituents. Applying the perfect gas equation for the j-th chemical species:

$$P = \frac{R_a T}{V_a} + \frac{R_b T}{V_b} + \frac{R_c T}{V_c} + \dots = \frac{\mathcal{R}T}{\mathfrak{M}V_{mix}} \quad (3.30)$$

with V_j the reaction-chamber volume per unit component mass. The volumetric proportions for each gas species in a gas mixture are determined from their molar concentration n_j expressed as kg-mol per kg of mixture. If n is related to the total number of kg-mol of all species per kilogram of uniform gas mixture, the mol fraction X_j becomes:

$$X_j = \frac{n_j}{n} \quad (3.31)$$

$$n = \sum_{j=1}^m n_j \quad (3.32)$$

Where the index m represents the total number of different gaseous species in the equilibrium combustion gas mixture. The average molecular mass is defined as:

$$\mathfrak{M} = \frac{\sum_{j=1}^m n_j \mathfrak{M}_j}{\sum_{j=1}^m n_j} \quad (3.33)$$

The molar specific heat for a gas mixture at constant pressure can be determined from n_j and their molar specific heats:

$$C_{p_{mix}} = \frac{\sum_{j=1}^m n_j C_{p_j}}{\sum_{j=1}^m n_j} \quad (3.34)$$

with a specific heat ratio equals to:

$$\gamma_{mix} = \frac{C_{p_{mix}}}{C_{p_{mix}} - \mathcal{R}} \quad (3.35)$$

When all the reactants are consumed and transformed into products, the reaction is defined stoichiometric. In rocket propulsion systems, it is usually not advantageous to operate under this condition but in a fuel rich mixture. This allows low molecular mass, reducing \mathfrak{M} which in turn increases the exhaust velocity of reaction products. Chemical equilibrium occurs in a reversible chemical reaction when the rate of product formation exactly equals the reverse reaction and once this equilibrium is reached, no further changes in concentration take place. The heat of reaction is the sum of the heats of formation of products and reactants:

$$\Delta_r H^0 = \sum [n_j (\Delta_f H^0)_j]_{products} - \sum [n_j (\Delta_f H^0)_j]_{reactants} \quad (3.36)$$

and can be positive or negative depending on whether the reaction is exothermic or endothermic. It is defined as the energy released or absorbed when 1 mol of chemical compound is formed from its constituent atoms at 0.1 MPa and isothermally at 298.15K. The symbol Δ implies an energy change and the superscript 0 means that each product or reactant is at its thermodynamic standard state. If stable equilibrium is reached, the system is in minimum energy configuration. The Gibbs free energy is a convenient function for the chemical system describing its thermodynamic potential and is directly related to the internal energy U , pressure P , molar specific volume V , enthalpy h , temperature T and entropy S . It is defined as:

$$G_j = U_j + P_j V_j - T_j S_j = h_j - T_j S_j \quad (3.37)$$

For a series of different species, the total free energy is:

$$G = \sum_{j=1}^m n_j G_j \quad (3.38)$$

The free energy represents the driving force for a chemical substance to enter into a chemical change and for a perfect gas is function of temperature and pressure. Changes in free energy result in the following equation:

$$\Delta G = \sum_{j=1}^m [n_j (\Delta_f G^0)_j]_{products} - \sum_{j=1}^r [n_j (\Delta_f G^0)_j]_{reactants} \quad (3.39)$$

where the index m accounts for the number of gas species in the combustion products and r for the reactants. At equilibrium:

$$\frac{d(\Delta G)}{dn} = 0$$

If the reacting propellants are liquid, energy will be needed to change phase and/or vaporize them or to break them down into other species. This energy must be subtracted from that available to heat the gases from the reference temperature to the combustion temperature. Therefore, values of ΔG^0 and ΔH^0 for liquid species are considerably different from those for same species initially in gaseous state. The change of entropy, another thermodynamic property that for an isentropic nozzle flow it is assumed to remains constant, is described by the following equation:

$$dS = \frac{dU}{T} + \frac{pdV}{T} = C_p \frac{dT}{T} - R \frac{dP}{P} \quad (3.40)$$

For a constant C_p the corresponding integral beacomes:

$$S - S^0 = C_p \ln \frac{T}{T_0} - R \ln \frac{P}{P_0}$$

with the subscript 0 applied to indicate the reference state. For mixtures, the total entropy is:

$$S = \sum_{j=1}^m S_j n_j \quad (3.42)$$

Here, S_j is measured in J/kg-mol-K. The entropy for each gaseous species is:

$$S_j = (S_T^0)_j - R \ln \frac{n_j}{n} - R \ln P \quad (3.43)$$

where S_T^0 represents the standard state entropy at a temperature T. Typical thermochemical values from [2] of various species are listed below:

Substance	Phase ^a	Molar Mass (g/mol)	$\Delta_f H^0$ (kJ/mol)	$\Delta_f G^0$ (kJ/mol)	S^0 (J/mol-K)	C_p (J/mol-K)
Al (crystal)	s	29.9815	0	0	28.275	24.204
Al ₂ O ₃	l	101.9612	-1620.567	-1532.025	67.298	79.015
C (graphite)	s	12.011	0	0	5.740	8.517
CH ₄	g	16.0476	-74.873	-50.768	186.251	35.639
CO	g	28.0106	-110.527	-137.163	197.653	29.142
CO ₂	g	44.010	-393.522	-394.389	213.795	37.129
H ₂	g	2.01583	0	0	130.680	28.836
HCl	g	36.4610	-92.312	-95.300	186.901	29.136
HF	g	20.0063	-272.546	-274.646	172.780	29.138
H ₂ O	l	18.01528	-285.830	-237.141	69.950	75.351
H ₂ O	g	18.01528	-241.826	-228.582	188.834	33.590
N ₂ H ₄	l	32.0453	+50.434	149.440	121.544	98.666
N ₂ H ₄	g	32.0453	+95.353	+159.232	238.719	50.813
NH ₄ ClO ₄	s	117.485	-295.767	-88.607	184.180	128.072
N ₂ O ₄	l	92.011	-19.564	+97.521	209.198	142.509
N ₂ O ₄	g	92.011	9.079	97.787	304.376	77.256
NO ₂	g	46.0055	33.095	51.258	240.034	36.974
HNO ₃	g	63.0128	-134.306	-73.941	266.400	53.326
N ₂	g	28.0134	0	0	191.609	29.125
O ₂	g	31.9988	0	0	205.147	29.376
NH ₃	g	17.0305	-45.898	-16.367	192.774	35.652

Figure 3.4 Thermochemical properties of various species

For the analysis of the flow inside the nozzle, there are several calculation methods that depend mainly on the type of assumptions made. Generally, once the hot gases reach the supersonic nozzle, they experience an adiabatic and reversible expansion, with a substantial drop in temperature and pressure and a conversion in kinetic energy. For an ideal rocket with frozen composition, the state of the gas throughout expansion in the nozzle is fixed by the entropy of the system, which is invariant with pressure reduction. In the real case

it is appropriate to consider all the losses mentioned above. Chemical composition during nozzle expansion may be treated analytically in the following ways:

- When the expansion is sufficiently rapid, composition may be considered invariant throughout the nozzle, that is, there are no chemical reactions or phase changes and the reaction products composition at the nozzle outlet are identical to those of the chamber. This is defined as frozen equilibrium and tends to underestimate the system's performance of 1 to 4%.
- Instantaneous chemical equilibrium among all molecular species may be significant in some cases under variable pressure and temperature during expansion. Here, product composition do shift because the chemical reactions and phase change equilibria between gaseous and condensed phase in all exhaust gas species are fast compared to the nozzle transit time. This composition is defined as shifting equilibrium and tends to overestimate the nozzle performance of 1 to 4%.
- Although rapid, chemical reactions take a finite amount of time. Reaction rates for specific reactions are often estimated, depending on temperature, magnitude of deviation from the equilibrium composition, nature of the reactions involved.

3.4 Software-assisted analysis

All analyses previously discussed are generally executed by computational software. The most common ones are listed below:

- NASA Chemical Equilibrium with Applications (CEA) is based on equilibrium composition, with the assumption of one-dimensional forms of the continuity, momentum and energy equations, isentropic expansion in the nozzle, ideal gas behaviour and chemical equilibrium in the chamber.
- One-Dimensional Kinetics (ODK) incorporates finite chemical reaction rates for temperature-dependant composition changes in the flow direction with uniform flow properties across any nozzle section.
- Two-Dimensional Kinetic code (TDK) incorporates finite kinetic chemical reaction rates and radial variation in flow properties.
- Rocket Propulsion Analysis (RPA) is based on minimizing the Gibbs free energy to obtain the combustion composition, analysis of nozzle flows with shifting and frozen chemical equilibrium.

Unfortunately, not all the mentioned computer codes are available, as they are generally owned by private companies and government offices. The following discussion is based on the use of NASA CEA and RPA to

solve the chemical equilibrium for rocket performance evaluation. The current mission is characterized by the following input data:

Table 3.1 Mission requirements

Parameter	Requirements	Unit
Fuel	MMH	
Oxidizer	MON-X	
Isp Required	> 310	s

To estimate the performance of a rocket using such combination of fuel and oxidizer, as mentioned in the previous section, software such as CEA NASA and RPA are used, which allow to solve the chemical equilibrium of the considered mixture. The choice of propellant type is dictated by the requirements listed in Section 3.1. Since the fuel is a fixed input data, the only variable to be investigated will be the percentage of nitric oxide within the NTO. The main properties of MMH are listed below:

Table 3.2 Monomethylhydrazine main properties

MMH PROPERTIES		
Parameter	Value	Unit
Freezing point	221.15	K
Boiling point	364.15	K
Heat of formation	54.14	KJ/mol
Molecular weight	46.07174	g/mol
Vapor Pressure [293.15 K]	0.005	MPa

The density, as a function of temperature is shown in the following graph:

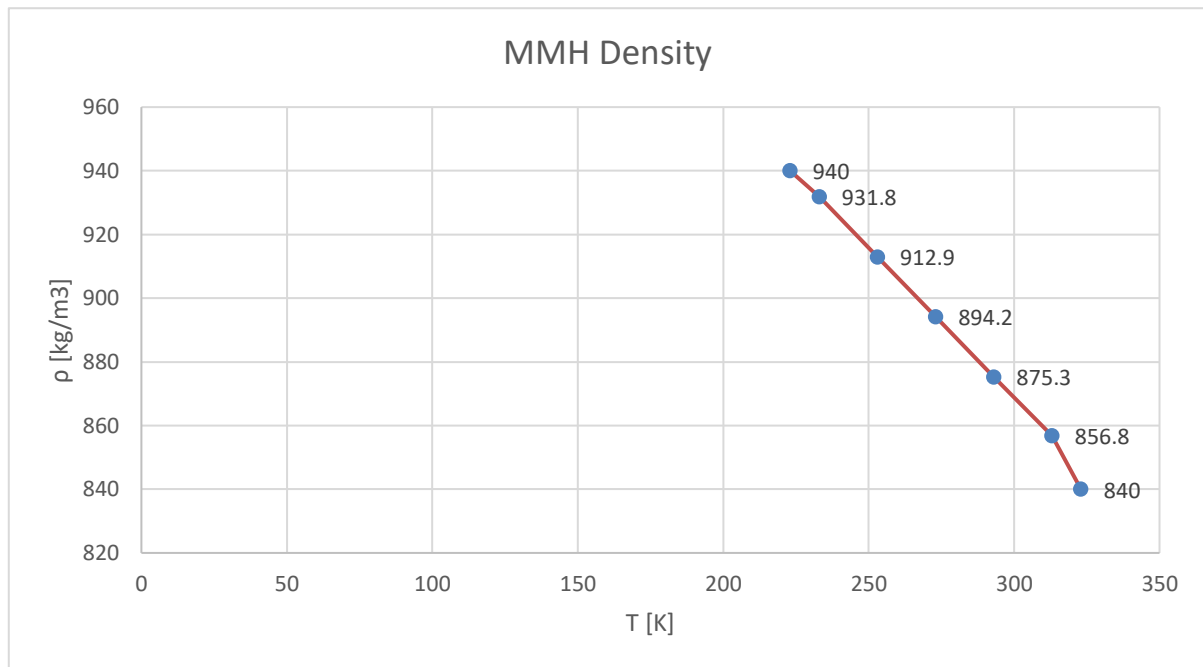


Figure 3.5 Variation of MMH density as a function of temperature

For a temperature of 298.15 [K], a density of 874 [kg/m³] is assumed. It is also shown the trend of the specific heat:

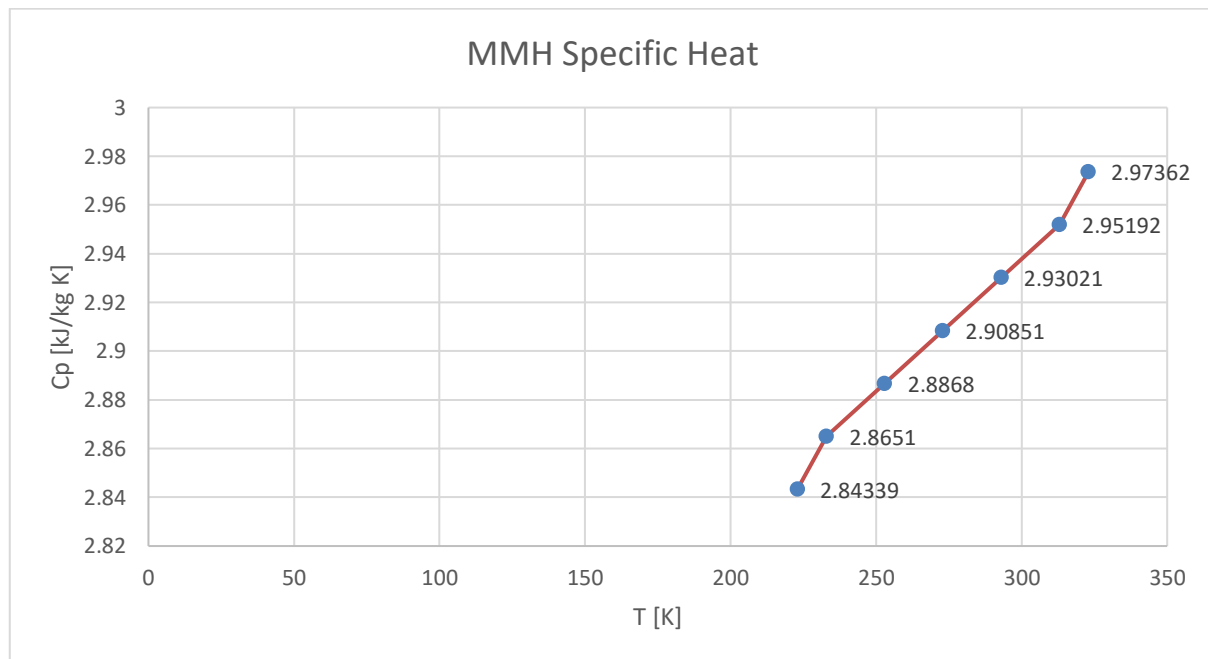


Figure 3.6 Variation of MMH specific heat as a function of temperature

For a temperature of 298.15 [K], a specific heat of 2.935 [kJ/kg K] is assumed. At this point the principal properties of the oxidizer are evaluated. As mentioned in Section 3.1 the addition of a given percentage of

NO changes the freezing point of the Mixed Oxides of Nitrogen and its vapor pressure. According to [3] this trend is given below:

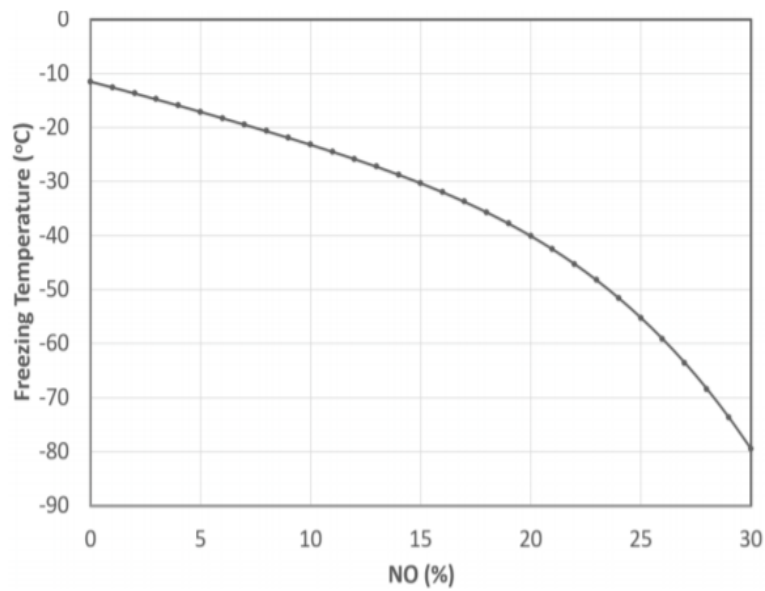


Figure 3.7 Variation of MON-x freezing point as a function of NO%

Freezing temperature is changed from 260.15 K (-13 °C) with 1% of nitric oxide to 218.15 (-52 °C) with a percentage of 25%. Vapor pressure increases as the percentage of NO increases:

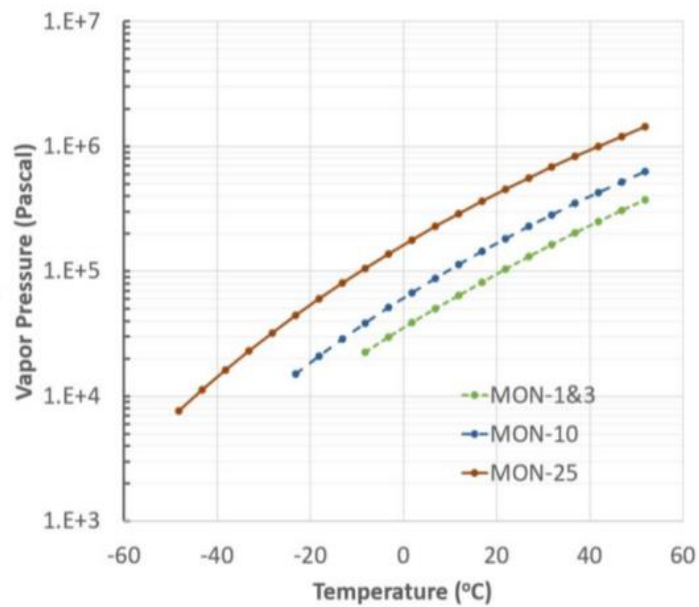


Figure 3.8 Variation of MON-x vapor pressure as a function of temperature and NO%

As can be seen from the graphs shown above, the addition of NO into NTO results in a lowering of the freezing point for the mixture, a wider operating temperature range than NTO/MMH and subsequently a reduction of the heater power requirements. In addition, an increase in nitric oxide reduces the formation of iron nitrate, which in turn reduces the corrosiveness of the materials. It also true that a significant increase in the percentage of NO can affect tank design and the maximum pressure of the system. According to Ref [3], as liquid MON-25 flows through sharp-curvature lines, bubble are formed due to local flow-field pressure drop below the propellant vapor pressure, causing undesirable propellant flow oscillations that can lead to chamber pressure fluctuation. In the following, the performance of the MON-X/MMH pair will be analysed. As the mixture ratio varies, all performance indexes listed in Section [] will exhibit a maximum and minimum at the stoichiometric point. c^* and C_F both have a different maximum point: the tendency generally goes towards the maximum of the following product:

$$c^* C_F = c = \frac{T}{\dot{m}} \quad (3.44)$$

representing the theoretical minimal consumption. The specific impulse, as a function of MR is shown in the following graph for a different percentage of NO:

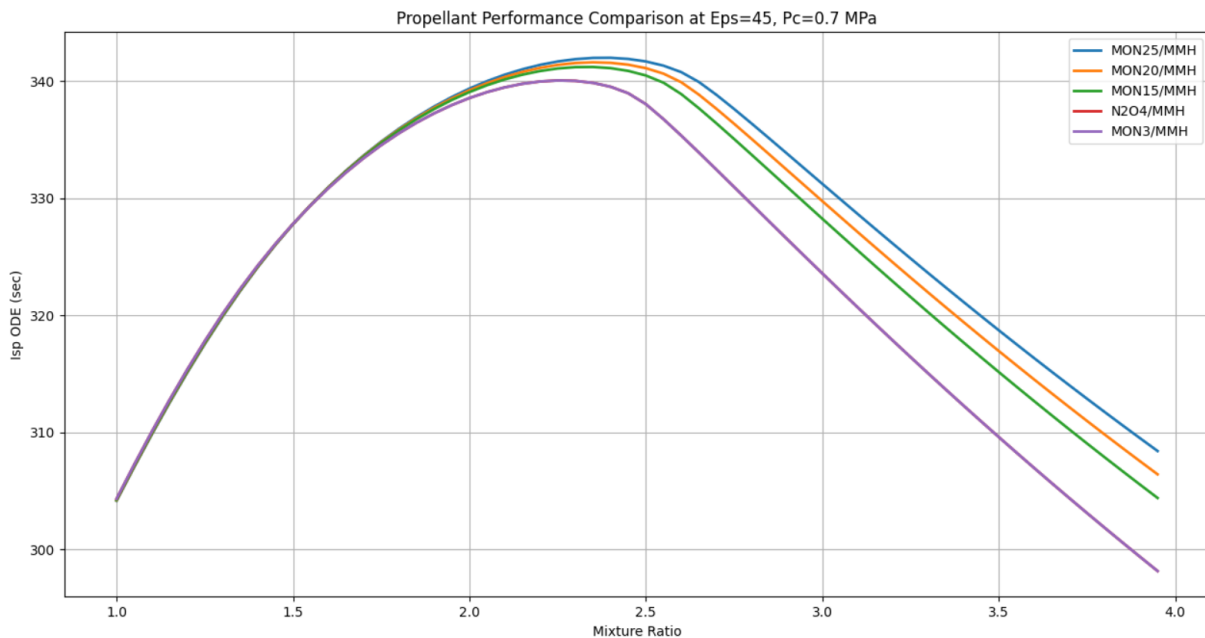


Figure 3.9 Variation of specific impulse as a function of mixture ration and NO%

The vacuum I_{sp} for a shifting equilibrium ranges from 340 to 343 seconds for reasonable expansion ratio values of 45 and a chamber pressure of 0.7 MPa. The c^* has the following trend:

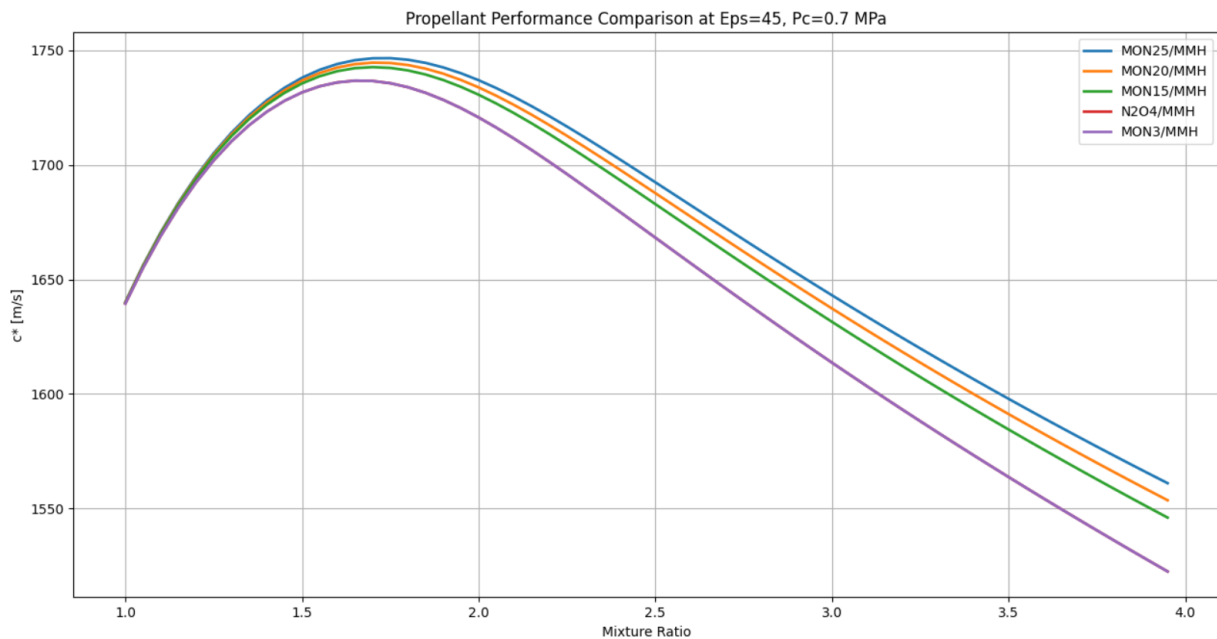


Figure 3.10 Variation of characteristic velocity as a function of mixture ratio and NO%

with a from 1738 to 1747 m/s for the same values of P_c and ε_e . The vacuum thrust coefficient will be da ratio between $I_{sp}g_0$ and c^* and oscillates between values of 1.93 and 1.915. Stoichiometric conditions for specific impulse are achieved for a mixture ratio value ranging between 2.2 and 2.4, as noted in fig. 3.9 and depends essentially on the propellant combination used. Although the MON25/MMH pair has the highest performance, considering the problems previously mentioned the choice for the current mission falls on the use of MON3/MMH, because of its wide availability on the market. As noted in the graphs above, the addition of 3% of nitric oxide within the NTO does not lead to any change in performance, but only a slight reduction in freezing point. According to RocketCEA documentation v1.1.24 [4] the calculator input parameters for the oxidizers of interest are essentially the same:

MON3

```
oxid N2O4 (L)  N 2 O 4  wt%=100.00
h,cal=-4676.0  t (k)=298.15
```

N2O4

```
oxid N2O4 (L)  N 2 O 4  wt%=100.00
h,cal=-4676.0  t (k)=298.15
```

The main properties of MON3 are listed below:

Table 3.3 Mixed oxides of nitrogen main properties

MON3 MAIN PROPERTIES		
Parameter	Value	Unit
Freezing point	257.15	K
Boiling point	294.25	K
Heat of formation	-19.564	KJ/mol
Molecular weight	92.011	g/mol
Vapor Pressure [293.15 K]	0.1	Mpa

Once the propellant is selected, its major characteristics can be analysed as the mixture ratio changes using NASA Chemical Equilibrium and Applications as computational software. The latter requires the following input parameters:

- P_c or an interval of P_c .
- Fuel(s).
- Oxidizer(s).
- MR or an interval of MR .
- Exit conditions.
- Selecting frozen/shifting equilibrium.
- Selecting an infinite/finite area combustor, depending on the contraction ratio. For an infinite contraction ratio, as will be seen below, the pressure at the injector face is the same as the pressure in the chamber combustion end plenum. Vice versa, for a finite area combustor pressure losses will occur in the mentioned sections (Rayleigh line losses).

Considering shifting equilibrium and an infinite area combustor as first approximation, the MON3/MMH pair has the following characteristics:

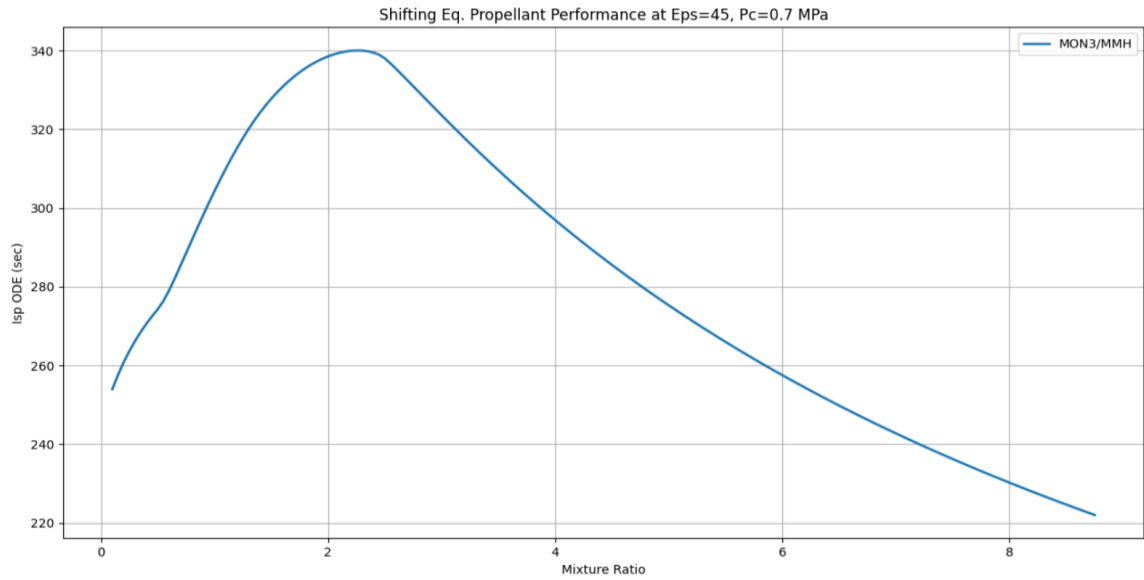


Figure 3.11 Variation of specific impulse as a function of mixture ratio for the MON3-MMH pair

The maximum value of specific impulse is 340.065 s and corresponds to a mixture ratio of 2.25. The temperature trend is shown in the subsequent graph:

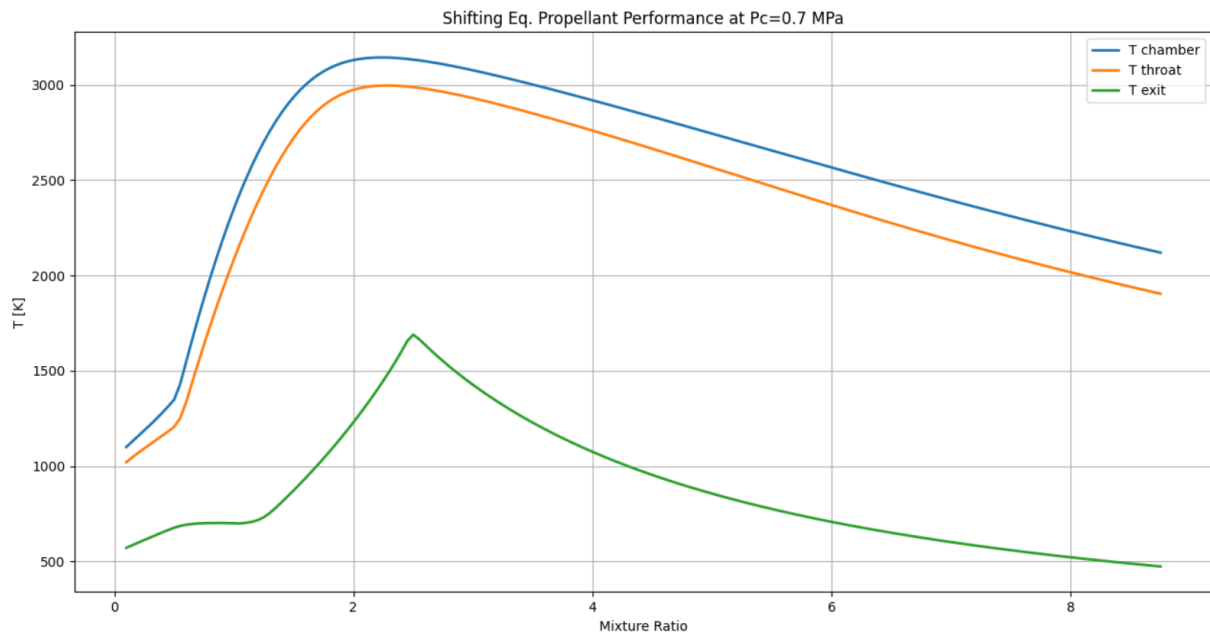


Figure 3.12 Variation of temperatures as a function of mixture ratio

It is noted that the maximum of T_c is obtained in the stoichiometric condition and in chamber section, with a value of 3144.4012 K. The temperatures in the throat section and at nozzle outlet are also shown, with values of 2997.221 and 1689.3969 K respectively. As will be seen in the following, the throat appears to be a

crucial section due to the manifestation of the maximum heat flux and the consequent erosion problems. It is then appropriate to size a cooling method. The shifting equilibrium performances are shown in the graph below:

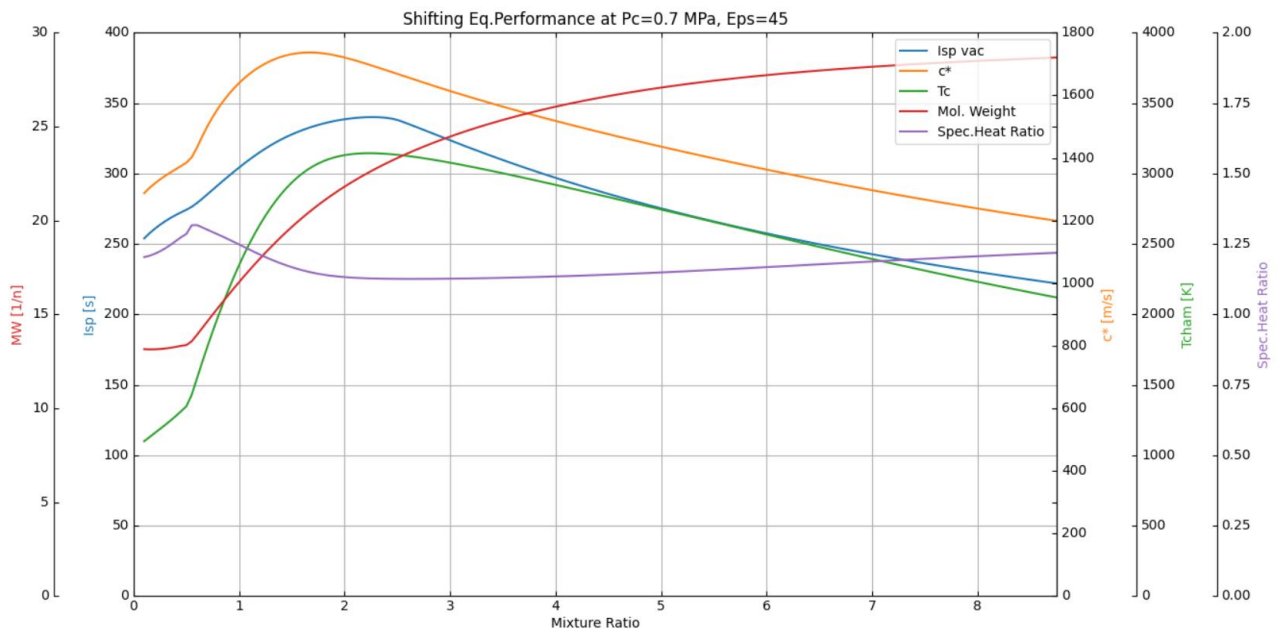


Figure 3.13 Shifting equilibrium performances of the MON3-MMH pair

As expected, in addition to the parameters previously discussed, the specific heat ratio exhibits a minimum at stoichiometric point, with a value of 1.12589 and the molecular weight increases as the mixture ratio increases. The specific heat presents the following trend:

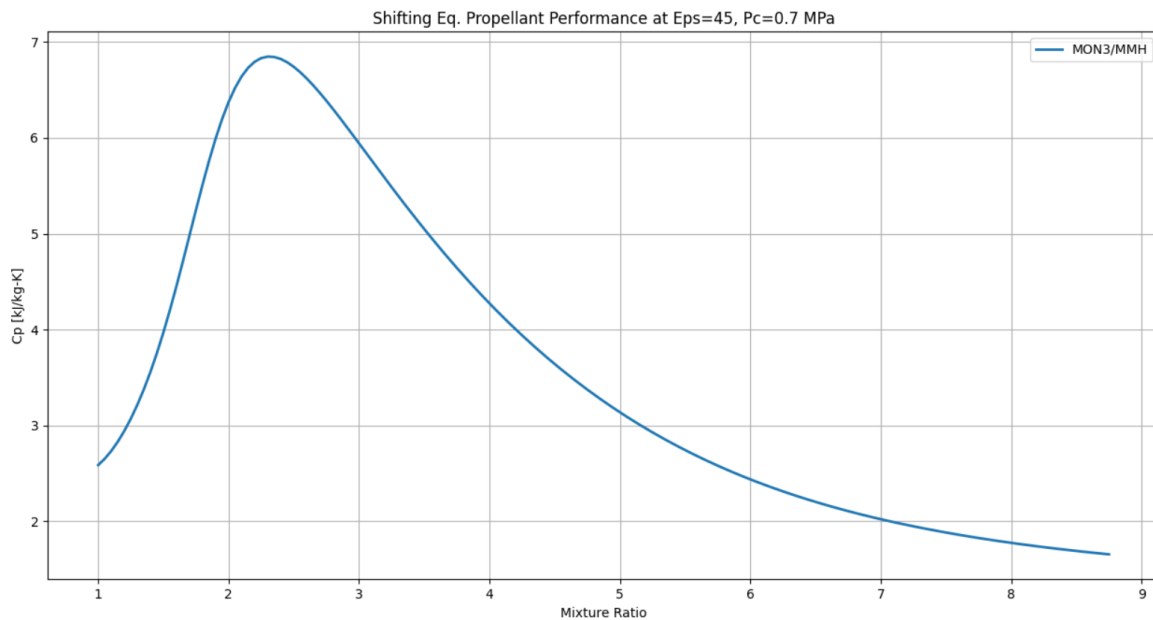


Figure 3.14 Variation of specific heat as a function of the mixture ratio

and reaches a maximum value of 6.8469 kJ/kg-K. Finally, other properties of the propellant are presented such as Prandtl number, viscosity, and the thermal conductivity:

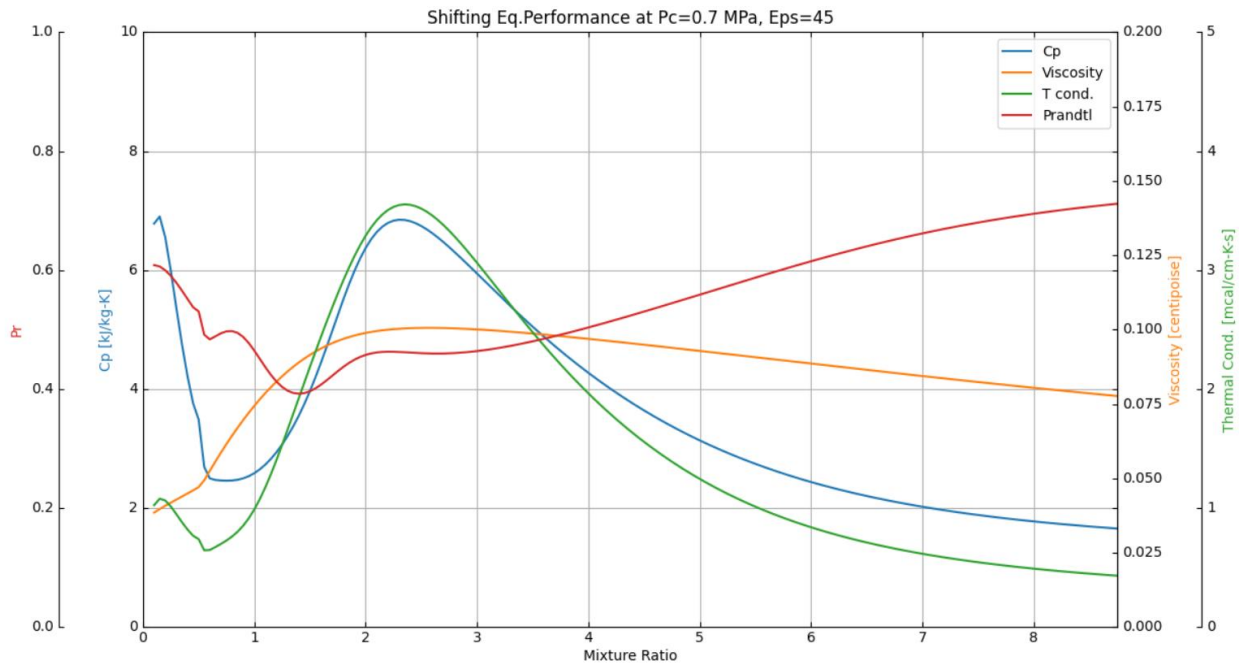


Figure 3.15 Variation of several parameters as a function of mixture ratio for MON3-MMH pair

In particular, Prandtl number reaches a value of 0.463 under stoichiometric conditions, while viscosity and conductivity reach 0.1 centipoise and 3.531 mcal/cm-K-s, respectively. A comparison in terms of performance using frozen equilibrium is shown in the following:

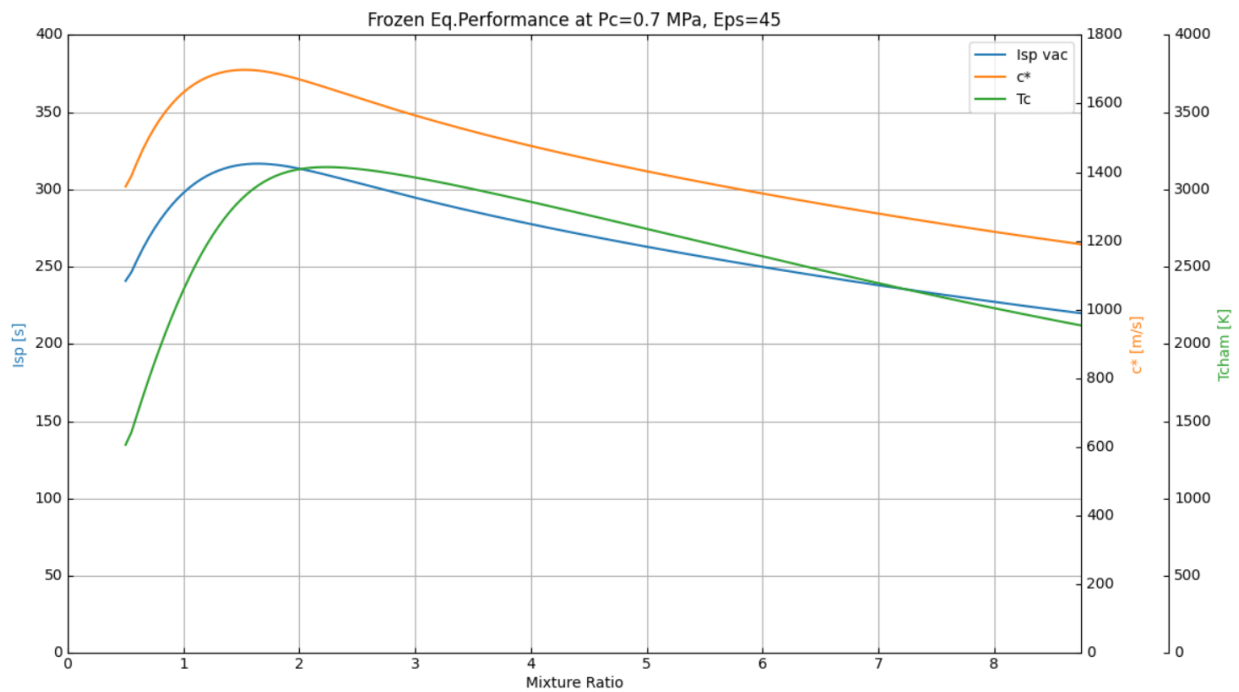


Figure 3.16 Frozen equilibrium performances for the MON3-MMH pair

A reduction in the specific impulse is noted, which reaches a maximum value of 316.654 s for a mixture ratio of 1.65, which represents the new stoichiometric point for a frozen composition of propellant. The characteristic velocity is decreased to a value of 1698.08 m/s. The temperature trend for a frozen composition is analysed in the following graph:

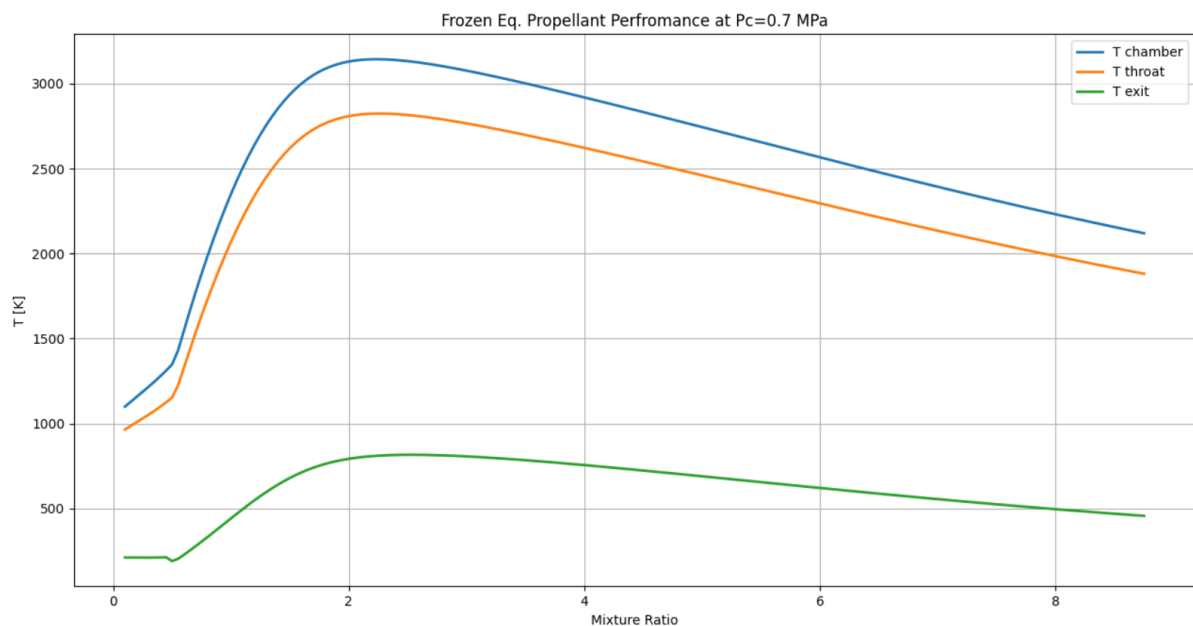


Figure 3.17 Variation of temperatures as a function of mixture ratio

The chamber temperature remains unchanged, while a reduction in the throat and at the nozzle outlet can be noted, with values of 2824.61 K and 816.337 K respectively. The transport properties are shown below:

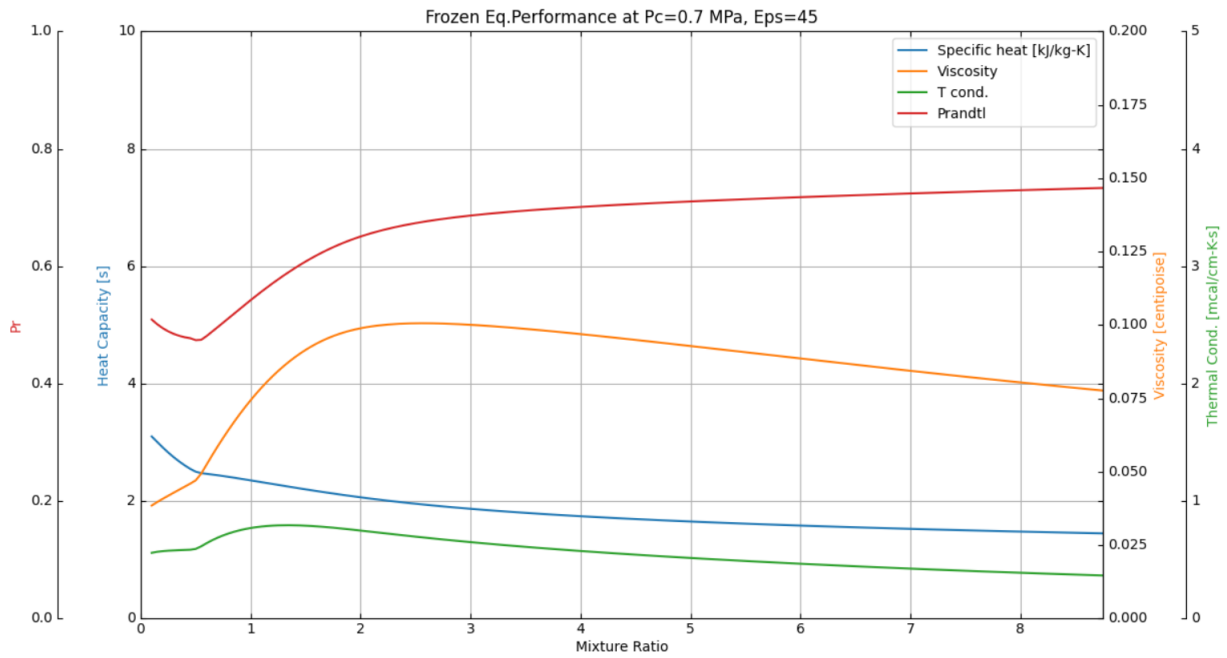


Figure 3.18 Variation of several parameters as a function of mixture ratio

Prandtl number reaches a value of 0.62 under stoichiometric conditions, while viscosity and conductivity reach 0.0946 centipoise and 0.7819 mcal/cm-K-s respectively. For the sake of completeness, P_c and ε_e will be varied in the following sections. As expected, fixing the value of expansion ratio of 45, a change in chamber pressure results in an increase in rocket performance, as shown in the following graphs:

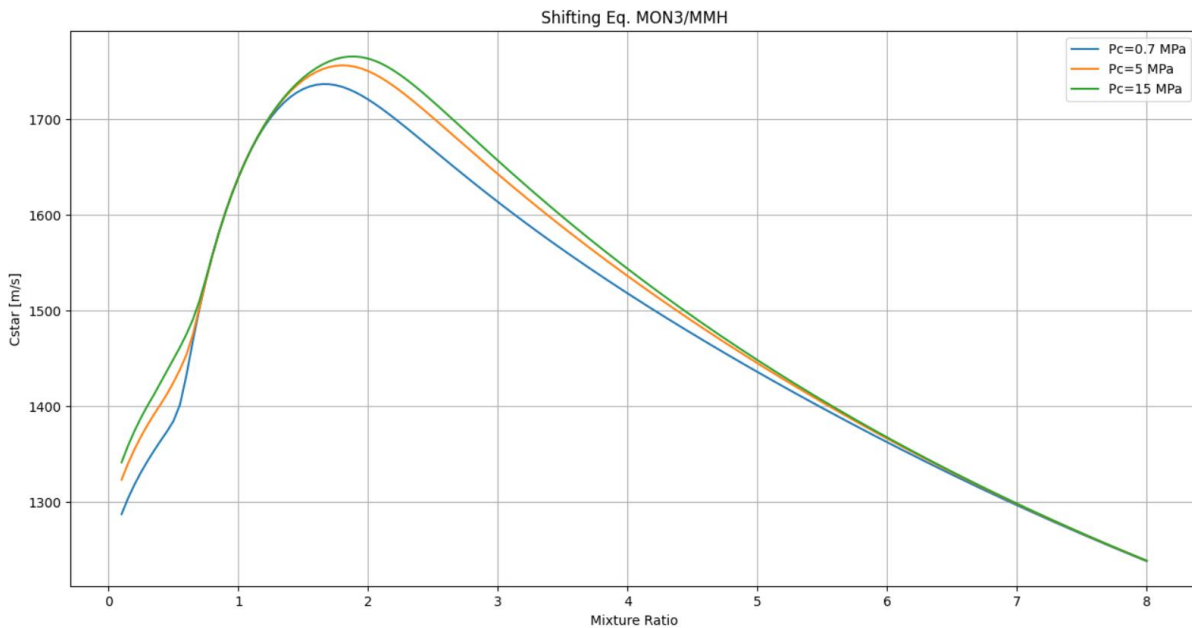


Figure 3.19 Variation of characteristic velocity as a function of mixture ratio and chamber pressure

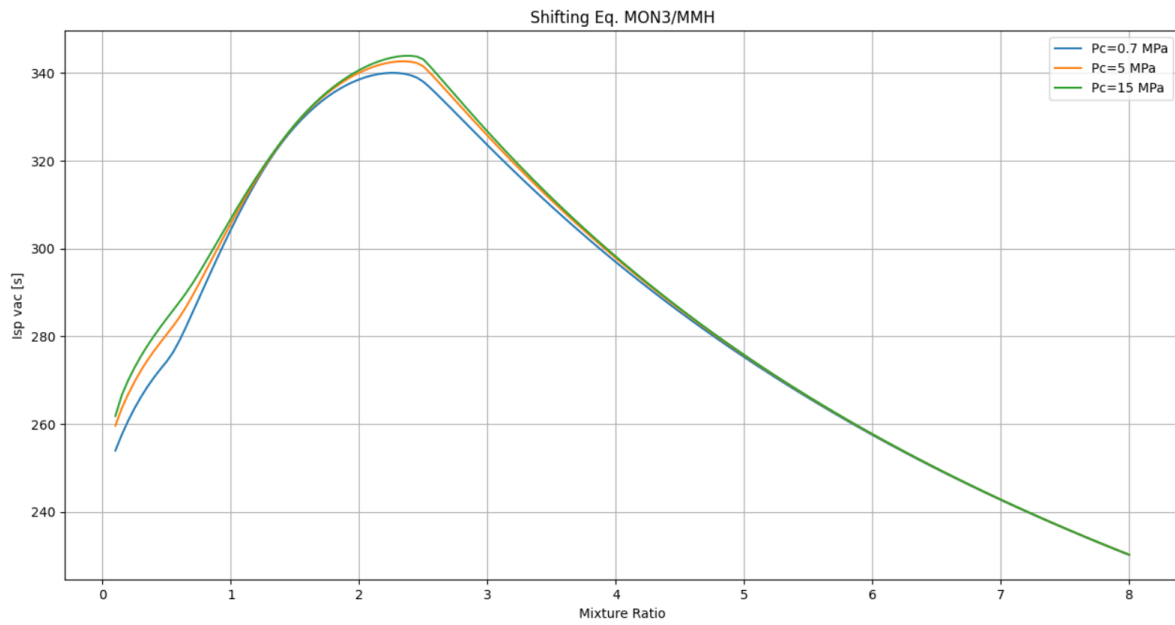


Figure 3.20 Variation of specific impulse as a function of mixture ratio and chamber pressure

The same principle is applied on the specific impulse graph, by fixing P_c and varying ϵ_e :

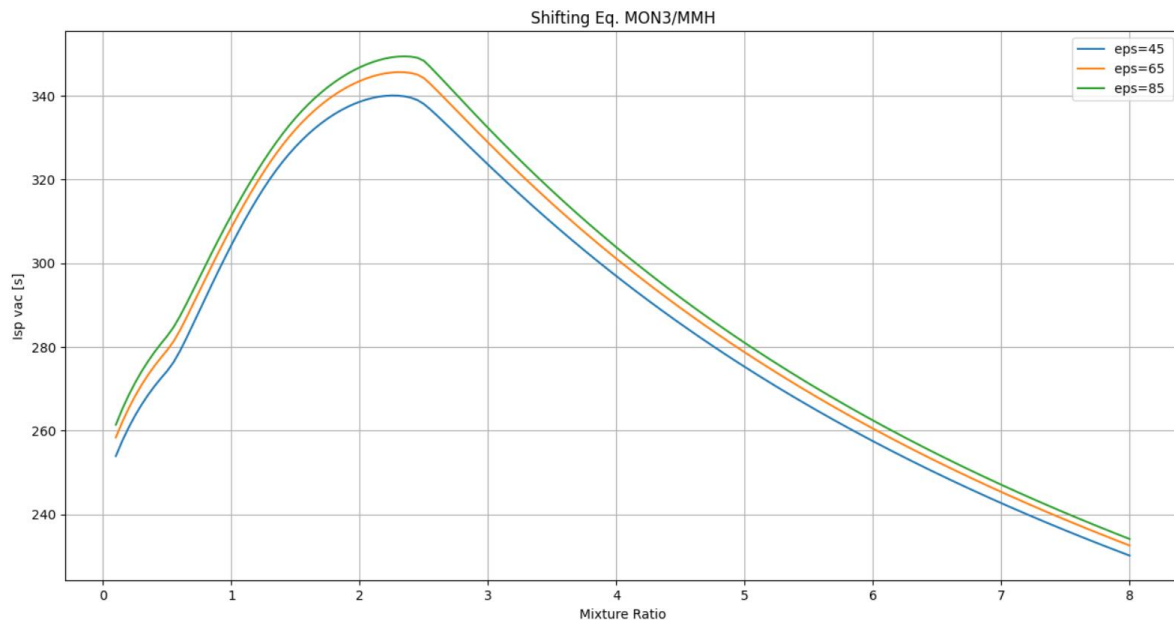


Figure 3.21 Variation of specific impulse as a function of mixture ratio and expansion area ratio

For frozen composition, the same trend is observed with a slight decrease in performance:

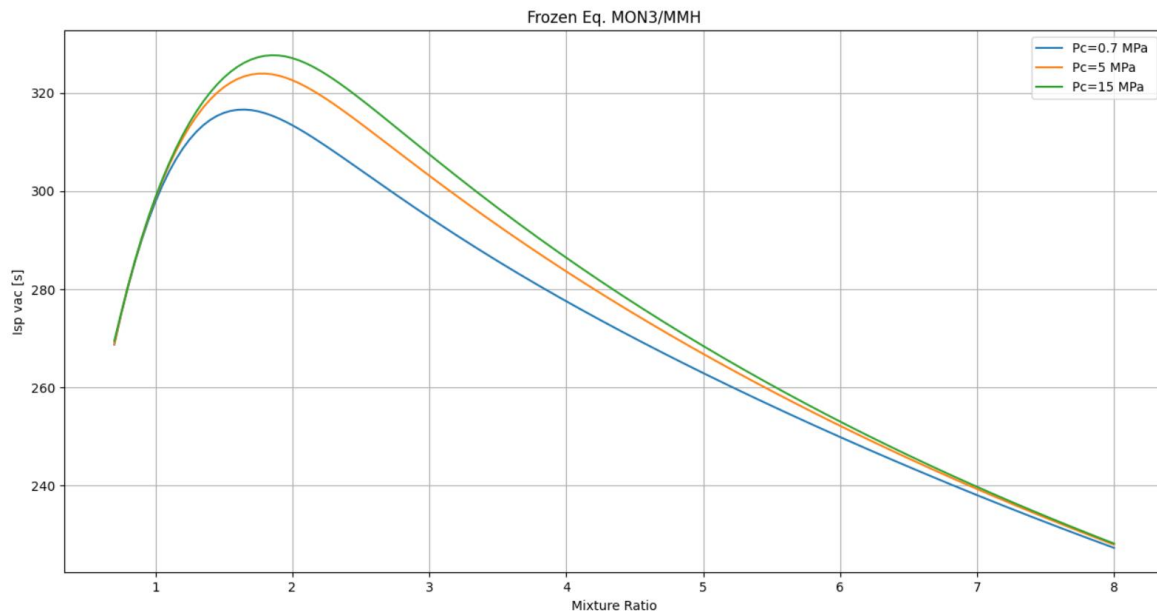


Figure 3.22 Variation of specific impulse as a function of mixture ratio and chamber pressure

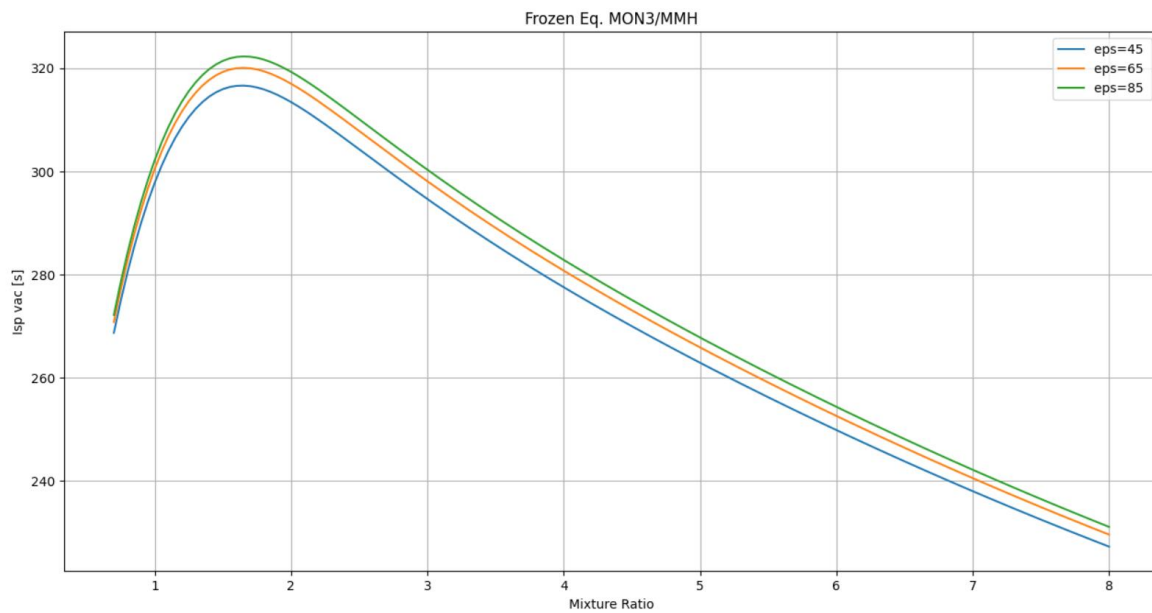


Figure 3.23 Variation of specific impulse as a function of mixture ratio and expansion area ratio

Once the performance of the rocket has been evaluated, it is appropriate to choose a reasonable mixture ratio value. The trend exhibited by upper stage rockets used for other missions that include such an oxidizer/fuel pair is generally based on a mixture ratio of 1.65 due to a lower value of the molecular weight of the propellant compared to stoichiometric conditions. With such value, the following characteristics are tabulated for shifting and frozen equilibrium:

Table 3.4 Shifting equilibrium performance for the MON3-MMH pair

SHIFTING EQUILIBIRUM PERFORMANCE		
Parameter	Value	Unit
MR	1.65	
Pc	0.7	MPa
εe	45	
Isp	332.196	s
c*	1736.39	m/s
T chamber	3028.32	K
T throat	2836.34	K
T exit	970.35	K
Cf	1.876791942	
Cp	4.713	kJ/kg-K
Viscosity	0.000094615	Pa-s
Thermal Conductivity	1.07	W/m K
Pr	0.415	

Table 3.5 Frozen equilibrium performance for the MON3-MMH pair

FROZEN EQUILIBIRUM PERFORMANCE		
Parameter	Value	Unit
MR	1.65	
Pc	0.7	MPa
εe	45	
Isp	316.654	s
c*	1736.39	m/s
T chamber	3028.32	K
T throat	2708.98	K
T exit	727.39	K
Cf	1.788985	
Cp	2.1572	kJ/kg-K
Viscosity	9.46E-05	Pa-s
Thermal Conductivity	0.327	W/m K
Pr	0.62345	

As previously mentioned, a comparison is made with Rocket Propulsion Analysis (RPA) to calculate the chemical equilibrium. This multi-platform tool also allows the generation of the rocket geometry and the evaluation of an appropriate cooling system. Therefore, if the performance calculation for this type of propellant coincides with that of NASA CEA, it can be reasonably assumed that the data obtained are correct and usable within that software for subsequent rocket sizing. RPA v2.3 standard edition [5] requires the following input parameters:

- P_c
- Fuel(s) and its initial temperature/pressure
- Oxidizer(s) and its initial temperature/pressure
- MR
- Exit conditions.
- Selecting frozen/shifting equilibrium.
- Selecting an infinite/finite area combustor.

The thrust chamber sizing also requires:

- Nominal Thrust, mass flow rate or throat diameter.
- Selecting chamber thermal analysis. If not specified, radiation cooling is assumed for whole chamber.

Propellant analysis is performed by imposing shifting equilibrium for the previous input data and analysing the main quantities. It is noted that:

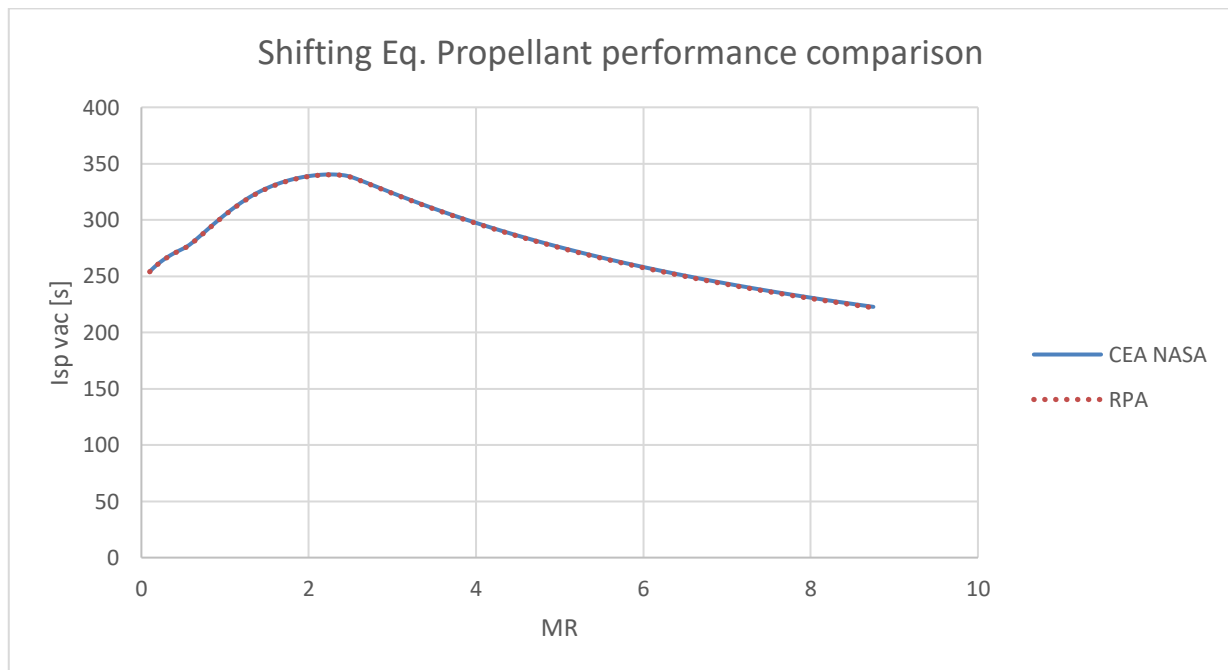


Figure 3.24 Comparison of computed specific impulse with CEA and RPA

for the specific impulse there is a perfect correspondence of values. The characteristic velocity follows the same trend:

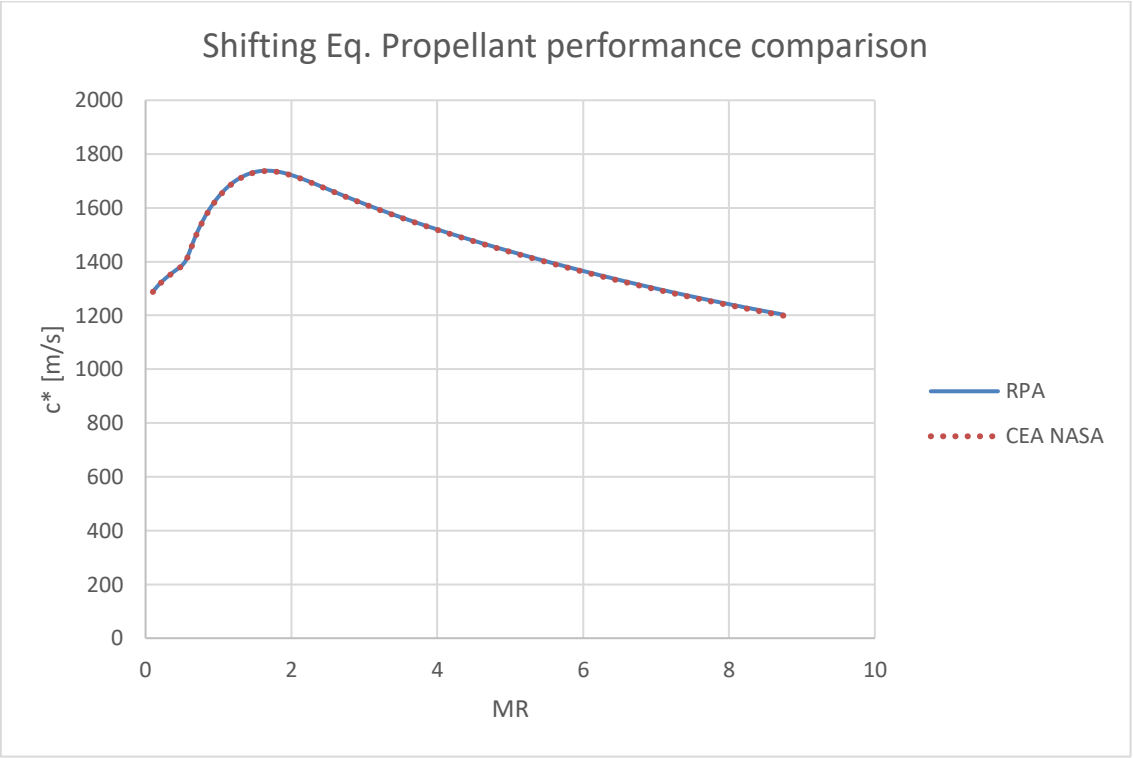


Figure 3.25 Comparison of computed characteristic velocity with CEA and RPA

Thrust coefficient and temperature trends are also shown:

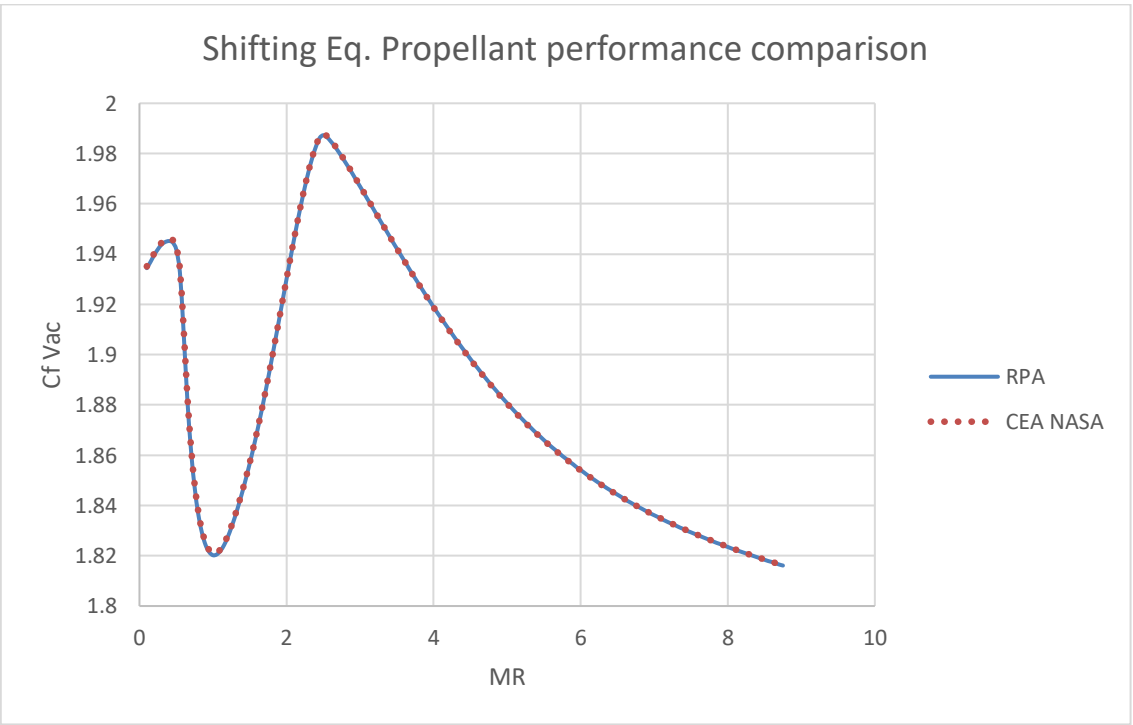


Figure 3.26 Comparison of computed thrust coefficient with CEA and RPA

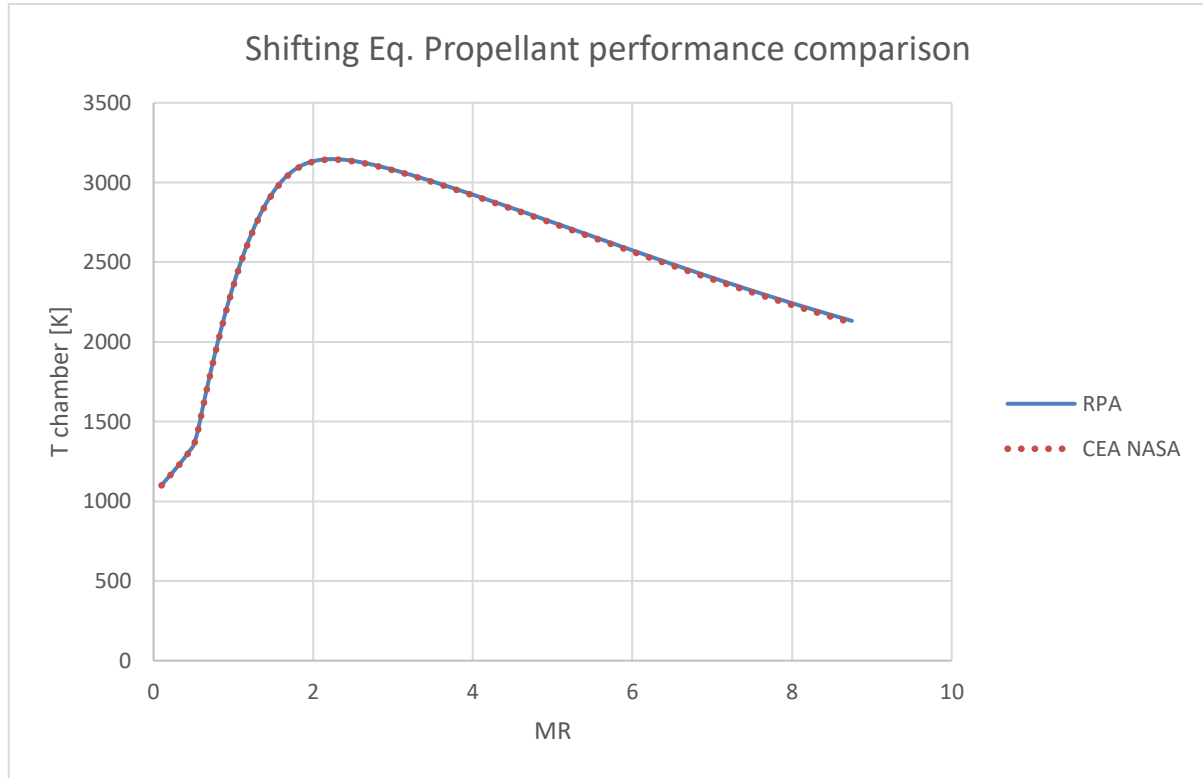


Figure 3.27 Comparison of computed chamber temperature with CEA and RPA

As expected, in accordance with what is stated in RocketCEA documentation, the MON3/MMH pair has an excellent agreement between the two codes, with a data discrepancy only at high values of mixture ratio and expansion ratio. For simplicity of the discussion, the trend of the parameters for a frozen-type chemical equilibrium is not presented, but a perfect match between the data is expected in this case as well. The real performances lie in the middle between the two equilibrium conditions. Therefore, the approach followed is to apply correction factors that account for the losses mentioned in Section 3.2. For specific propulsion systems, where accurately measured data are available, these factors, defined as the ratio between actual and ideal performance, allow for simple prediction of true behaviour of the engine. In the ordinary testing of rocket propulsion systems, the combustion chamber pressure, the propellant mass flow rates, the thrust force, and the throat and exit areas are typically measured. These measurements yield two direct ratios, namely thrust correction factor and discharge factor, defined as:

$$\eta_T = \frac{T_a}{T_i} \quad (3.45)$$

$$\eta_d = \frac{\dot{m}_a}{\dot{m}_i} \quad (3.46)$$

Unlike incompressible flows, in rocket propulsion systems the value of η_d could be larger than 1.0 (up to 1.15) because actual flow rates may exceed the ideal one because of the following reasons, mentioned in [2]:

- Incomplete combustion (a lower combustion temperature), which results in increases of the exhaust gas densities.
- Cooling the walls that reduces boundary layer temperatures and thus the average gas temperature.
- Changes in specific heat ratio and molecular mass in an actual nozzle that affect the flow rate and thus the discharge coefficient.

The c^* efficiency or simply η_* is defined as:

$$\eta_* = \frac{c_a^*}{c_i^*} \quad (3.47)$$

It represents the combined effectiveness of the combustion chamber and injector design and ranges between 0.87 to 1.03. The effective exhaust velocity correction factor, in accordance with equation (3.15), is expressed by the following ratio:

$$\eta_v = \frac{\eta_T}{\eta_d} = \eta_* \eta_{CF} \quad (3.48)$$

and varies between 0.85 to 0.98. η_{CF} or simply thrust coefficient efficiency represents the effectiveness of the nozzle design at its operating conditions and ranges between 0.92 to 1.0. It is defined thermodynamic nozzle efficiency the ratio between actual and ideal enthalpy changes:

$$\eta_n = \frac{\Delta h_a}{\Delta h_i} \simeq \eta_v^2 \quad (3.49)$$

The approximate sign above becomes an equality when optimum expansion is obtained. Finally, under strictly chemically-frozen-composition flow assumptions, the equation (3.27) leads to a useful relation between the ideal and actual chamber stagnation temperature:

$$\frac{T_{c_a}}{T_{c_i}} = \eta_*^2 \quad (3.50)$$

The main correction factors such as η_v , η_* and η_{C_F} are used within RPA to provide an understanding of the actual performance of the rocket. For practical purpose, what is of most interest is to choose an appropriate value of vacuum specific impulse such that it can be used for subsequent propulsion system sizing. In fact, as it will be seen in the following, the I_{sp} is related to the lander mass ratio through the delta-v, another fundamental parameter that expresses the propellant consumption to perform a given manoeuvre.

4. Preliminary mass estimation

4.1 Selection of input parameters

To estimate the masses required for the current mission, it is appropriate to choose the specific impulse consistently with the propellant used, the input parameters such as chamber pressure, expansion ratio and shifting/frozen equilibrium of the mixture, for all the reasons mentioned in Chapter 2. Emphasis will be placed on new generation liquid propellant rockets, whose main characteristics are presented in the following table, in accordance with Ref. [6]:

Table 4.1 Several upper stage engine

Parameter	OMS	Aestus (L7)	Aestus (II)	RS-72	ATE	AJ10-118K
Propellant	MMH/NTO	MMH/NTO	MMH/NTO	MMH/NTO	MMH/NTO	A-50/NTO
Cycle	Pressure-fed	Pressure-fed	Pump-fed	Pump-fed	Pump-fed	Pressure-fed
Thrust vac [kN]	26.7	27.5	46	55.4	20	43.4
Throttling Capability		No	No	No	90-100	-
Thrust Vector Control [deg]	6° pitch	4°	6°	6°	15°	Fixed
Isp [s]	316	320	337.5	338	345	320.5
Overall MR	1.65	2	2.05	2.05	2	1.9
Propellant density [kg/m ³]	1141	1189	1189	1189	1189	
Max. single burn time [s]	1250	1100			3600	
Cumulative life span	15h	100min				
Number of missions	>100	5			1	1
Number of starts/mission	10	20	Multiple	Multiple	>10	3
Engine Mass [kg]	118	110	148	154	74.2/57.9	124.5
T/W ratio	23.3	25.5	31.7	36.6	27.4/35.2	35.5
Overall length [m]	1.956	2.2	2.2	2.286	>1.4	2.7
Maximum Diameter [m]	1.168	1.27			0.38	1.53
Production cost 2000 (M\$)					1.6	>3.5

Although rocket engines show large differences depending on mission profile and staging of the launcher it is possible to separate them in four major classes:

- Booster
- Main stage
- Upper stage
- Satellite propulsion and attitude control

The current mission is oriented on the use of pressure-fed upper stage engines. In the following discussion, the differences between these classes will not be explained because it strays from the primary purpose, which is to evaluate the appropriate specific impulse. In any case, the feed system used will be analysed in detail in Chap.6. As noted in the table above, the I_{sp} ranges between 316 s and 320.5 s, depending on the overall mixture ratio, expansion ratio and chamber pressure. The OMS engine utilizes an expansion ratio of 55 and a chamber pressure of 0.86 MPa, while Aestus respectively of 84 and 1.1 MPa. The AJ10-118K is characterized by a thrust value similar to that of the Apollo LEM of 46.7 KN, an expansion ratio of 65 and a chamber pressure of 0.896 MPa, but with a slightly different propellant combination compared to that used in the current mission. In particular, the fuel used is Aerozine-50, a mixture of 50% Hydrazine and 50% UMDH. In accordance with [1] these results, when in conjunction with NTO, in a slight difference of specific impulse and stoichiometric mixture ratio, as shown in the table below:

Propellant Combination	^a Specific Impulse (s)	Density Impulse (s-gm/cc)	Freezing and Boiling Points (°F), Oxidizer/Fuel (FP)(BP)/(FP)(BP)	Mixture Ratio (O/F)	Combustion Temperature (°F)	Remarks
F ₂ /H ₂	474	241	(-364)(-307)/(-435)(-423)	9.3	6440	Hypergolic
^b O ₂ /H ₂	456	143	(-362)(-298)/(-435)(-423)	4.7	5110	Nonhypergolic
OF ₂ /B ₂ H ₆	430	424	(-371)(-299)/(-265)(-135)	3.5	7010	Hypergolic
OF ₂ /B ₂ H ₆	420	357	(-371)(-299)/(-265)(-135)	2.15	5910	Hypergolic
F ₂ /N ₂ H ₄	419	551	(-364)(-307)/(35)(236)	2.4	7285	Hypergolic
OF ₂ /CH ₄	417	451	(-371)(-299)/(-300)(-260)	5.6	6700	Nonhypergolic
O ₂ /B ₂ H ₆	408	303	(-362)(-298)/(-265)(-135)	2.0	5960	Nonhypergolic
N ₂ H ₄ /B ₂ H ₆	402	254	(35)(236)/(-265)(-135)	1.2	4085	Nonhypergolic
N ₂ O ₄ /B ₂ H ₆	375	340	(11)(70)/(-265)(-135)	2.9	5710	Nonhypergolic
^b N ₂ O ₄ /N ₂ H ₄	341	409	(11)(70)/(35)(236)	1.23	5513	Hypergolic
^b MON/EMHF	341	407	(-23)(29)/(-76)(144)	2.2	5330	Hypergolic
^b MON/MMH	338	401	(-23)(29)/(-63)(189)	2.4	5370	Hypergolic
^b N ₂ O ₄ /50-50	339	408	(11)(70)/(18)(170)	2.1	5175	Hypergolic
^b N ₂ O ₄ /MMH	339	407	(11)(70)/(-63)(189)	2.3	5290	Hypergolic

Figure 4.1 Properties of several propellant combination [1]

Using the following input parameters:

- $\varepsilon_e = 65$
- $P_c = 0.896 \text{ MPa}$

the resulting I_{sp} will have the subsequent trend:

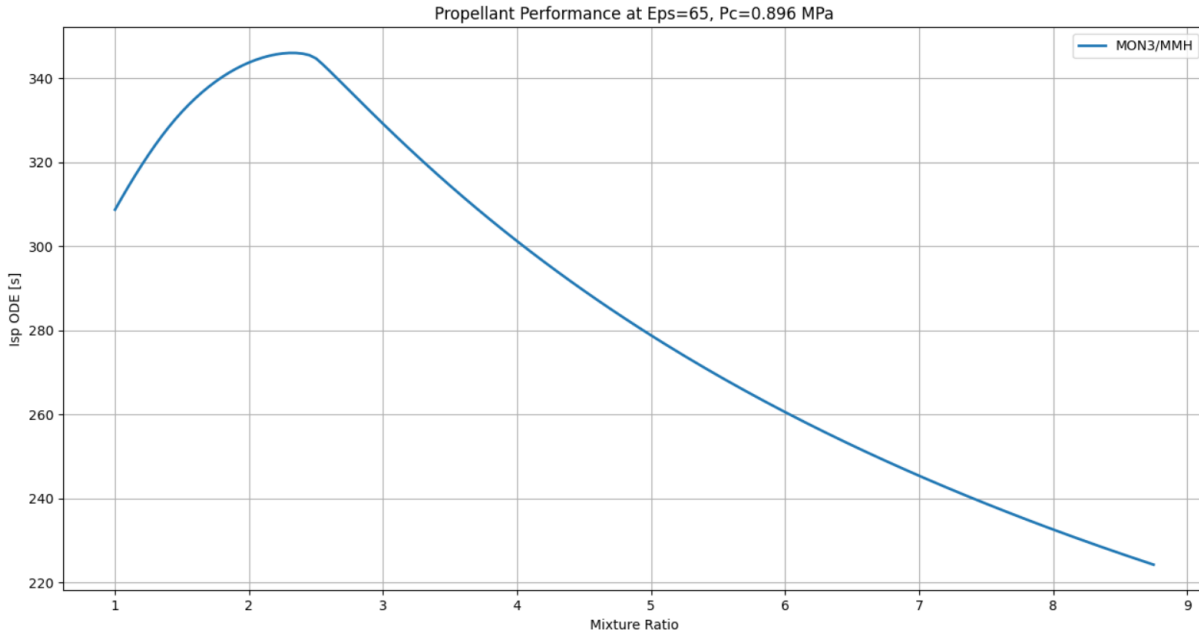


Figure 4.2 Variation of specific impulse as a function of mixture ratio for MON3-MMH pair

Choosing a mixture ratio of 1.65, the specific impulse will be equal to 336.6375 s. In accordance with [1], a well-designed combustion chamber is characterized by a η_* that ranges between 0.97 and 0.98. An average value of 0.975 is chosen to be inserted as first approximation within RPA. An η_{CF} of 0.9776 is estimated by the program based on defined exit condition and for a bell nozzle with 80% of bell. The rocket geometry will be better analysed in Chap.7. The resulting η_v will be 0.9531 and the vacuum specific impulse equal to 321.20 s. Using the following input parameters:

- $\varepsilon_e = 55$
- $P_c = 0.86 \text{ MPa}$

the resulting vacuum specific impulse will be equal to 319.35 s. Because of uncertainties, a reasonable value of 320 s is chosen to be used for subsequent propulsion system sizing. To understand how this parameter is related to the mass of the lander, the rocket equation is considered. Assuming an ideal case where no external forces like gravity and drag are acting on the vehicle, the total momentum of system which includes the vehicle, and the propellant remains constant. However, the momentum of the expelled propellant ejected backward at some relative velocity can be exchanged with the vehicle. In accordance with [7] the following schematic is shown:

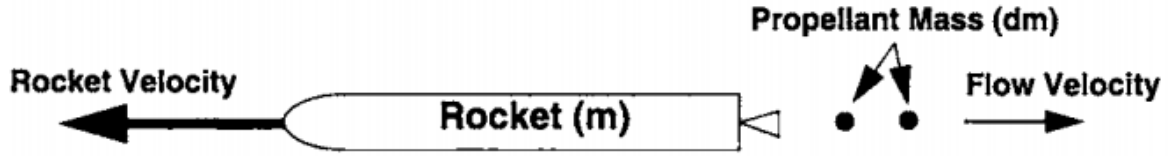


Figure 4.3 Rocket engine schematic Ref. [7]

It is assumed a reference frame which moves at the vehicle's velocity before thrust begins because. As the thrust accelerate it, the vehicle attains a velocity v relative to this frame. If an infinitesimal propellant mass dm is expelled in the opposite direction of vehicle's motion at a relative velocity v_e , the momentum imparted to the vehicle is equal to the propellant's momentum:

$$(m - dm)dv = -dmv_e \quad (4.1)$$

where dv is the infinitesimal change in relative velocity and m is the mass of rocket before propellant expulsion. By neglecting the higher order terms, the equation can be rewritten as follows:

$$dv = -v_e \frac{dm}{m} \quad (4.2)$$

and integrating both members:

$$\int_0^{\Delta V} dv = -v_e \int_{m_i}^{m_f} \frac{dm}{m} \quad (4.3)$$

the classical form of rocket equation, or simply the Tsiolkovsky equation, is obtained:

$$\Delta V = -v_e \ln \left(\frac{m_f}{m_i} \right) \quad (4.4)$$

where m_f is the final or dry vehicle's mass and m_i is the initial or gross one. According to the equation (3.1), in vacuum P_a is zero and the product $A_e P_e$ is negligible with respect to the first term. Therefore, it is possible to confuse the exhaust velocity with effective exhaust velocity. The rocket equation is rewritten as follows:

$$\Delta V = -c \ln \left(\frac{m_f}{m_i} \right) = -I_{sp} g_0 \ln \left(\frac{m_f}{m_i} \right) \quad (4.5)$$

This equation will be further manipulated so that the masses useful for sizing the rocket propulsion system can be calculated.

4.2 Preliminary mass budget

As previously mentioned, the renewed interest in lunar exploration and the goal of establishing a constant human presence on the Moon requires the development of new lunar human landing systems which would deliver the crew from a lunar station, commonly referred to as the Gateway, to the surface of the Moon and back. This Gateway will follow a near-rectilinear halo orbit, or NRHO for a long-term mission planning. To estimate the masses required for a preliminary design of the lander, the Apollo LEM (Lunar Excursion Module) is considered as the best historical data point from which all the assumptions made in the following discussion will be based on. As a first approximation, it is possible to identify the inert mass, or dry mass, as the total mass of the stage excluding the used propellant. This leads to the following schematization:

$$m_{dry} = m_{gross} - m_p \quad (4.6)$$

where m_{gross} is the initial or total mass of the stage before the specific maneuver and m_p is the propellant mass, including Flight Performance Reserve (FRP) and trapped fuel. The latter is calculated using the Tsiolkovsky equation:

$$\frac{m_{gross}}{m_{dry}} = e^{\frac{\Delta V}{I_{sp} * g_0}} \quad (4.7)$$

$$\frac{m_p}{m_{dry}} = e^{\frac{\Delta V}{I_{sp} * g_0}} - 1 \quad (4.8)$$

The velocity change or simply ΔV is the measure of the impulse per unit of spacecraft mass that is needed to perform a maneuver, g_0 is the Earth's gravitational acceleration and I_{sp} is the specific impulse. Since the

mission involves the use of a two-stage architecture, it is necessary to make a further distinction by evaluating the characteristics of the Ascender and Descender separately. For the first stage, it is possible to calculate the propellant mass, from the knowledge of the ΔV and the dry mass, simply by using the above equation:

$$m_{p_{Ascender}} = m_{dry_{Ascender}} * \left(e^{\frac{\Delta V_{Ascender}}{Isp_{Ascender} * g_0}} - 1 \right) \quad (4.9)$$

As the purpose of the Descender is to land on the Moon, the propellant mass needed to perform this manoeuvre is necessarily related to the total mass of the Ascender by the following equation:

$$m_{p_{Descender}} = (m_{gross_{Ascender}} + m_{dry_{Descender}}) * \left(e^{\frac{\Delta V_{Descender}}{Isp_{Descender} * g_0}} - 1 \right) \quad (4.10)$$

To obtain starting values for the preliminary sizing of the current mission, it is essential to evaluate the masses of the LEM because it was the only known architecture tested on the Moon. The data collected on the Apollo mission are listed below:

Table 4.2 Apollo masses from Ref. [8]

Apollo Reference [8]

Parameter	Value	Unit
Crew Compartment	2427	kg
Ascent stage propellant	2372	kg
Ascent engine mass	91	kg
Ascent stage (including crew)	4960	kg
Descent stage propellant	8848	kg
Descent engine mass	158	kg
Landing gear	220	kg
LM total mass	16430	kg
Ascent DV	1874	m/s
Descent ΔV (no margin)	2045	m/s
Descent ΔV (with margin)	2454	m/s
Crew size	2	
Crew Mass (2 crew)	160	kg
Mission Duration	4	days

Sample mass to orbit	95	kg
Payload mass to surface	557	kg
Isp ascent/descent	311	s

Table 4.3 Apollo masses from Ref. [9]

Apollo Reference [9]

Parameter	Ascent Stage	Descent Stage	Total
Structure	628.1	666.6	1294.7
Stabilization and control	35.8	5.8	41.7
Navigation and guidance	155.5	19.9	175.5
Crew provisions	66.2	106.1	172.3
Environmental control	134.7	93.4	228.1
Instrumentation	59.9	3.6	63.5
EPS	334.2	356.9	691.1
Propulsion	212.6	493.8	706.5
Reaction control	109.7	0	109.7
Communications	51.7	0	51.7
Controls and displays	105.2	1.3	106.5
Explosive devices	13.1	11.8	24.9
Landing gear	0	220.4	220.4
Lunar experiment and equipment	184.1	549.6	733.8
Liquid and gases excluding prop	61.7	251.7	313.4
Inert weight	2152.8	2781.4	4934.2
Propellant			
Main	2371.8	8846.7	11218.5
RCS	274.3	0	274.3
Total Weight	4799.1	11628.1	16427.2

Table 4.4 Apollo masses from Ref. [10]

Apollo Reference [10]		
Parameter	Value	Unit
Total weight including crew and propellant	16374.7	kg
LM (dry)	4898.8	kg
Ascent stage dry	2131.9	kg
Descent stage dry	2766.9	kg
Pressurized Volume	6.6	m3
Habitable Volume	4.5	m3
Propellant		
Ascent stage	2358.7	kg
Descent stage	8845.1	kg

Table 4.5 Apollo masses from Ref. [11]

Apollo LMDE Reference [11]		
Parameter	Value	Unit
Propulsion		
Fuel Tank	108.3	kg
Oxidizer Tank	108.3	kg
Pressurization	90.7	kg
Engine assembly	209.5	kg
Other		
Avionics	522.4	kg
Structure (incl. Ascent & Propellant	3508.8	kg
Thermal/Heatshield/Aerobrake	-	
Environmental Control	315.1	kg
Crew (incl. Astronauts)	325.1	kg
Power & Electrical	656.6	kg
Landing/Docking	253.9	kg
ACS	141.04	kg
Contingency (Parking orbit, Tank Failure & Checkout RCS)	21.7	kg
Dry Mass	6262.1	kg

Propellants		
Unusable (MPS)	206.3	kg
Unusable (ACS)	17.6	kg
Vented Propellant	0	kg
Usable (MPS incl. Reserves)	7485.2	kg
Usable (ACS incl. Reserves)	202.2	kg
Total Mass	14173.7	kg

Table 4.6 Apollo masses from Ref. [11]

Apollo LMAE Reference [11]

Parameter	Value	Unit
Propulsion		
Fuel Tank	41.7	kg
Oxidizer Tank	41.7	kg
Pressurization	47.6	kg
Engine assembly	102.4	kg
Other		
Avionics	388.2	kg
Structure (incl.Ascent & Propellant)	525.1	kg
Thermal/Heatshield/Aerobrake	-	
Environmental Control	151.4	kg
Crew (incl. Astronauts)	325.1	Kg
Power & Electrical	351.02	kg
Landing/Docking	0	
ACS	141.04	kg
Contingecy (Parking orbit, Tank Failure & Checkout RCS)	21.7	kg
Dry Mass	2137.4	kg
Propellants		
Unusable (MPS)	58.04	kg
Unusable (ACS)	17.6	kg
Vented Propellant	0	kg
Usable (MPS incl. Reserves)	2114.2	kg
Usable (ACS incl. Reserves)	202.2	kg

Total Mass	4529.7	kg
------------	--------	----

with the relative propellant-to-dry mass ratio:

Table 4.7 Apollo propellant-to-dry mass ratios

Apollo propellant-to-dry mass ratio

Stage	Value	Reference
Ascender	0.91	[8]
Descender	1.16	
Ascender	1.10	[9]
Descender	1.16	
Ascender	1.10	[10]
Descender	1.21	
Ascender	1.1	[11]
Descender	1.26	

It is noted that the propellant mass of both stage is approximately equal to the corresponding dry mass but considering that this will strictly depend on the type of manoeuvre used, the added margins and the ΔV required. The estimated LEM masses are listed below:

Table 4.8 Apollo masses estimation

Apollo mass estimation

Parameter	Value	Unit
ΔV descender	2470	m/s
ΔV ascender	2220	m/s
Isp descender (Ref.SME)	303	s
Isp ascender (Ref.SME)	306	s
(Propellant mass)/(Total mass) ascender	0.5	
(Propellant mass)/(Dry mass) ascender	1.09	
(Propellant mass)/(Total mass) descender	0.56	
(Propellant mass)/(Dry mass) descender	1.29	

DRY ascender	2137.7	kg
Propellant Ascender	2340.8	kg
Total Mass Ascender	4478.5	kg
DRY Descender (Asc not included)	2745	kg
Propellant Descender	9358.4	kg
Total Mass Descender (incl Ascender PS and propellant)	16582.1	kg

4.2.1 Scaling relationship method

In accordance with what was previously said, it is therefore appropriate to use scaling relationships from Refs [11,12] with respect to the Apollo data, to obtain further information on the masses of the mission examined. This implies a schematization of the respective components as follows:

$$m_{cabin} = 1250 + 525n_{crew} \quad (4.11)$$

$$m_{consumables} = 9.4n_{crew}t_{support} + 2.3t_{support} + 4.5N_{EVA\ cycles} \quad (4.12)$$

$$m_{dryAscender}^{PM} = A_a m_{launch} + B_a m_{pAscender} + C_a \quad (4.13)$$

$$m_{dryAscender} = m_{dryAscender}^{PM} + m_{cabin} \quad (4.14)$$

$$m_{grossAscender} = m_{dryAscender} + m_{consumables} + m_{pAscender} \quad (4.15)$$

$$m_{dryDescender} = A_d m_{deorbit} + B_d m_{pDescender} + C_d \quad (4.16)$$

$$m_{grossDescender} = m_{dryDescender} + m_{pDescender} \quad (4.17)$$

where n_{crew} is the number of crew, $t_{support}$ is the total number of days the crew cabin provides life support, $N_{EVA\ cycles}$ is the number of EVA (Extra-Vehicular Activity) cycles to be performed on the surface of the Moon, $m_{consumables}$ are the consumables required for the mission, m_{cabin} is the mass of the crew cabin, $m_{dry\ Ascender}^{PM}$ is the mass of the ascender propulsion module, A_i , B_i , C_i are coefficient defined as follows:

Table 4.9 Propellant input parameter for scaling relationship

Propellant specifications

Type	ρ oxidizer [kg/m3]	ρ fuel [kg/m3]	MR	Isp	Bt	Ct
MMH/NTO	1442	870	1.9	320	0.04253	2454
A-50/NTO (LEM)	1434	897	1.6	311	\	\

$$A_d = A_a = 0.0640 \quad (4.18)$$

$$C_d = C_a = 390 \text{ [kg]} \quad (4.19)$$

$$B_d = 0.0506 \left(\frac{\rho_{Bulk}^{LEM}}{\rho_{Bulk}^{Descender}} \right) \quad (4.20)$$

$$B_a = 0.0506 \left(\frac{\rho_{Bulk}^{LEM}}{\rho_{Bulk}^{Ascender}} \right) \quad (4.21)$$

where ρ_{Bulk} is the bulk or mean density of the propellant, defined as:

$$\rho_{Bulk} = \frac{\rho_{Oxidizer}\rho_{Fuel}(1 + MR)}{MR\rho_{Fuel} + \rho_{Oxidizer}} \quad (4.22)$$

The estimated coefficients are summarized in the following table:

Table 4.10 Scaling relationship coefficient for a specified propellant

Estimated coefficients

Parameter	Value	Unit
A	0.064	
C	390	kg
ρ bulk Ascender	1175.4	kg/m3
ρ bulk Descender	1175.4	kg/m3
ρ bulk LEM	1165.6	kg/m3
Ba	0.050174468	
Bd	0.050174468	

It is also assumed in first approximation to use the same I_{sp} for both stage and a MR greater than the estimated one in Chap. 3, in agreement with Ref. [12]. It is possible to rewrite the Tsiolkovsky equation in a generic form:

$$\frac{m_{f_i}}{m_{0_i}} = e^{-\frac{\Delta V}{I_{sp} * g_0}} = E_i \quad (4.23)$$

$$m_{f_i} - m_{0_i} E_i = 0 \quad (4.24)$$

where m_{f_i} is the final mass at the end of the specific maneuver and m_{0_i} is the initial one. With this schematization it is possible to derive a system of linear equations for the 2-stage architecture. It is assumed that:

- the Lander consist of a two-stage architecture.
- the Descender transfer the payload from a NRHO orbit to a Low Lunar orbit (LLO) and then performs the descent manoeuvre to the lunar surface.
- after the EVA cycles, the Ascender brings the crew and the lunar samples to the LLO leaving the descent stage on the surface.
- the ascent stage returns from the LLO to the Gateway.

In accordance with Ref. [12], the ΔV s required for this type of maneuver are summarized in the following table:

Table 4.11 Velocity change estimation for the listed manoeuvres

ΔV Estimation

Parameter	Value	Unit
ΔV GW-LLO	780	m/s
ΔV LLO-LS	1900	m/s
ΔV LS-LLO	1900	m/s
ΔV LLO-GW	820	m/s

These values are reasonably l to those of the current mission. The resulting system of linear equations is written in the following matrix shape:

$$\begin{bmatrix} 1 - E_a & -E_a & 0 & 0 & 0 \\ A_a - 1 & A_a + B_a & 0 & 0 & 0 \\ 1 - E_{d_1} & 1 - E_{d_1} & 1 - E_{d_1} & -E_{d_1} & 1 - E_{d_1} \\ A_d & A_d & A_d - 1 & B_d & A_d + B_d \\ 1 - E_{d_2} & 1 - E_{d_2} & 1 - E_{d_2} & 0 & -E_{d_2} \end{bmatrix} \begin{bmatrix} m_{dryAscender}^{PM} \\ m_{pAscender} \\ m_{dryDescender} \\ m_{pDescender_1} \\ m_{pDescender_2} \end{bmatrix} = \begin{bmatrix} -(1 - E_a)m_{up} \\ -A_a m_{up} - C_a \\ -(1 - E_{d_1})m_{down} \\ -A_d m_{down} - C_d \\ -(1 - E_{d_2})m_{down} \end{bmatrix} \quad (4.25)$$

where:

$$m_{pDescender} = m_{pDescender_1} + m_{pDescender_2} \quad (4.26)$$

$$E_a = e^{-\frac{\Delta V_{LS-LLO} + \Delta V_{LLO-GW}}{Isp * g_0}} \quad (4.27)$$

$$E_{d_1} = e^{-\frac{\Delta V_{GW-LLO}}{Isp * g_0}} \quad (4.28)$$

$$E_{d_2} = e^{-\frac{\Delta V_{LLO-LS}}{Isp * g_0}} \quad (4.29)$$

$$m_{up} = m_{cabin} + m_{consumables} + m_{PLD_{up}} \quad (4.30)$$

$$m_{down} = m_{cabin} + m_{consumables} + m_{PLD_{down}} \quad (4.31)$$

It is noted that extra components have been added in terms of payload, in addition to m_{cabin} and $m_{consumables}$, which are identified as $m_{PLD_{up}}$ and $m_{PLD_{down}}$. Using the following input data:

Table 4.12 Input data from Ref. [12]

Input data		
Parameter	Value	Unit
n crew	4	
t support	7	days
n EVA	7	cycles
m PLD down	500	kg
m PLD up	250	kg

the corresponding results are obtained:

Table 4.13 Results from Ref.[12]

Estimated results		
Parameter	Value	Unit
m cabin	3350	kg
m consumables	310.8	kg
Lander dry Mass	8477.9	kg
Lander total mass	38883.7	kg

The current mission is characterized by:

Table 4.14 Current mission parameters

Mission parameters		
Parameter	Value	Unit
Isp	320	s
MR	1.65	
Dry mass Descender	5198	kg
Dry mass Ascender	6792	kg
ΔV GW-LLO	780	m/s
ΔV LLO-LS	1983	m/s
ΔV LS-LLO	1901	m/s
ΔV LLO-GW	901	m/s

Table 4.15 Current mission input data

Mission input parameter		
Parameter	Value	Unit
n crew	4	
t support	3.5	days
n EVA	3.5	cycles
m PLD down	500	kg
m PLD up	250	kg

and the corresponding results are:

Table 4.16 Current mission propellant specifications

Propellant specifications		
Parameter	Value	Unit
A	0.064	
C	390	kg
ρ bulk Ascender	1155.3	kg/m ³
ρ bulk Descender	1155.3	kg/m ³
ρ bulk LEM	1165.6	kg/m ³
Ba	0.051049275	
Bd	0.051049275	

Table 4.17 Current mission estimated results

Mass estimation		
Parameter	Value	Unit
m cabin	3350	kg
m consumables	155.4	kg
Lander dry Mass	8650.5	kg
Lander wet mass	40491.8	kg

The output data were shown in relation to the dry and total mass of the lander, defined as:

$$m_{dryLander} = m_{dryAscender} + m_{dryDescender} \quad (4.32)$$

$$m_{grossLander} = m_{grossAscender} + m_{grossDescender} \quad (4.33)$$

since the relationships used previously provide approximate results of the individual quantities. It is therefore more correct to consider the total-to-dry ratios and to compare this proportionality with respect to the Apollo mission, to obtain reasonable results of the current one. A table with the summarized values is shown below:

Table 4.18 Mass-ratio summary for several estimation

Mass ratios summary			
References	Gross to dry ratio	Lander Total [kg]	Lander dry [kg]
Ref. [8]	3.15	16430	5210
Ref. [9]	3.32	16427.21088	4934.2404
Ref. [10]	3.34	16374.685	4898.7976
Ref. [11]	2.26	14173.69615	6262.1315
Ref. [12]	4.58	38883.77579	8477.9593
Scaling Relationships Method	4.68	40491.82456	8650.5458

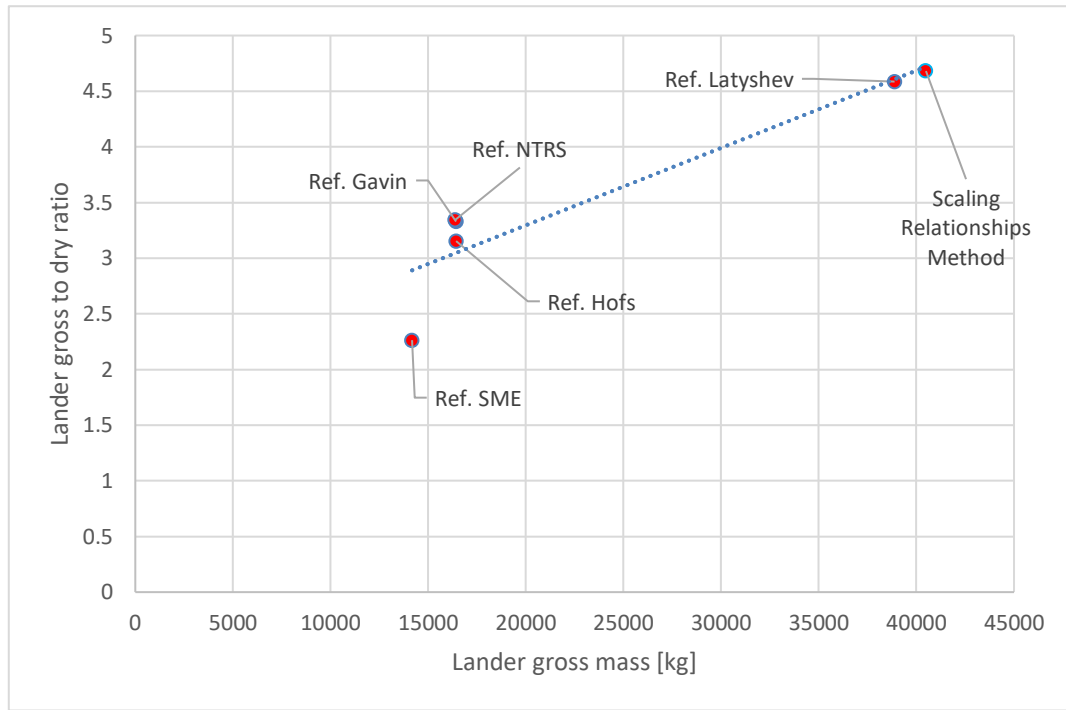


Figure 4.4 Comparison of lander gross-to-dry mass ratio as a function of lander gross mass for several estimations

A weighted average is applied to estimate the total mass of the current lander:

$$x = \frac{\sum_i (Lander_{Grosstodryratio_i} * m_{dryLander_i})}{\sum_i m_{dryLander_i}} = 3.715$$

The dry mass is equal to 11990 kg with a gross mass of approximately 44543 kg. The results are summarized in the following table:

Table 4.19 Current mission preliminary mass breakdown

Summarized results		
Parameter	Value	Unit
Isp Descender	320	s
Isp Ascender	320	S
Propellant to dry ratio Ascender	1.09	
Propellant to dry ratio Descender	1.29	
Ascender dry mass	6792	kg
Ascender Propellant	7427.05	kg
Ascender gross mass	14219.05	kg

Descender dry mass	5198	kg
Propellant Descender	25125.67	kg
Lander gross mass	44542.72	kg

It is noted that the propellant-to-dry ratios are consistent with those of the LEM, so it can be reasonably assumed that they are acceptable starting values for subsequent sizing:

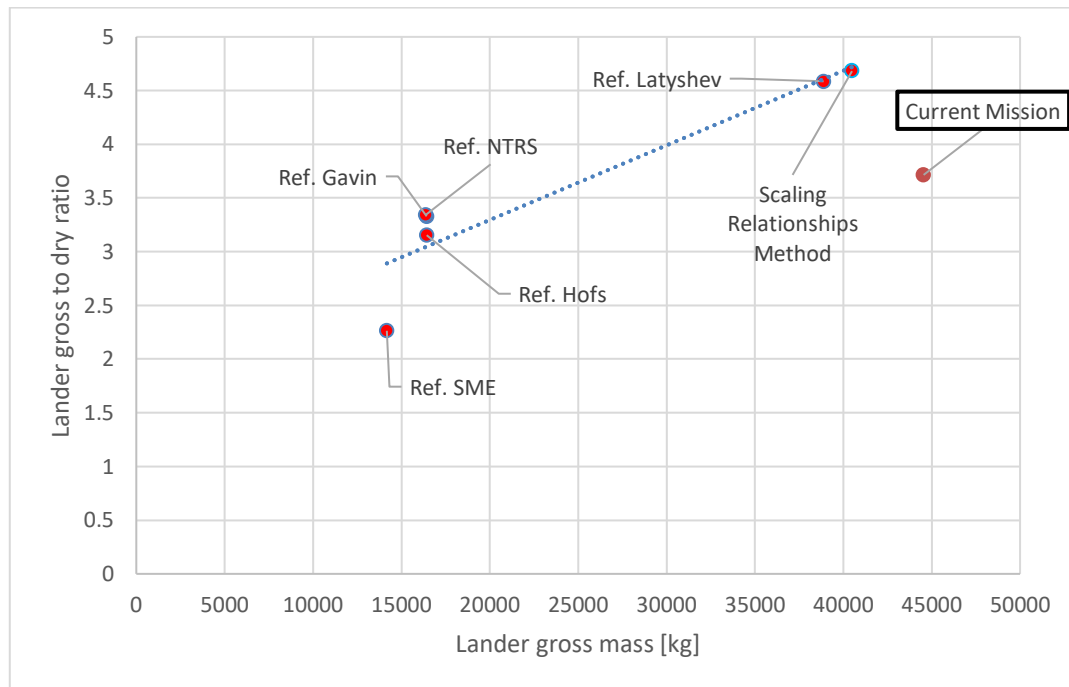


Figure 4.5 Comparison of lander gross-to-dry mass ratio as a function of lander gross mass for several estimations

5. FEED SYSTEM AND TANK SIZING

5.1 High-pressure gas feed system overview

Propellant feed systems have two principal functions:

- To raise the pressure of the propellants
- To supply them at design mass flow rates to one or more thrust chamber

The energy for these functions comes either from high-pressure gas, centrifugal pumps, or a combination of the two. Generally, the selection of a particular feed system and its components is governed by the rocket application, duration, number or type of thrust chambers, past experience, mission and by requirements of simplicity of design, ease of manufacture, low cost, and minimum inert mass. All feed systems, as noted below, consist of piping, a series of valves, provisions for filling and draining the liquid propellant, filters, and control device. Typically, systems with small propellant quantities have gas-pressurized propellant tanks because the weight penalty to design the propellant tanks at high pressure is not significant compared to the complexity of a turbopump feed system. Alternatively, weight considerations require that large systems utilize low-pressure propellant tanks with the propellant pressure increased downstream by pumps. Generally, the main parameters for any feed system's description in liquid rocket engine involve oxidizer and fuel magnitudes together with local pressures. An example of flow diagram, in accordance with Ref. [2] is shown below:

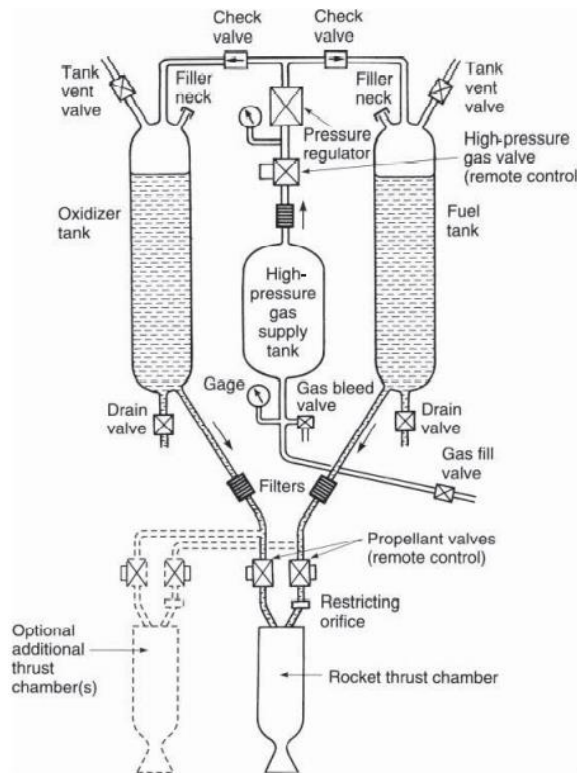


Figure 5.1 Typical high-pressure gas feed system Ref.[2]

The gas flows into two branches, the propellant splits and then is routed into pipes leading to each thrust chamber where the combustion phenomena begin. The highest pressure resides in the high-pressure gas supply tank. From this section, as the fluid flows through the various subsystems such as pipes, valves and regulators, several pressure losses will occur. Therefore, the knowledge of local flow and pressure is of extreme importance for the following reasons:

- This information is used in stress and thermal analysis of related subsystems.
- It is required for engine calibration, so that it operates at the design mixture ratio, chamber pressure and thrust.
- The measurement of actual flows and local pressures during engine ground tests and subsequent comparison with predicted values makes it possible to identify discrepancies between practice and theory.

The current mission is oriented on the use of gas pressure feed system, which will be analysed in detail below. It is not the purpose of the discussion to examine turbopump systems as well. One of the simplest and most reliable methods of pressurizing liquid propellant and force them to flow out of the tanks is to use high-pressure gas. There are two common types of pressurized feed systems. The first uses gas pressure regulator in the gas feed line with the engine operating at essentially constant tank pressure. This is shown in fig [UP] and consists of a high-pressure gas tank, a gas starting valve, a pressure regulator, propellant tanks, propellant valves, and feed lines. Additional components such as filling and draining provisions, check valves,

filters, pressure sensor or gauges are also often incorporated. After all tanks are filled, the high-pressure gas valve is remotely actuated and admits gas through the pressure regulator at a constant pressure to the propellant tanks. Check valves prevent mixing of the oxidizer with fuels, particularly when the unit is not in an upright position. Propellants are fed to the thrust chamber by opening valves. Any variations in this system, such as combination of several valves into one or the elimination and addition of certain components depend on the application. If a unit is to be used and flown repeatedly, such as a space-maneuvre rocket, it may include several additional features such as a thrust-regulating device and a tank level gauge. The second common type of gas pressure feed system is called blow-down feed system. It is shown in the following figure:

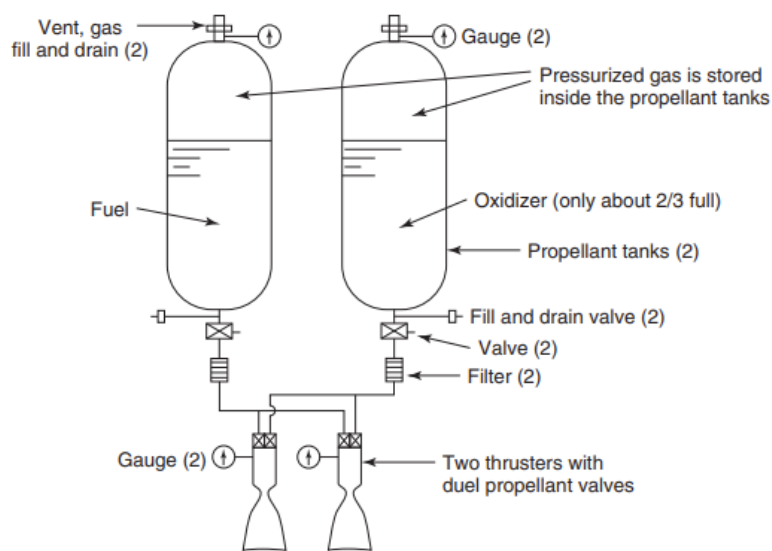


Figure 5.2 Typical blow-down feed system Ref.[2]

Here the propellant tanks are larger because they store not only the propellant but also the pressurizing gas at an initial maximum propellant tank pressure. There is no separate high-pressure gas tank and no pressure regulator. The expansion of the gas already in the tanks provide for the expulsion of the propellants. Blow-down systems can be lighter than a regulated pressure system, but gas temperatures, pressures and the resulting thrust all steadily decrease as propellants are consumed. A comparison of these two common types is shown in the table below:

Type	Regulated Pressure	Blowdown
Pressure/thrust	Stays essentially constant ^a	Decreases as propellant is consumed
Gas storage	In separate high-pressure tanks	Gas is stored inside propellant at tank pressure with large ullage volume (30–60%)
Required components	Needs regulator, filter, gas valves, and gas tank	Larger, heavier propellant tanks
Advantages	Nearly constant-pressure feed gives essentially constant propellant flow and approximately constant thrust, I_s and r	Simpler system. Less gas required. Can be less inert mass.
Disadvantages	Better control of mixture ratio	No high-pressure gas tank
	Slightly more complex	Thrust decreases with burn duration
	Regulator introduces a small pressure drop	Somewhat higher residual propellant due to less accurate mixture ratio control
	Gas stored under high pressure, often for a long time	Thruster must operate and be stable over wide range of thrust values and modest range of mixture ratios
	Requires more pressurizing gas	Propellants stored under pressure; slightly lower I_s toward end of burning time

Figure 5.3 Comparison of high-pressure gas and blow-down feed systems Ref. [2]

There are several sources of pressurizing gas used in tank pressurization systems. The main ones are listed as follows:

- High-pressure inert gases stored at ambient temperature, such as helium, nitrogen, and air.
- Heated high-pressure inert gases, which reduce the amount of required gas and thus the inert mass of the pressurizing system.
- Gases created by chemical reactions using either liquid bipropellants or a monopropellant, or alternatively a solid propellant, all at mixture ratios or compositions that result in “warm gas”.
- Evaporated flow of small portion of cryogenic liquid propellant.
- Direct injection of a small stream of hypergolic fuel into the main oxidizer tank and a small flow of hypergolic oxidizer into the fuel tank.
- Self-pressurization of cryogenic propellants by evaporation.

In order to design or analyse pressurizing system, in accordance with [1], it is necessary to have information on main engine parameters, such as propellant flow, thrust, duration, pulse width, propellant tank volume, percentage of ullage, storage temperature range, propellant and pressurizing gas properties, amount of unavailable residual propellant. A key task in the design is determining the required mass of pressurizing gas, which is influenced by several factor listed below:

- Evaporation of propellant at the interface between the pressurizing gas and the liquid propellant. In particular, the evaporated propellant dilutes the gas and changes its expansion properties, and this change depends essentially on the temperature difference between gas and liquid, sloshing, vapor pressure of propellant, turbulence, and local gas impingement velocities.

- The temperature of those propellant tank walls which form part of exterior vehicle surfaces exposed to the atmosphere are affected by aerodynamic heating, which may vary during flight.
- The solubility of a gas in a liquid is affected by temperature and pressure.
- Condensation of certain gaseous species can dilute the propellant.
- Changes in the gas temperature may take place during operation: compressed gases undergoing an adiabatic expansion can cause noticeable gas cooling.
- Chemical reactions in some species of pressurizing gas with liquid propellant have occurred, some that can generate heat or increase the pressure.
- Turbulence, impingement, and irregular flow distributions of the entering gas will increase the heat transfer between liquid and gas.
- Sloshing can quickly change the gas temperature.
- In many rocket engines, a portion of the pressurizing gas is used for purposes other than tank pressurization, such as actuation of valves or controls. The amount required, once determined, must be added to the total gas mass needed.

It is appropriate to use a simplified method for calculating the mass of pressurizing gas. It is considered a system characterized by compressed gas stored in a separate tank with respect to those of the propellant, at ambient temperature. When tank is insulated and the operation of the rocket engines is relatively short, the expansion process in the gas tank is close to adiabatic. At the other extreme is the isothermal expansion, a considerably slower process requiring longer times for temperature equilibration. It assumed a perfect gas behaviour, no evaporation and dissolution of the liquid propellant, absence of sloshing or vortexing. The initial condition in the gas tank is indicated with subscript 0, the final one with g and the gas in the propellant tank with subscript p. Supposing that the expansion of the pressurizing gas is an isentropic process, the corresponding energy balance is written as follows:

$$e_0 m_0 = e_g m_g + e_p m_p + P_p V_p \quad (5.1)$$

As noted, the initial energy of the gas in its initial state is equal to the sum of the energy of the gas remaining in the gas reservoir, the energy of the gas in propellant tank and the pressure work performed by the gas. V_p is the volume of propellant that has been expelled up to the instant considered. Assuming that the specific heats are constant (calorically perfect gas), the internal energy can be expressed as follows:

$$e = c_v (T - T_{ref}) \quad (5.2)$$

with T_{ref} a reference temperature. Substituting the equation (5.2) in (5.1) yields:

$$m_0 c_v T_0 = m_g c_v T_g + m_p c_v T_p + P_p V_p \quad (5.3)$$

From the perfect equation of state:

$$P = \rho R T = \frac{m}{V} R T \quad (5.4)$$

$$m T = \frac{P V}{R} \quad (5.5)$$

it is possible to rewrite the equation (5.3) as follows:

$$m_0 c_v T_0 = \frac{c_v}{R} P_g V_0 + \frac{c_v}{R} P_p V_p + P_p V_p = \frac{c_v}{R} P_g V_0 + \frac{c_p}{R} P_p V_p \quad (5.6)$$

where:

$$c_p = \frac{\gamma R}{\gamma - 1} \quad (5.7)$$

$$c_v = \frac{R}{\gamma - 1} \quad (5.8)$$

Substituting the equation (5.7) in (5.6) gives:

$$m_0 = \frac{1}{R T_0} (P_g V_0 + \gamma P_p V_p) = m_0 \frac{P_g}{P_0} + \frac{P_p V_p}{R T_0} \gamma = \frac{P_p V_p}{R T_0} \left(\frac{\gamma}{1 - \left(\frac{P_g}{P_0} \right)} \right) \quad (5.9)$$

At the end, when the tank is completely emptied, V_p will be equal to V_{tank} and P_g higher or equal to P_p .

Assuming a condition such that $P_p = P_g$, the equation (5.9) is rewritten as follows:

$$m_0 = \left(\frac{\gamma}{1 - \left(\frac{P_p}{P_0} \right)} \right) \frac{P_p V_{tank}}{RT_0} = \frac{P_p V_{tank}}{\mathcal{R}T_0} \left(\frac{\gamma \mathfrak{M}}{1 - \left(\frac{P_p}{P_0} \right)} \right) \quad (5.10)$$

where γ , R and \mathfrak{M} are referred to the gas. As noted in the above equation, to reduce the mass of pressurizing gas and thus the overall weight of the structure, it will need to have a low γ value. Also, once the P_p is fixed, the mass will decrease as the initial pressure of the gas contained in its reservoir increases. The pressurizing gas, moreover, should not react with the propellant (typically inert is chosen) nor should it be soluble. At this point it is possible to evaluate the sizing of the relative vessels. For simplicity it is indicated as pressure vessel the recipient containing the pressurizing gas and as propellant tank the recipients of oxidizer and fuel.

5.2 Reservoir sizing

5.2.1 Spherical reservoirs

To properly size the reservoirs, it is necessary to choose the type of gas that will pressurize the propellant. The selection falls on the use of Helium because of its low molecular weight, stored at a reference temperature of 293.15 K. This will present the following characteristics:

Table 5.1 Gas properties

Helium properties		
Parameter	Value	Unit
γ	1.66	
R	2077.26	J/kg-K
\mathfrak{M}	4.0026	u
T_0	293.15	K

The P_0 is set at 31 MPa, a value consistent with those found on vessel market. The propellant masses evaluated in the previous chapter are shown below for simplicity:

Table 5.2 Summary of propellant mass required

Stage masses		
Parameter	Value	Unit
Ascender Propellant	7427.05	kg
Descender Propellant	25125.67	kg

Propellants affect tank design mainly by their physical and chemical characteristics. The boiling point or storage temperature of a propellant determines the operating temperature range of the tank assembly. Once these ranges are known, it is possible to evaluate the shape and the arrangement of the reservoirs, which essentially depends on vehicle mission and size. Typically, a spherical geometry offers the smallest surface-to-volume ratio and the smallest shell stress for a given internal pressure, but the combination of several spheres into a certain envelope may cause sizable weight and volume penalty. Thus, both vehicle configuration and tank pressure will determine the shape of propellant tanks. In accordance with [1], vehicles of relatively large length-to-diameter ratios and of limited space envelopes will use cylindrically shaped tanks. Relatively high tank pressures and less-stringent space conditions may favour spherical tanks. The ends or domes of cylindrical tanks can have either spherical or ellipsoidal shapes. The basic cylindrical tank with spherical ends weighs less than one with ellipsoidal ends; but overall, an ellipsoidally-ended tank may weigh less owing to shorter interstage structure. In some designs, the propellant tank ends will have special shapes to accommodate structural loads, minimize residual propellants and utilize available envelope. The required propellant tank volume is the sum of usable volume, trapped-propellant volume, boiled-off volume, and tank ullage (portion of tank not occupied by liquid):

$$V_{tank} = V_{usable} + V_{trapped} + V_{boil} + V_{ullage} \quad (5.11)$$

The current mission is characterized by non-cryogenic storable propellants, therefore V_{boil} is equal to zero. From literature it is possible to consider the sum of $V_{trapped}$ and V_{ullage} as 15% of the usable volume, also considering a growth in weights as mission development progresses. The total volume branches into oxidizer and fuel volume, as noted in the following equations:

$$V_{tank} = V_{oxidizer} + V_{fuel} \quad (5.12)$$

$$V_{oxidizer} = \frac{m_{oxidizer}}{\rho_{oxidizer}} \quad (5.13)$$

$$V_{fuel} = \frac{m_{fuel}}{\rho_{fuel}} \quad (5.14)$$

The calculated values for oxidizer and fuel for the two-stage architecture are listed below:

Table 5.3 Descender tank requirements

Descender propellant specifications		
Parameter	Value	Unit
Oxidizer Mass	15644.2	kg
Fuel Mass	9481.3	kg
Oxidizer Volume	12.5	m3
Fuel Volume	12.5	m3

Table 5.4 Ascender propellant tank requirements

Ascender propellant specifications		
Parameter	Value	Unit
Oxidizer Mass	4624.3	kg
Fuel Mass	2802.6	kg
Oxidizer Volume	3.7	m3
Fuel Volume	3.7	m3

The propellant masses are obtained from eq. (3.11),(3.12) and depend on mixture ratio used. To evaluate the mass of pressuring gas used to expel the propellant from the tanks and direct it into the thrust chamber, it is appropriate to provide a reasonable value of P_p , i.e., the pressures at which the oxidizer and fuel are stored respectively. These may differ from each other due to the different line pressure losses but for simplicity a single equal value will be used for the oxidizer and fuel tanks. Generally, P_p also referred to as regulating pressure, is provided by the following equation, in accordance with [7]:

$$P_p = \Delta P_{feed} + \Delta P_{cool} + \Delta P_{inj} + \Delta P_{dyn} + P_c \quad (5.15)$$

where ΔP_{feed} is the pressure drop in the feed system and ranges between 0.035 and 0.05 Mpa, ΔP_{cool} is the pressure drop in a regenerative cooling system and can vary between 10% and 20% of chamber pressure, ΔP_{inj} is the pressure drop across injector face and should be about 20% or more of the chamber pressure for unthrottled engines. This drop should isolate chamber-pressure oscillations from the feed system, reducing pressure coupling between the combustion chamber and the feed system which could lead to instabilities or oscillations in the flow that are driven by variations in combustion and in performance. The actual pressure drop is also a function of throttling and a complex function of geometry. The rule of thumb for throttled systems is a 30% drop of chamber pressure. Generally, the major source of loss through injector is from an increase in dynamic pressure. Small injector orifices accelerate the flow so the high-speed propellant streams can atomize and vaporize more easily. However, some flow losses are associated with forcing the propellant through the small holes. The current, as it will be seen in the following, is characterized by a throttleable descent engine, unlike the ascent engine that is characterized by fixed thrust. Finally, ΔP_{dyn} is related to the velocity of propellant leaving the tanks. It is expressed by the below relationship:

$$\Delta P_{dyn} = \frac{1}{2} \rho v^2 \quad (5.16)$$

Assuming the total pressure remains constant, the static pressure must drop to allow the increase in dynamic pressure, because as the propellant leaves the tank its velocity goes from zero to required flow velocity with a typical number of 10 m/s. Considering a reasonable chamber pressure value for both stage of 0.9 Mpa as a first approximation, the estimated pressure losses are schematized in the table below:

Table 5.5 Pressure losses through engine

Pressure losses		
Parameter	Value	Unit
ΔP_{feed}	0.05	MPa
ΔP_{cool}	0.18	MPa
$\Delta P_{inj_Descender}$	0.27	MPa
$\Delta P_{inj_Ascender}$	0.18	MPa
$\Delta P_{dyn_Oxidizer}$	0.0717	MPa
ΔP_{dyn_Fuel}	0.0437	MPa

The corresponding regulating pressure for the descent and ascent stage will be greater than or equal to:

Table 5.6 Descender regulating pressure requirements

Descender Regulating Pressure		
Parameter	Value	Unit
P _{P_Oxidizer}	1.292	MPa
P _{P_Fuel}	1.4437	MPa

Table 5.7 Ascender regulating pressure requirements

Ascender Regulating Pressure		
Parameter	Value	Unit
P _{P_Oxidizer}	1.202	MPa
P _{P_Fuel}	1.354	MPa

The substantial differences between pressure losses are related to propellant density, associated with ΔP_{dyn} , and to the type of coolant used in thrust chamber associated with ΔP_{cool} . As mentioned above, although these losses may differ substantially depending on whether the tanks used are of oxidizer or fuel, for simplicity the following can be considered:

$$P_{p_{Descender}} \geq 1.4437 \text{ MPa}$$

$$P_{p_{Ascender}} \geq 1.354 \text{ MPa}$$

The mass of the pressurizing gas is calculated from the eq. (5.10), modifying it as follows:

$$m_0 = \frac{P_p m_p}{\rho_{bulk} \mathcal{R} T_0} \left(\frac{\gamma \mathfrak{M}}{1 - \left(\frac{P_p}{P_0} \right)} \right) \quad (5.17)$$

$$V_{tank} = \frac{m_p}{\rho_{bulk}} \quad (5.18)$$

and the respective volume is:

$$V_0 = \frac{T_0 m_0 \mathcal{R}}{P_0 \mathfrak{M}} \quad (5.19)$$

Because of the uncertainties, a slightly higher regulating pressure is placed than previously highlighted, limiting the growth in pressurizing gas volume and thus the number of vessels required, compared to what the market can provide. The calculated parameters are shown in the following table:

Table 5.8 Descender pressure vessel requirements

Descender: Vessel Parameters		
Parameter	Value	Unit
$P_{p_Descender}$	1.59	MPa
m_0	99.4	kg
V_0	1.9	m ³

Table 5.9 Ascender pressure vessel requirements

Ascender: Vessel Parameters		
Parameter	Value	Unit
$P_{p_Ascender}$	1.65	MPa
m_0	30.5	kg
V_0	0.6	m ³

In the subsequent section, the geometry of the reservoirs will be evaluated. As structural members, the reservoirs must be designed to withstand a combination of the following probable structural loads, in accordance with [1]:

- Internal pressures and their dynamic effects.
- Axial thrust loads and their dynamic effects.
- Bending moments due to vehicle transverse accelerations, wind loads, and shifting of the center of gravity.
- Aerodynamic forces.
- Thrust-vector-control forces.

- Vibration and shock loads.
- Loads produced by mounting arrangement.
- Loads caused by thermal transients and gradient.
- Loads produced during ground handling.

In most vehicle systems, internal reservoir pressure loads, and axial-thrust loads are the principal ones. These and other loads require careful evaluation, including experimental testing. When calculating the allowable operating stress, generally a standardization is frequently imposed, with a minimum of proof test and burst factor of respectively 1.25 and 1.5. If these are not specified, the following safety factors are recommended for vital equipment:

$$\sigma_{allowable} = \frac{\sigma_y}{1.25} \quad (5.20)$$

$$\sigma_{allowable} = \frac{\sigma_u}{1.5} \quad (5.21)$$

where σ_y and σ_u are the yield and tensile strength respectively and depend on the construction material of reservoirs. In recent years, in accordance with [13] the trend is to employ continuous fiber, polymer matrix composites for the development of stiff and strong, but lightweight, structures for commercially available pressure vessels. These can be divided into several classes:

- Type I vessels are purely metallic.
- Type II vessels have a metallic structure, reinforced with circumferential composite layers in their central portion.
- Type III vessels have a metallic liner, reinforced with composite layers over their entire body.
- Type IV vessels have a plastic liner, and their load bearing structure is entirely made of composite layers.
- Type V do not include liner and are wound over a collapsible mandrel; the composite materials carry all loads [14].

Typically, high-performance carbon fiber made of polyacrylonitrile (PAN) are used for these types of vessels, generally manufactured by Toray. The main characteristics of these materials, more simply called Torayca, are presented in the following table, according to the Ref. [15]:

	Product No.	Filaments	Tensile strength (MPa)	Tensile strength (kgf/mm ²)	Modulus of elongation (GPa)	Modulus of elongation (kgf/mm ²)	Elongation (%)	Fineness tex (g/1000m)	Density (g/cm ³)
T300	T300-1000	1000	3530	360	230	23500	1.5	66	1.76
	T300-3000	3000	3530	360	230	23500	1.5	198	1.76
	T300-6000	6000	3530	360	230	23500	1.5	396	1.76
T300B	T300B-1000	1000	3530	360	230	23500	1.5	66	1.76
	T300B-3000	3000	3530	360	230	23500	1.5	198	1.76
	T300B-6000	6000	3530	360	230	23500	1.5	396	1.76
T400HB	T400HB-3000	3000	4410	450	250	25500	1.8	198	1.8
	T400HB-6000	6000	4410	450	250	25500	1.8	396	1.8
T700SC	T700SC-12000	12000	4900	500	230	23500	2.1	800	1.8
	T700SC-24000	24000	4900	500	230	23500	2.1	1650	1.8
T800SC	T800SC-24000	24000	5880	600	294	30000	2	1030	1.8
T800HB	T800HB-6000	6000	5490	560	294	30000	1.9	223	1.81
	T800HB-12000	12000	5490	560	294	30000	1.9	445	1.81
T830HB	T830HB-6000	6000	5340	545	294	30000	1.8	223	1.81
T1000GB	T1000GB-12000	12000	6370	650	294	30000	2.2	485	1.8
T1100GC	T1100GC-12000	12000	7000	715	324	33000	2	505	1.79
	T1100GC-24000	24000	7000	715	324	33000	2	1010	1.79
M35JB	M35JB-6000	6000	4510	460	343	35000	1.3	225	1.75
	M35JB-12000	12000	4700	480	343	35000	1.4	450	1.75
M40JB	M40JB-6000	6000	4400	450	377	38500	1.2	225	1.77
	M40JB-12000	12000	4400	450	377	38500	1.2	450	1.77
M46JB	M46JB-6000	6000	4200	430	436	44500	1	223	1.84
	M46JB-12000	12000	4020	410	436	44500	0.9	445	1.84
M50JB	M50JB-6000	6000	4120	420	475	48500	0.9	216	1.88
M55J	M55J-6000	6000	4020	410	540	55000	0.8	218	1.91
M55JB	M55JB-6000	6000	4020	410	540	55000	0.8	218	1.91
M60JB	M60JB-3000	3000	3820	390	588	60000	0.7	103	1.93
	M60JB-6000	6000	3820	390	588	60000	0.7	206	1.93
M30SC	M30SC-18000	18000	5490	560	294	30000	1.9	760	1.73

Figure 5.4 Torayca composite properties Ref. [15]

Considering propellant tanks, most of the market still offers competitive solutions with materials such as titanium alloys. For the current mission, T800 is chosen as the material for the pressure vessel and Ti-6Al-4V as that for propellant tank, characterized by the following tensile strengths:

Table 5.10 Propellant tank material and tensile strength

Propellant tank		
Parameter	Value	Unit
Material	Ti-6Al-4V	
σ_u	833	MPa

Table 5.11 Pressure vessel material and tensile strength

Pressure vessel		
Parameter	Value	Unit
Material	T800	
σ_u	5490	MPa

The shape of a reservoir can be spherical or cylindrical with domes of different geometry, as mentioned earlier. For spherical reservoir, the following pressure distribution is valid:

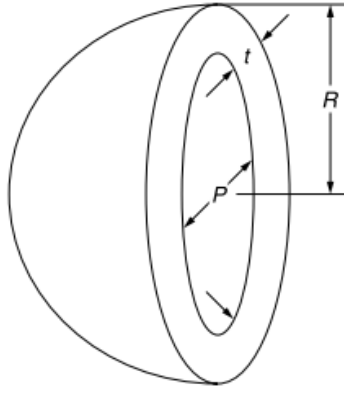


Figure 5.5 Section of spherical tank

$$P_0 \pi r^2 k = 2 \pi r t \sigma_{allowable} \quad (5.22)$$

Referring to fig.5.5, k is the safety factor, r is the radius of the reservoir and t is the thickness. The overwritten equation can be put into system with the next to:

$$m_{reservoir} = N 4 \pi r^2 t \rho \quad (5.23)$$

$$V_0 = N \frac{4}{3} \pi r^3 \quad (5.24)$$

so that the desired t and r can be calculated. The parameter N represents the number of reservoirs to be used for the mission and depends essentially on what the market offers and affects the configuration and weight of the structure. The equation (5.22) can be rewritten as follows:

$$1.5 P_0 \pi r^2 = 2 \pi r t \sigma_u \quad (5.25)$$

Simplifying the terms appropriately:

$$1.5 P_0 r = 2 t \sigma_u$$

the thickness will be:

$$t = \frac{1.5P_0r}{2\sigma_u} \quad (5.26)$$

In accordance with Ref. [16], if the radius-to-thickness ratio is greater than or equal to 10, the reservoirs shell offers no resistance to bending stresses. The wall will be subjected only to direct or hoop and longitudinal stresses, depending on geometry, which are assumed to be uniformly distributed over the thickness. However, any discontinuity along the wall, such an abrupt change in radius of curvature or wall thickness, will introduce discontinuity and bending stresses. At a sufficient distance from the juncture between the reservoir ends and the central shell body, where interaction does not occur, the maximum stress in the reservoir wall due to internal pressure P_0 should be calculated using the membrane stress formula only. For a spherical shell, the radii of curvature are equal in the hoop and longitudinal directions, so the loads due to this pressure is equal to:

$$\sigma_{hoop} = \frac{P_0r}{2t} \quad (5.27)$$

Using the overwritten equations, for spherically shaped vessel is obtained:

Table 5.12 Descender spherical pressure vessel requirements

Descender: Pressure Vessel		
Parameter	Value	Unit
Vessel Mass	44.9	kg
N	9	
Vessel radius	0.3	m
Vessel thickness	0.0015	m
V0 each tank	0.21	m3
r/t	273.9	
σ	3660	MPa
Body Geometry	Sphere	

Table 5.13 Ascender spherical pressure vessel requirements

Ascender: Pressure Vessel		
Parameter	Value	Unit
Vessel Mass	13.8002201	kg
N	3	
Vessel Radius	0.3	m
Vessel thickness	0.0015	mm
V0 each tank	0.2	m ³
r/t	236.1	
σ	3660	MPa
Body Geometry	Sphere	

The same applies to propellant tanks:

Table 5.14 Descender spherical propellant tank requirements

Descender: Propellant Tanks		
Parameter	Value	Unit
Body Geometry	Sphere	
N Oxidizer	6	
N Fuel	6	
V0 Oxidizer each tank	2.09	m ³
V0 Fuel each tank	2.09	m ³
Oxidizer Tank radius	0.79	m
Fuel Tank radius	0.79	m
Oxidizer Tank thickness	0.001	m
Fuel Tank thickness	0.001	m
Oxidizer Tank Mass	238.6	kg
Fuel Tank Mass	237.3	kg
σ	555.3	MPa

Table 5.15 Ascender spherical propellant tank requirements

Ascender: Propellant Tanks

Parameter	Value	Unit
Body Geometry	Sphere	
N Oxidizer	3	
N Fuel	3	
V0 Oxidizer each tank	1.2	m ³
V0 Fuel each tank	1.2	m ³
Oxidizer Tank radius	0.6	m
Fuel Tank radius	0.6	m
Oxidizer Tank thickness	0.0009	m
Fuel Tank thickness	0.0009	m
Oxidizer Tank Mass	73.2	kg
Fuel Tank Mass	72.8	kg
σ	555.3	MPa

5.2.2 Cylindrical reservoirs

For a cylindrical shell body subjected to P_0 , the following schematic is considered:

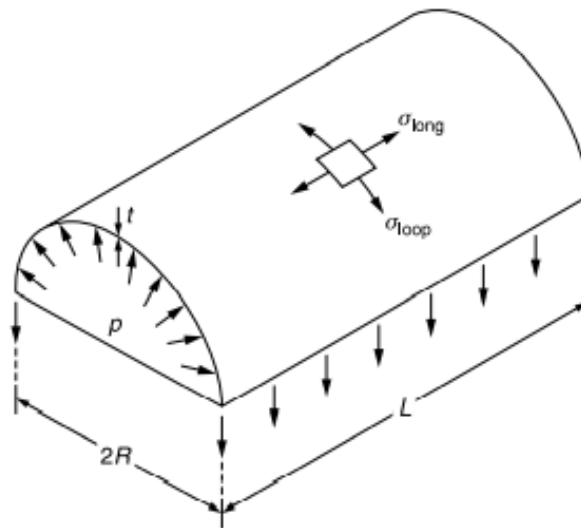


Figure 5.6 Section of cylindrical tank

$$P_0 L 2r = 2\sigma_{allowable} t L k \quad (5.28)$$

$$m_{reservoir} = N 2\pi r L t \rho \quad (5.29)$$

$$V_0 = N\pi r^2 L \quad (5.30)$$

where L is the length of cylinder. The equation (5.28) can be rewritten as follows:

$$P_0 r = 1.5\sigma_u t$$

the thickness is:

$$t = \frac{1.5P_0 r}{\sigma_u} \quad (5.31)$$

The shell will be, as in the case of the sphere, long and thin so that the occurring stresses will be uniformly distributed along the thickness. Considering equilibrium across the cut section in fig. 5.6, the following equation is valid:

$$P_0 L 2r = 2\sigma_{hoop} t L \quad (5.32)$$

which gives:

$$\sigma_{hoop} = \frac{P_0 r}{t} \quad (5.33)$$

Considering a cross-section of the shell perpendicular to its axis, it is obtained that:

$$P_0 \pi r^2 = 2\pi r t \sigma_{long} \quad (5.34)$$

which gives:

$$\sigma_{long} = \frac{P_0 r}{2t} \quad (5.35)$$

The domes can be of different geometries, as shown in the following figure:

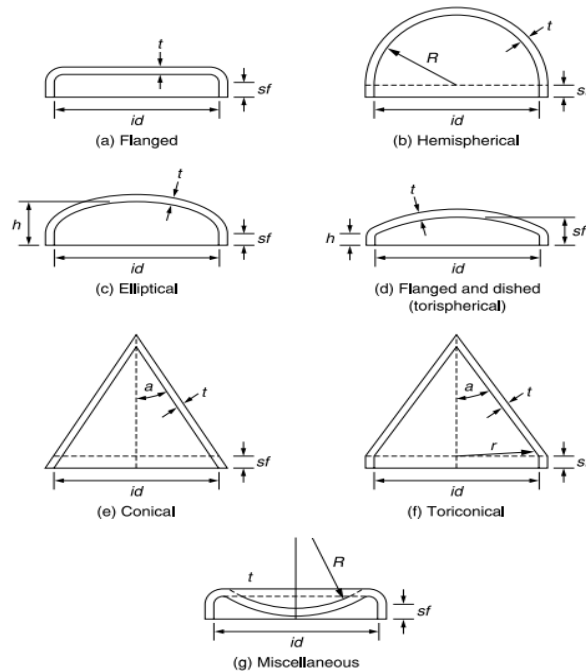


Figure 5.7 Typical tank head shapes

but generally, the market offers mainly hemispherical or elliptical shapes. For the current preliminary design, cylindrical-body and hemispherical-domes reservoirs are considered, with a comparison to those of spherical shapes in terms of weight, radius, and thickness. For a cylindrical-shape with hemispherical-domes reservoirs:

Table 5.16 Descender cylindrical pressure vessel with hemispherical dome requirements

Descender: Pressure Vessel		
Parameter	Value	Unit
Vessel Mass	68.9	kg
N	9	
Vessel radius	0.25	m
Vessel thickness	0.002	m
V0 each tank	0.2	m ³

r/t	118.1	
L cylinder	0.7	m
L tot	1.27	m
σ_{hoop}	3660	MPa
σ_{long}	1830	MPa
Body Geometry	Cylinder	
Domes Geometry	Hemispherical	

Table 5.17 Ascender cylindrical pressure vessel with hemispherical dome requirements

Ascender: Pressure Vessel		
Parameter	Value	Unit
Vessel Mass	21.4	kg
N	3	
Vessel radius	0.25	m
Vessel thickness	0.002	m
V0 each tank	0.2	m3
r/t	118.1	
L cylinder	0.6	m
L tot	1.18	m
σ_{hoop}	3660	MPa
σ_{long}	1830	MPa
Body Geometry	Cylinder	
Domes Geometry	Hemispherical	

Table 5.18 Descender cylindrical propellant tank with hemispherical dome requirements

Descender: Propellant Tanks		
Parameter	Value	Unit
Body Geometry	Cylinder	
Domes Geometry	Hemispherical	
N Fuel	6	

N Oxidizer	6	
V0 Fuel each tank	2.09	m3
V0 Oxidizer each tank	2.09	m3
r	0.6	m
L fuel	1.03	m
L oxidizer	1.03	m
L Fuel tot	2.2	m
L Oxidizer tot	2.2	m
Fuel Tank thickness	0.0017	m
Oxidizer Tank thickness	0.0017	m
Fuel Tank Mass	385.3	kg
Oxidizer Tank Mass	387.1	kg
σ hoop	555.3	MPa
σ long	277.6	MPa

Table 5.19 Ascender cylindrical propellant tank with hemispherical dome requirements

Ascender: Propellant Tanks		
Parameter	Value	Unit
Body Geometry	Cylinder	
Domes Geometry	Hemispherical	
N Fuel	3	
N Oxidizer	3	
V0 Fuel each tank	1.2	m3
V0 Oxidizer each tank	1.2	m3
r	0.6	m
L fuel	0.29	m
L oxidizer	0.29	m
L Fuel tot	1.49	m
L Oxidizer tot	1.49	m
Fuel Tank thickness	0.0017	m
Oxidizer Tank thickness	0.0017	m
Fuel Tank Mass	132.805	kg
Oxidizer Tank Mass	133.353	kg
σ hoop	555.3	MPa

σ long	277.6	MPa
---------------	-------	-----

As stated above, spherical reservoirs offer the lowest surface-to-volume ratio and the smallest shell stress, or for equal stress, the smallest thickness. For the same material and number of tanks, as can be seen from the tables above, spherical reservoirs also have the lowest weight. On the other hand, spherical tanks have a large footprint and are not very suitable when space requirements are stringent. In the next chapter, the preliminary tank sizing will be compared with what the market offers. Once this choice has been made, it is possible to size the architecture of the various propulsion systems.

6. Propulsion system architecture

As mentioned in previous chapters, the current mission is based on the use of storable propellants, specifically on MON3/MMH as oxidizer and fuel pair. The design of tanks for storable liquid propellants uses the same general design practices applied to other propellant tanks, except in the area of compatibility. Most of these will remain stable for long periods if stored in tanks constructed of compatible materials. To minimize propellant decomposition and tank-material corrosion, the surface of tank walls in contact with the propellants must be smooth and clean. In addition, under zero or oscillatory g-loading conditions, the propellant's location in tank becomes uncertain and thus requires a means to prevent gas from being expelled with the propellant. To provide proper propellant orientation within the tanks, positive displacement with moving surfaces or propellant properties such as surface tension are used to continuously confine the liquid to the vicinity of the tank outlet. Therefore, tanks must be equipped with Propellant Management Devices (PMD's). Generally, a positive-expulsion propellant tank consists of an outer structural shell and an inner movable expulsion device, such as a metallic diaphragm or bladder, bellows, and pistons. A surface-tension propellant tank consists of an outer structural shell and an inner compartment that confines a small portion of the propellant at the outlet. The inner compartment may be very simple or extremely complex, depending on the possible orientations of propellant within the tank when flow to the engine is required.

6.1 Space market: pressure vessels and propellant tanks

To choose the types and number of tanks needed for the current mission, it is convenient to analyse the space market and what it has to offer. As will be seen below, the limiting factors for the optimal choice in terms of weight and volume will be related to the maximum capacity of the tank and its main dimensions. It is noted that the descent stage is the binding structure, as it is characterized by the largest volume required for pressurizer and propellant, due to the large masses involved. This implies that an excessive increase in the number of reservoirs leads an increase in overall weight of structure and problems of tank arrangement, while few large capacity reservoirs with spaceflight heritage are difficult to find on space market. Major companies in the space sector were analysed, such as ArianeGroup, Cobham, MT Aerospace, MOOG, VACCO, NuSpace, Northrop Grumman, Infinite Composites (IC), IHI AeroSpace, Omnidea-RTG. Considering pressure vessels, the following brochures are presented below:

COMPOSITE PRESSURE VESSELS Continued													
Part No.	Minimum Capacity		MEOP/ Service Pressure		Burst Safety Factor	Diameter		Length		Maximum Weight		Port Type	Size Code
	ci	liter	psi	bar		in	mm	in	mm	lb	kg		
7234*	1250	19.7	4100	283	3.0	12.92	328.2	15.31	388.9	17.40	7.9	ASS202	-16
6280-3	1299	21.3	3295	227	3.4	8.86	225.0	29.03	737.4	20.01	9.1	ASS202	-16
7106*	1300	21.3	9700	669	2.0	11.50	292.1	22.40	569.0	35.80	16.3	ASS202	-08*
7173*	1378	22.6	6200	428	2.0	10.40	264.2	26.06	661.9	21.80	9.9	ASS202	-10*
6280-5	1400	23.0	3295	227	3.4	8.86	225.0	30.64	778.3	21.02	9.6	ASS202	-16
6193	1471	24.1	1850	128	3.4	9.25	235.0	29.00	736.6	17.30	7.9	ASS202	-08
6220	1500	24.6	1850	128	3.4	8.98	228.1	31.30	795.0	17.40	7.9	ASS202	-08
6283	1624	26.6	3295	227	3.4	9.59	243.6	30.42	772.7	24.70	11.2	SCBA ASS202	7/8", -16
6289	1624	26.6	4500	310	3.4	9.84	249.9	30.83	783.1	30.00	13.6	ASS202	-16
6366*	1624	26.6	6000	414	3.4	10.18	258.6	31.05	788.7	41.30	18.8	ASS202	-12
7130*	1728	28.3	6000	414	2.0	10.40	264.2	30.89	784.6	28.00	12.7	ASS202	-10*
6208	1910	31.3	5000	345	3.4	8.40	213.4	48.01	1219.5	40.00	18.2	ASS202	-16
6247	1910	31.3	5000	345	3.4	8.55	217.2	48.20	1224.3	46.00	20.9	ASS202	-16
6364	1910	31.3	6000	414	3.4	8.60	218.4	48.25	1225.6	48.50	22.0	ASS202	-16
7109*	2100	34.4	4100	283	4.0	15.46	392.7	20.17	512.3	48.30	22.0	ASS202	-04/-08*
6184	2640	43.3	3100	214	3.4	9.19	233.4	51.00	1295.4	42.00	19.1	ASS202	-16
7176*	2650	43.4	4600	317	1.5	14.84	376.9	25.57	649.5	23.50	10.7	ASS202	-10*
6295	2756	45.2	1850	128	3.4	10.10	256.5	41.93	1065.0	24.70	11.2	ASS202	-08
8108	2756	45.2	4300	297	3.4	10.57	268.5	42.42	1077.5	41.70	19.0	ASS202	-08
7226	2756	45.2	5500	379	2.6	10.53	267.5	42.41	1077.2	40.48	18.4	ASS202	-16
7189-02*	4300	70.5	3625	250	2.5	10.95	278.1	56.65	1438.9	43.60	19.8	ASS202	-16*
7127*	4770	78.2	3300	228	2.0	18.10	459.7	27.17	690.1	43.00	19.5	ASS202	-06*
7189-03*	4820	79.0	3625	250	2.0	10.83	275.1	62.71	1592.8	40.60	18.5	ASS202	-16*
7189-01*	5900	96.7	3625	250	2.5	10.95	278.1	75.54	1918.7	58.00	26.4	ASS202	-16*
7169*	16350	268.0	1750	121	1.5	35.45	900.4	24.31	617.5	48.75	22.2	Stub Tube	0.25" OD*
7193*	47111	772.3	400	28	2.0	40.00	1016.0	46.30	1176.0	101.50	46.1	Stub Tube	0.25" OD*

Figure 6.1 Cobham composite pressure vessels Ref. [17]

The overwritten table shows the specifications of Cobham carbon composite pressure vessels characterized by the higher reservoirs' capacity. It is noted that, for a P_0 of 31 MPa or 310 bar, the suitable vessel will be the one characterized by 45.2 L or 0.0452 m³. In accordance with tables 5.8 and 5.9, for a total gas volume of 1.953 m³, the following requirements are presented for the descent stage:

Table 6.1 Descender pressure vessel requirements with COBHAM's reservoirs

Descender: Space market pressure vessel		
Parameter	Value	Unit
N Vessels	44	
Industry	COBHAM	
V0	45.2	L
V0 totale	1988.8	L
Vessel Mass	18.4	kg
Total Vessel Mass	809.6	kg
L	1.0772	m
Diameter	0.2675	m
Material	Carbon Composite	

For the ascent stage, with a gas volume of 0.6003 m³, it is obtained:

Table 6.2 Ascender pressure vessel requirements with COBHAM's reservoirs

Ascender: Space market pressure vessel		
Parameter	Value	Unit
N Vessels	14	
Industry	COBHAM	
V0	45.2	L
V0 totale	632.8	L
Vessel Mass	18.4	kg
Total Vessel Mass	257.6	kg
L	1.0772	m
Diameter	0.2675	m
Material	Carbon Composite	

Imposing the Maximum Expected Operating Pressure (MEOP) of 37.9 MPa for which the vessel was designed, as expected in accordance with eq. (5.19), this results in a reduction of the pressurizing gas volume, as shown in the following tables:

Table 6.3 Descender pressure vessel requirements with different MEOP

Descender: Vessel Parameters		
Parameter	Value	Unit
m_0	98.435672	kg
V_0	1.5815905	m ³

Table 6.4 Ascender pressure vessel requirements with different MEOP

Ascender: Vessel Parameters		
Parameter	Value	Unit
m_0	13.66236767	kg
V_0	0.48595718	m ³

This implies:

Table 6.5 Descender pressure vessel requirement with COBHAM's reservoirs and vessel design MEOP

Descender: Space market pressure vessel		
Parameter	Value	Unit
N Vessels	35	
Industry	COBHAM	
V0	45.2	L
V0 totale	1582	L
Vessel Mass	18.4	kg
Total Vessel Mass	644	kg
L	1.0772	m
Diameter	0.2675	m
Material	Carbon Composite	

Table 6.6 Ascender pressure vessel requirement with COBHAM's reservoirs and vessel design MEOP

Ascender: Space market pressure vessel		
Parameter	Value	Unit
N Vessels	11	
Industry	COBHAM	
V0	45.2	L
V0 totale	497.2	L
Vessel Mass	18.4	kg
Total Vessel Mass	202.4	kg
L	1.0772	m
Diameter	0.2675	m
Material	Carbon Composite	

Even with a slight reduction in feed system requirements, the setting of a higher MEOP does not change the fact that this company does not offer a good solution for the current mission due to the high number of pressure vessels. This arrangement would conflict with the lander's space constraints, considering that in addition to these, propellant tanks will also need to be evaluated. The same is valid for IHI AeroSpace, whose pressure vessels reach a maximum of 0.104 m^3 , as shown in the following brochure:

Volume [L]	Size [mm]	Material
16	310 ID Sphere	CFRP/Ti-6Al-4V
17	262 ID x 480 length	CFRP/A6061
57	480 ID Sphere	CFRP/Ti-6Al-4V
104	585 ID Sphere	CFRP/Ti-6Al-4V

Figure 6.2 IHI AeroSpace pressure vessels Ref. [18]

and for Northrop Grumman, whose vessels reach a maximum of 0.087 m³ for a MEOP of 31 MPa. MT Aerospace provides reservoirs that approach the standards desired in preliminary sizing, as shown below:





PVG Family 80-120

High Pressure Tank (HPV) – Helium/Nitrogen – COTS with delta Qual

HERITAGE		Extension of 40-75 litre HeHPV Family
FLUIDS		Helium, Nitrogen
MATERIALS	Shell	Ti-6Al-4V
	Tube	Ti-3Al-2.5V
	Overwrap	Epoxy-based CFRP / T800
MOUNTING INTERFACE		polar
TOTAL VOLUME (unpressurized)	80-120 l	3.967 in ³
TEMPERATURE RANGE	-30 / +60 °C	-22 / +140°F
TANK DRY MASS	23,5 kg	51,81 lbs
DIAMETER (max. pressurized)	432,0 mm	17,01 in
LENGTH (max. pressurized)	? mm	? in
MEOP*	310,0 bar	4.496 psi
PROOF PRESSURE (x 1,25)	387,5 bar	5.620 psi
BURST PRESSURE (x 1,50)	465,0 bar	6.744 psi
BURST PRESSURE TESTED	633,0 bar	9.181 psi

Figure 6.3 MT Aerospace composite pressure vessel Ref. [19]

Using a MEOP of 31 MPa, the requirements for the descent and ascent stage are presented in the following table:

Table 6.7 Descender pressure vessel requirements with MT AeroSpace's reservoirs

Descender: Space market pressure vessel		
Parameter	Value	Unit
N Vessels	17	
Industry	MT Aerospace	
V0	120	L
V0 totale	2040	L
Vessel Mass	23.5	kg

Total Vessel Mass	399.5	kg
L	-	m
Diameter	0.432	m
Material	T800	

Table 6.8 Ascender pressure vessel requirements with MT AeroSpace's reservoirs

Ascender: Space market pressure vessel

Parameter	Value	Unit
N Vessels	6	
Industry	MT Aerospace	
V0	120	L
V0 totale	720	L
Vessel Mass	23.5	kg
Total Vessel Mass	141	kg
L	-	m
Diameter	0.432	m
Material	T800	

Among others, the most suitable pressure vessel for the current mission can be found at Infinite Composites (IC) company. The specifications are listed in the brochure below:


														
Tank Specifications														
	Diameter		Length		Design Pressures			Volume		Weight				
PN	in	mm	in	mm	MEOP (psig)	Proof (psig)	Min Burst (psig)	in. ³	L	lb	kg	Fluids Held	Fiber	Categories
CFZ055050	5.9	151.0	5.7	144.0	4351.0	5438.0	6527.0	85.0	1.4	1.0	0.5	H2O, He, CA, GN2	T-800	High-Pressure
CFZ001008	25.6	650.2	37.3	946.4	500	750	2000	15622	256	58	26.36	H2O, He, LN2, GN2	T-800	Cryogenic
CFZ001015	11.1	281.6	38.4	975.4	4000.0	6000.0	12000.0	2625.0	43.0	31.0	14.1	H2O, He, CA	H2250	High-Pressure
CFZ001017	13.3	338.0	13.4	340.0	5000.0	6250.0	7500.0	1355.0	22.2	10.5	4.8	H2O, K, He, CA	T-800	High-Pressure
CFZ001006	20.0	508.0	61.6	1564.6	5500.0	8250.0	11000.0	14406.0	236.1	135.0	61.4	H2O, GN2, He	T-800	High-Pressure
CFZ002015	10.9	276.9	87.78	2229.6	1,000	1,500	3,000	6,890	112.91	43	19.55	H2O, He, CA, LOX	H2250	Cryogenic
CFZ0240035	2.58	65.6	3.48	88.5	500	750	1,000	7	0.12	0.24	0.11	H2O, He, LN2, GN2	T-800	Cryogenic
CFZ001018	23.1	586.7	60.0	1524.0	4500.0	6750.0	10125.0	19954.8	327.0	185.0	84.1	H2O, CA, CH4	UTS50	High-Pressure
CFZ057471	5.95	151.1	47.62	1209.5	1,000	1,250	1,500	1,153	18.90	7	3.18	H2O, He, NO2	T-800	Low-Pressure
CFZ240001	23.9	607	25.4	645	500	750	1,000	6,713	110.01	24	10.91	H2O, He, LN2	T-800	Cryogenic
CFZ490001	10.5	268	20.9	531	150	300	600	1,664	27.27	2.52	1.15	H2O, CA	H2250	Low-Pressure

Figure 6.4 InfiniteComposite pressure vessels Ref. [20]

The selected high-pressure vessel, compatible with Helium as pressurizing gas, is characterized by the part number CFZ001006 and has a volume of 236 L. Using a MEOP of 31 MPa, the following requirement for the two-stage architecture are presented below:

Table 6.9 Descender pressure vessel requirements with IC's reservoirs

Descender: Space market pressure vessel		
Parameter	Value	Unit
N Vessels	9	
Industry	InfiniteComposite	
V0	236.1	L
V0 totale	2124.9	L
Vessel Mass	61.4	kg
Total Vessel Mass	552.6	kg
L	1.5646	m
Diameter	0.508	m
Material	T800	

Table 6.10 Ascender pressure vessel requirements with IC's reservoirs

Ascender: Space market pressure vessel		
Parameter	Value	Unit
N Vessels	3	
Industry	InfiniteComposite	
V0	236.1	L
V0 totale	708.3	L
Vessel Mass	61.4	kg
Total Vessel Mass	184.2	kg
L	1.5646	m
Diameter	0.508	m
Material	T800	

Imposing a vessel-design MEOP of 37.92 Mpa (or 5500 psig) results in:

Table 6.11 Descender vessel requirements with different MEOP

Descender: Vessel Parameters		
Parameter	Value	Unit
m_0	98.433398	kg
V_0	1.580719	m ³

Table 6.12 Ascender vessel requirements with different MEOP

Ascender: Vessel Parameters		
Parameter	Value	Unit
m_0	13.66203969	kg
V_0	0.48568922	m ³

Table 6.12 Descender pressure vessel requirements with IC's reservoirs and vessel design MEOP

Descender: Space market pressure vessel		
Parameter	Value	Unit
N Vessels	7	
Industry	InfiniteComposite	
V_0	236.1	L
V_0 totale	1652.7	L
Vessel Mass	61.4	kg
Total Vessel Mass	429.8	kg
L	1.5646	m
Diameter	0.508	m
Material	T800	

Table 6.13 Ascender pressure vessel requirements with IC's reservoirs and vessel design MEOP

Ascender: Space market pressure vessel		
Parameter	Value	Unit
N Vessels	3	
Industry	InfiniteComposite	
V_0	236.1	L
V_0 totale	708.3	L

Vessel Mass	61.4	kg
Total Vessel Mass	184.2	kg
L	1.5646	m
Diameter	0.508	m
Material	T800	

It can be observed that with a slight increase in pressure inside the helium vessel there is an overall reduction in the number of reservoirs in the descent stage which implies a reduction in the structure weight. However, a MEOP of 31 MPa is chosen for compatibility with the valve requirements used for individual propulsion systems. At this point, the selection of propellant tanks is made. In accordance with Tabs. [5.3], [5.4], it is necessary to limit also in this case the number of reservoirs and their weight. The main companies offering competitive solution are ArianeGroup and Northrop Grumman with volumes exceeding 2000 L, but NuSpace products will also be analyzed for the ascent stage. First it is considered the descent stage. ArianeGroup's proposed solution is a propellant tank compatible with that used by the current mission, whose specifications are shown below:



Figure 6.5 ArianeGroup propellant tank Ref. [21]

Table 6.14 Descender propellant tank requirements with ArianeGroup's reservoirs

Descender: Space market propellant tank		
Parameter	Value	Unit
N Vessels	12	
Industry	ArianeGroup	
V0	2100	L
V0 totale	25200	L
Vessel Mass	110	kg
Total Vessel Mass	1320	kg
L	2.6516	m
Diameter	1.1458	m
Material	Ti-6Al-4V	

The reservoir shown is compliant with both MMH and MON, therefore in the table above no distinction has been made between oxidizer and fuel. Generally, the tendency is to choose equal tanks to obtain a certain symmetry of the overall structure, but it all depends on the compatibility of the propellant with the tank shell. Northrop Grumman offers a 2310 L oxidizer-compatible tank as solution, with features listed below, according to Ref. [22]:

Part Number	Volume	Length	Mass
80576-2	2309.7 L (140,945 in ³)	2514.6 mm (99.00 in) boss-to-boss	63.9 kg (140.8 lb _m)
80576-1	2151.3 L (131,282 in ³)	2362.2 mm (93.00 in) boss-to-boss	60.6 kg (133.7 lb _m)

a derivative and longer solution of P/N 80507 tank, whose characteristics are presented in the next table:

Parameters	Requirements
Operating Pressure	18.7 bar (271 psig)
Proof Pressure	23.3 bar (338 psig)
Burst Pressure	>28.3 bar (>410 psig)
External Pressure	2.0 – 3.0 psig, Actual Collapse: 2.50 psig
Material of Construction	Shell: Solution Treated and Aged (STA) 6AL-4V Titanium Heads Inlet/Outlet Ports: 6AL-4V titanium tubes PMD: 6AL-4V and CP Titanium
Tank Mount(s)	Mounting skirt consists of 28 equally space mounting tabs
Inside Diameter	Ø1150 mm (Ø 45.29 in) ID
Skirt Interface Dimension	Ø1177 mm (Ø 46.321 in) with 28 equally spaced tabs
Propellant Capacity	Qualified to 1754 kg (3,866 lb _m) NTO for P/N 80507-5
Natural Frequency	64 Hz axial, 39 Hz lateral
Shell Leakage	<1x10 ⁻⁶ std cc/sec He max @ MEOP
Actual Burst Pressure	Tank ruptured @ 34.7 bar (503 psig). Normalized burst pressure @ 28.5 bar (413 psig).

Figure 6.6 Properties of P/N 80507 propellant tank

Employing such a tank, the specifications for the current mission will be:

Table 6.15 Descender oxidizer tank requirements with Northrop Grumman's reservoirs

Descender: Space market propellant tank		
Parameter	Value	Unit
Parameter	Value	
Propellant Compatibility	Oxidizer	
N Vessels	6	
Industry	Northrop Grumman	
V0	2310	L
V0 totale	13860	L
Vessel Mass	63.9	kg
Total Vessel Mass	383.4	kg
L	2.5146	m
Diameter	1.158	m
Material	Ti-6Al-4V	

Table 6.16 Descender fuel tank with ArianeGroup's reservoirs

Descender: Space market propellant tank		
Parameter	Value	Unit
Propellant Compatibility	Fuel	
N Vessels	6	
Industry	ArianeGroup	
V0	2100	L
V0 totale	12600	L
Vessel Mass	110	kg
Total Vessel Mass	660	kg
L	2.6516	m
Diameter	1.1458	m
Material	Ti-6Al-4V	

with a saving in total tank weight of 276.6 kg. Choosing the latter as a suitable option for the mission, the ascent stage is analysed below. The ArianeGroup's solution are listed as follows:

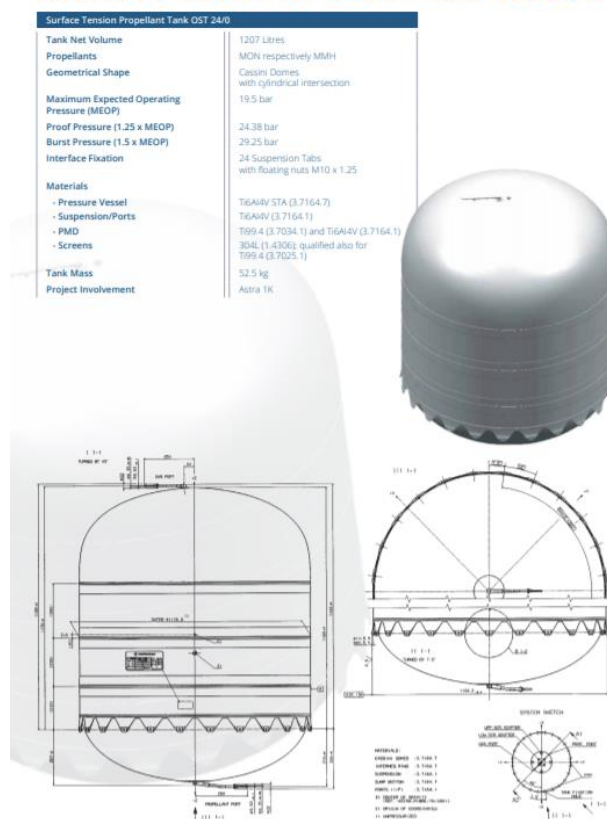


Figure 6.7 ArianeGroup propellant tank

Table 6.17 Ascender propellant tank requirements with ArianeGroup's reservoirs

Ascender: Space market propellant tank		
Parameter	Value	Unit
N Vessels	7	
Industry	ArianeGroup	
V0	1108	L
V0 totale	7756	L
Vessel Mass	49	Kg
Total Vessel Mass	343	kg
L	-	m
Diameter	-	m
Material	Ti-6Al-4V	

SURFACE TENSION PROPELLANT TANK OST 24/0



ArianeGroup - Orbital Propulsion - Robert-Koch-Straße 1 - 82024 Taufkirchen - Germany
 Susana Cortés Borgmeyer - susana.cortes.borgmeyer@ariane-group - Phone: +49 (0)89 6000 29244 - www.space-propulsion.com

Figure 6.8 ArianeGroup propellant tank

Table 6.18 Ascender propellant tank requirements with ArianeGroup's reservoirs

Ascender: Space market propellant tank

Parameter	Value	Unit
N Vessels	7	
Industry	ArianeGroup	
V0	1207	L
V0 totale	8849	L
Vessel Mass	52.5	Kg
Total Vessel Mass	367.5	kg
L	1.456	m
Diameter	1.146	m
Material	Ti-6Al-4V	



[General Brochure](#)

1309 to 1450 Litre Bipropellant Tank	
Volume (net)	1309 to 1450 litres
Propellants	MON, MMH
MEOP	19.5 bar
Proof pressure	24.375 bar (1.25 x MEOP)
Burst pressure	29.25 bar (1.5 x MEOP)
Mass	57 to 61 kg
Pressurant gas	Helium or nitrogen
Geometry	Cassini domes with variable length cylindrical intersection to match propellant capacity.
Interface fixation	24 suspension tabs with floating nuts M10 x 1.25
Materials	
- pressure vessel	Ti6Al4V sta (3.7164.7)
- suspension port	Ti6Al4V sta (3.7164.1)
- PMD	Ti6Al4V (3.7164.1)
- screens	304L (1.4306)
Dimensions	Diameter: 1141 mm Height: 1570 to 1683 mm

Figure 6.9 ArianeGroup propellant tank

Table 6.19 Ascender propellant tank requirements with ArianeGroup's reservoirs

Ascender: Space market propellant tank

Parameter	Value	Unit
N Vessels	6	
Industry	ArianeGroup	

V0	1309	L
V0 totale	7854	L
Vessel Mass	57	Kg
Total Vessel Mass	342	kg
L	1.570	m
Diameter	1.141	m
Material	Ti-6Al-4V	

The latter is the best in terms of overall weight and number of tanks. Although the propellant compatibility was not mentioned within the catalog, NuSpace offers a competitive solution characterized by the following design:


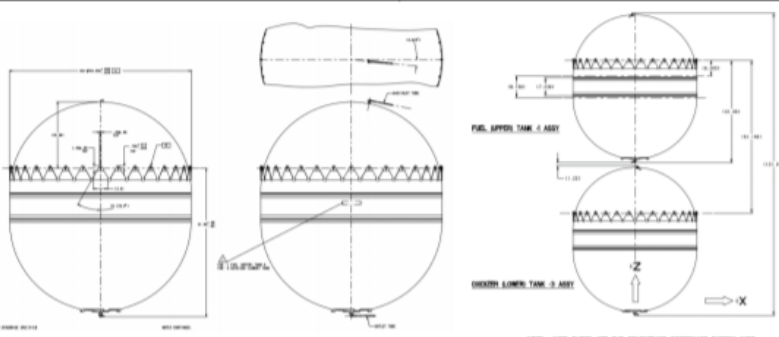
	Part Number:		Size:	
	1260000		49.25 OD x 59.92 Long	
	Tank Type:	Mount Style:	Location:	PMD Device:
	PMD	Tabs	Girth	
	Dual tank design for propellant and oxidizer.			
Applicable Documents	Tank Characteristics:		Tank Characteristics (Metric):	
Interface Control Doc. 1260000_ICD	Total Volume, in ³ :	77.805	Total Volume, L:	1275
	Propellant Volume, in ³ :		Propellant Volume, L:	
	Max Design Weight, lbs:	97.3	Max Design Weight, kg:	44.13
	Minimum Wall Thickness, in:		Minimum Wall Thickness, mm:	
	Operating Pressure, psia:	300	Operating Pressure, bar:	20.68
	Proof Pressure, psia:	375	Proof Pressure, bar:	25.86
	Cryo Proof, psia:	N/A	Cryo Proof, bar:	N/A
	Burst Pressure, psia:	450	Burst Pressure, bar:	31.03
	Notes:		Tube Type:	Size:
	Tanks similar in all aspects but inlet tube orientation.			
Applications Testing:		Qualifications Testing:		
				
11/15/2017		4401 Donald Douglas Dr. Long Beach, CA 90808		Telephone: 562-497-3200

Figure 6.10 NuSpace propellant tank

Table 6.20 Ascender propellant tank requirements with NuSpace's reservoirs Ref. [23]

Ascender: Space market propellant tank		
Parameter	Value	Unit
N Vessels	6	
Industry	NuSpace	
V0	1275	L
V0 totale	7650	L
Vessel Mass	44.13	Kg
Total Vessel Mass	264.78	kg
L	1.5219	m
Diameter	1.251	m
Material	Ti-6Al-4V	

with a saving in total tank weight of 77.22 kg. However, the configuration provided by ArianeGroup with six 1309-litre tanks is chosen for the current mission because of the larger amount of data provided, the perfect compatibility between tank shell and propellant, and the smaller diameter of reservoir which implies a reduced overall space requirement in the ascent stage. After the determination of the number of tanks, the architecture of the various propulsion systems is selected.

6.2 Descender architecture

As previously mentioned, the lander architecture is based on a high-pressure gas feed system. The preliminary estimation in Chapter 4, however, provides untrue values on the mass of propellant required and the volume of usable tanks. It is generally expected that with the mission ΔV 's and dry masses involved a propellant mass of about 16 tons, which would imply an overall reduction in lander requirements. In any case, the following is a conceptual description of what a flowchart associated with a descent engine should look like, dividing the entire system into three subsystems: pressurization system, propellant storage and feed system, engine assembly. The descent pressurization system, as mentioned above, consists of helium pressure vessels stored at 31 MPa and an ambient temperature of 298.15 K. After appropriate ground filling, to open the path from the vessels to propellant tank, an explosive valve is fired. After flowing through a stainless-steel filter used to prevent debris originating at the pyrotechnic valve that may contaminate downstream components, high-pressure gas passes through a relief valve, which is actuated in case of overpressure, and a pressure transducer. Helium then enters parallel arrangement where redundant pressure regulators reduce its pressure. A series redundancy ensures that if one fails, the pressure drop is

achieved by the other present on the same line. Parallel redundancy ensures the appropriate pressurization of propellant tanks in case of failure of the two-series regulators. The regulated gas then flows through a parallel path leading to double redundant check valves, which direct the fluid in a single direction and prevent mixing of the oxidizer with fuel or their vapours in the pressurization system, particularly when the unit is not in an upright position. The descent section propellant supply is contained in fuel and oxidizer tanks and each group of like propellant tanks is manifolded into a common delivery line connected to engine assembly. Pressurizing helium acting on the surface of the propellant, forces the fuel and oxidizer into the delivery lines through PMD that maintains the propellant near the tank outlet in negative or low-g conditions. Fuel and oxidizer then flow through a pressure transducer, trim orifice which provides appropriate propellant pressure at engine inlet, and a filter. The descent engine assembly is characterized by an oxidizer main line and fuel main line. Propellant flows through cavitating venturi flow control valves, which in conjunction with the pintle injector, regulate the engine thrust to achieve the desired performance. Throttling is obtained, as discussed in the next chapter, by a movable venturi pintle driven by an actuator connected in turn with injector sleeve. Propellant then enters the electrically operated shut-off valve, whose parallel redundancy ensures engine shutoff, should one valve fail to close. Vent valve located downstream of the shut-off valves prevent undesired engine ignition caused by propellant residue within the main flow lines. Fuel then flows into cooling system before being directed to injector, while oxidizer is directly injected into the thrust chamber. This prevents rough engine start and overheating problems caused by high temperatures during the combustion of hypergolic fluids.

6.3 Ascender architecture

Similar to the descent stage, the preliminary mass analysis provides estimated values for both propellant and required volumes. The hypothetical flowchart of the ascender is presented below, whose system as mentioned earlier is divided into three subsystems: pressurization system, propellant storage and feed system, engine assembly.

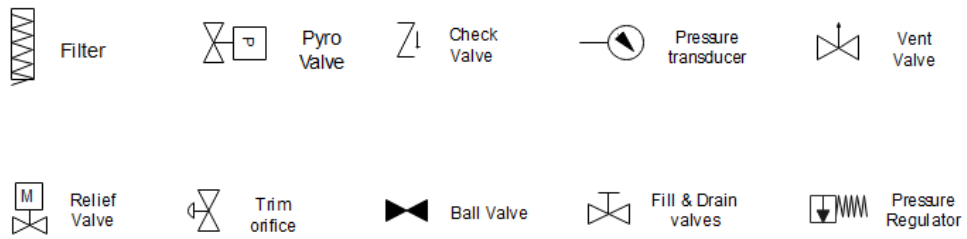


Figure 6.11 Ascender valve legend for current architecture

6.3.1 Ascender pressurization system

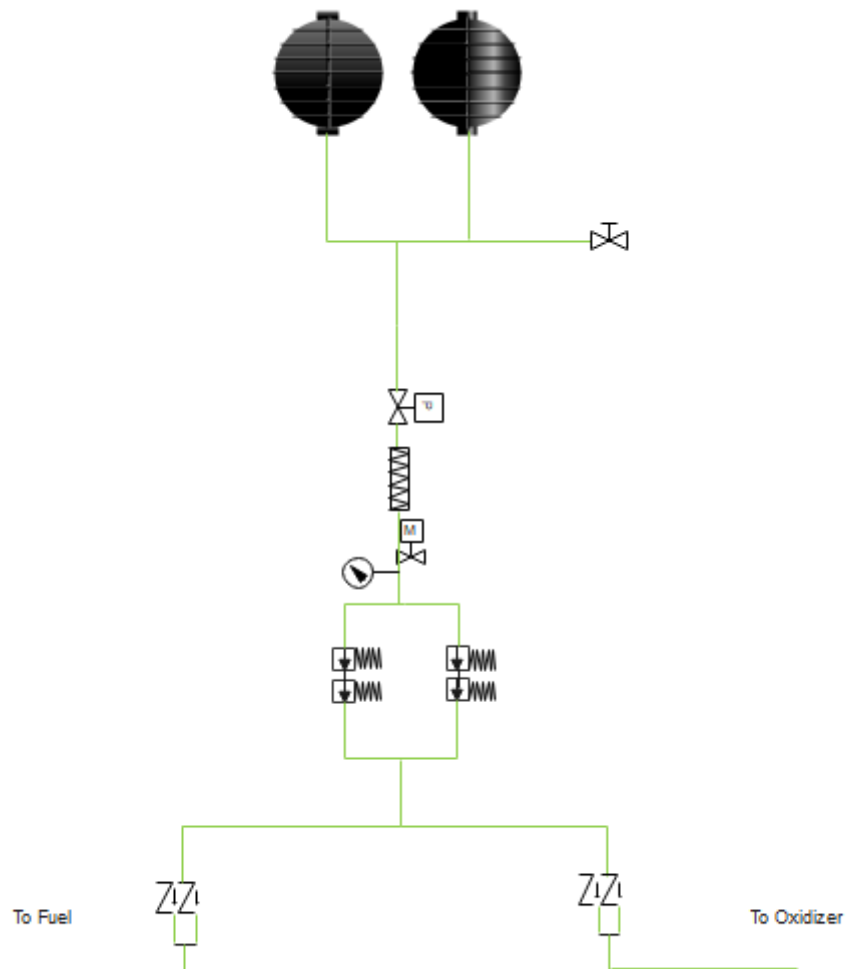


Figure 6.12 Ascender pressurization section

After all tanks are filled, the high-pressure gas flow is driven by a pyrotechnic valve. Helium enters filter to prevent debris that may contaminate downstream components, then flows into relief valve and pressure transducer. The main pressurization line then branches into two parallel lines, in which the high gas pressure is reduced to the regulated pressure by a redundant series and parallel arrangement of regulators. As in the descent architecture, the series redundancy ensures that if one fails the pressure drop is achieved by the other regulator present on the same line, while the parallel redundancy ensures a proper tank pressurization if two regulators in series fail. The regulated helium enters double redundancy check valves, which direct the fluid into propellant storage system and prevent the mixing of oxidizer and fuel in the pressurization system.

6.3.2 Ascender propellant storage and feed system

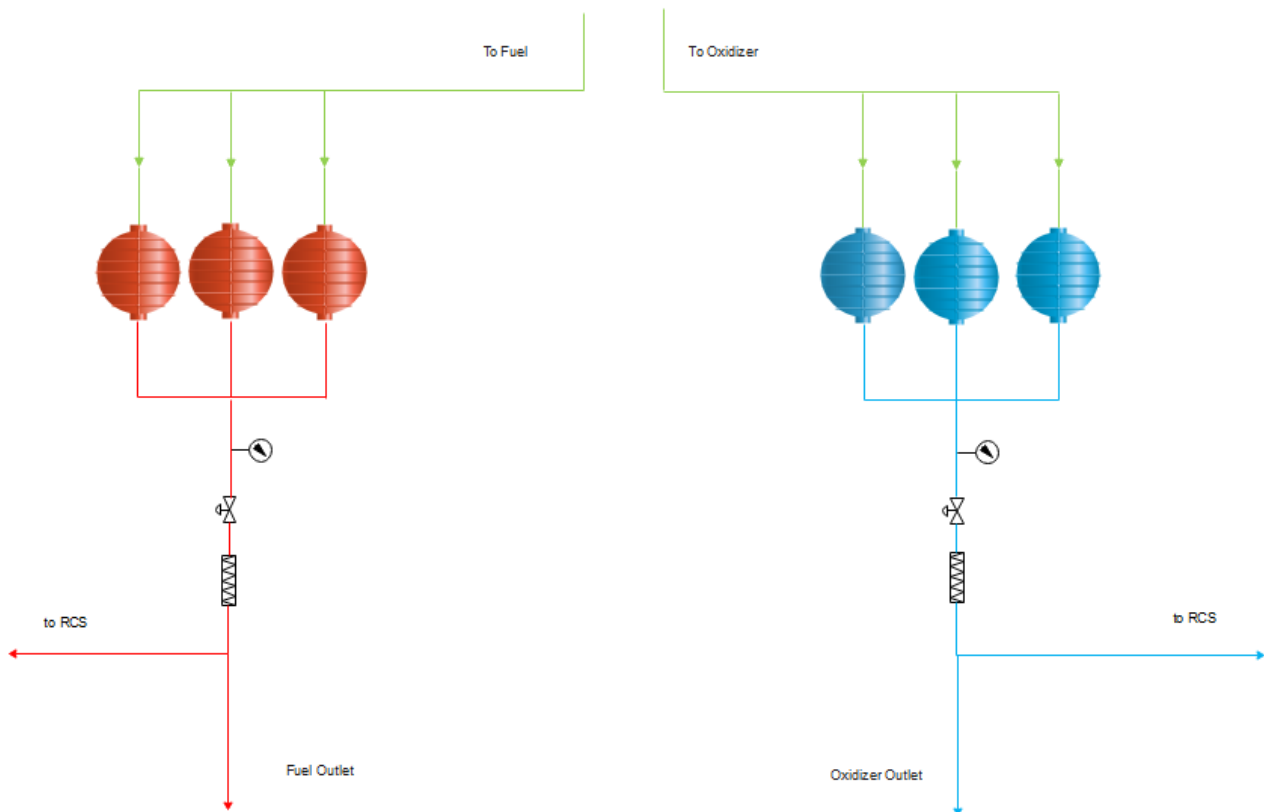


Figure 6.13 Ascender propellant storage and feed system

The ascent section propellant supply is contained in six fuel and oxidizer tanks and each three-group of like propellant tanks is manifolded into a common delivery line connected to engine assembly. Two secondary lines connect the ascent system with the reaction control system (RCS), in this way it is possible to use the available oxidizer and fuel to activate the group of sixteen thrusters to perform the attitude correction

required by the structure. Propellant then flows through trim orifices and filters, to obtain proper pressure at engine inlet and prevent debris that may lead problems in the thrust chamber during the combustion process.

6.3.3 Ascender engine assembly

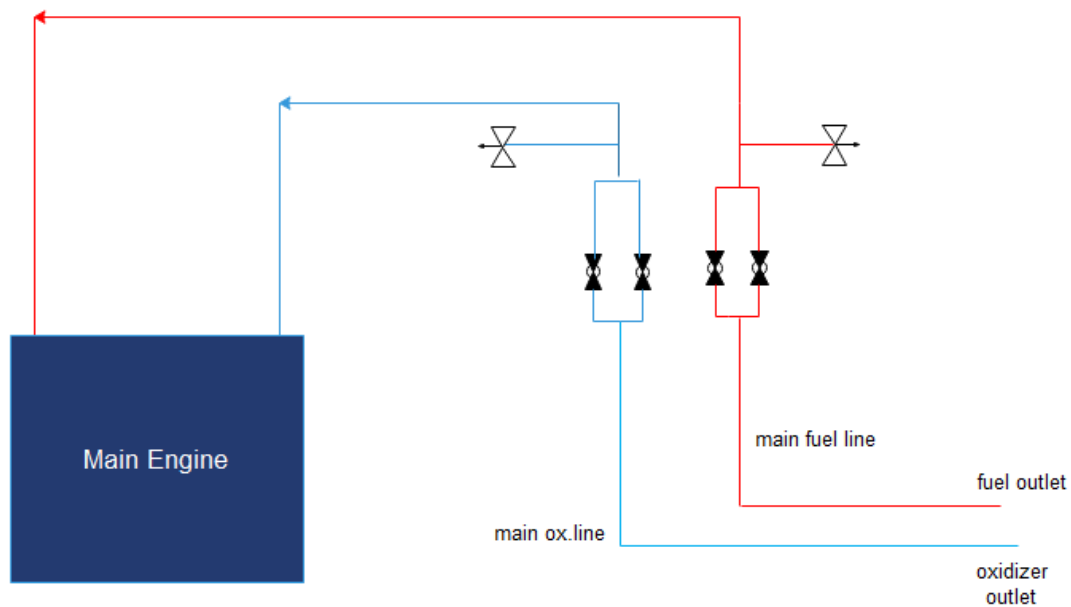


Figure 6.14 Ascender engine assembly

The ascent engine assembly is characterized oxidizer main line and fuel main line. Propellant flows through electrically actuated shut-off valves and then enters thrust chamber. The vent valves prevent undesired engine ignition by venting residual propellant locked inside the main lines to the outside. Fuel flows into the cooling system before being delivered to the injector, while the oxidizer is directly routed to the thrust chamber. The ascent stage is characterized by a fixed-thrust engine, so the injector will not be adjustable but will have a defined geometry.

6.4 Reaction control system (RCS) architecture

The reaction control system [24] provides thrust impulse that stabilize the lander during descent and ascent manoeuvres, controlling attitude and translation movement about and along the three main axes of the structure. It consists in a group of sixteen thrusters clustered in sets of four, mounted on four outriggers equally spaced around the ascent stage and using the same type of hypergolic propellant. In each cluster, two thrusters are mounted parallel to x-axis, facing in opposite directions; the other two are spaced 90° apart, in a plane normal to x-axis and parallel to y-axis and z-axis. In accordance with Apollo LEM, for redundancy the RCS is characterized by two totally independent systems, each consisting of two cluster of four thruster, a pressurization and a propellant storage and feed system, which under normal conditions, function together to provide complete attitude and translation control. The two systems are interconnected by a normally closed cross-feed arrangement that enables the crew to operate all sixteen thrusters for a single propellant supply. In addition, as noted in fig. [6.17], the thrusters can use the ascender propellant during ascent engine thrust, due to interconnection between the two systems. This allows the RCS propellant to be conserved for docking manoeuvres. Again, the division of the overall system into three subsystems is made, as for the descent and ascent stage.

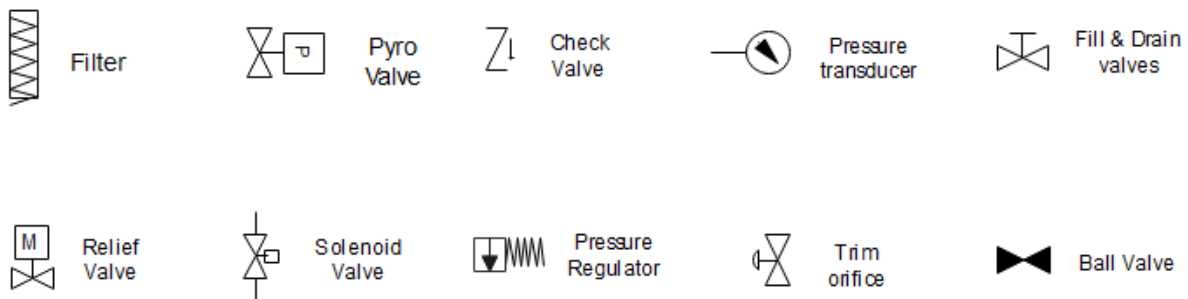


Figure 6.15 RCS valve legend for current architecture

6.4.1 Reaction control system pressurization section

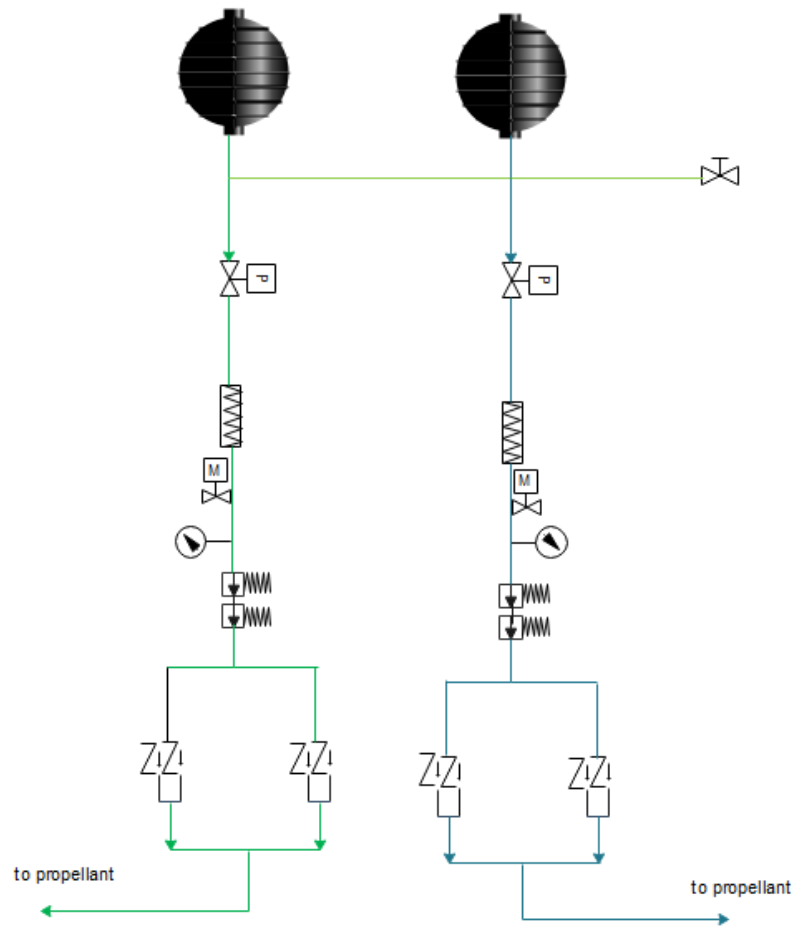


Figure 6.16 RCS pressurization system

The RCS pressurization system is characterized by helium stored at high pressure within two vessels, each corresponding to its own eight thruster system. Once the vessels are filled, pyrotechnic valves are actuated to allow gas to flow into the main flow lines. Helium then enters filters, relief valves and pressure transducers, before being regulated by a series of pressure regulators. The main flow lines branch-off into two parallel paths where redundant check valves are located. Regulated gas finally is directed to the propellant tanks.

6.4.2 Reaction control system propellant storage and feed system

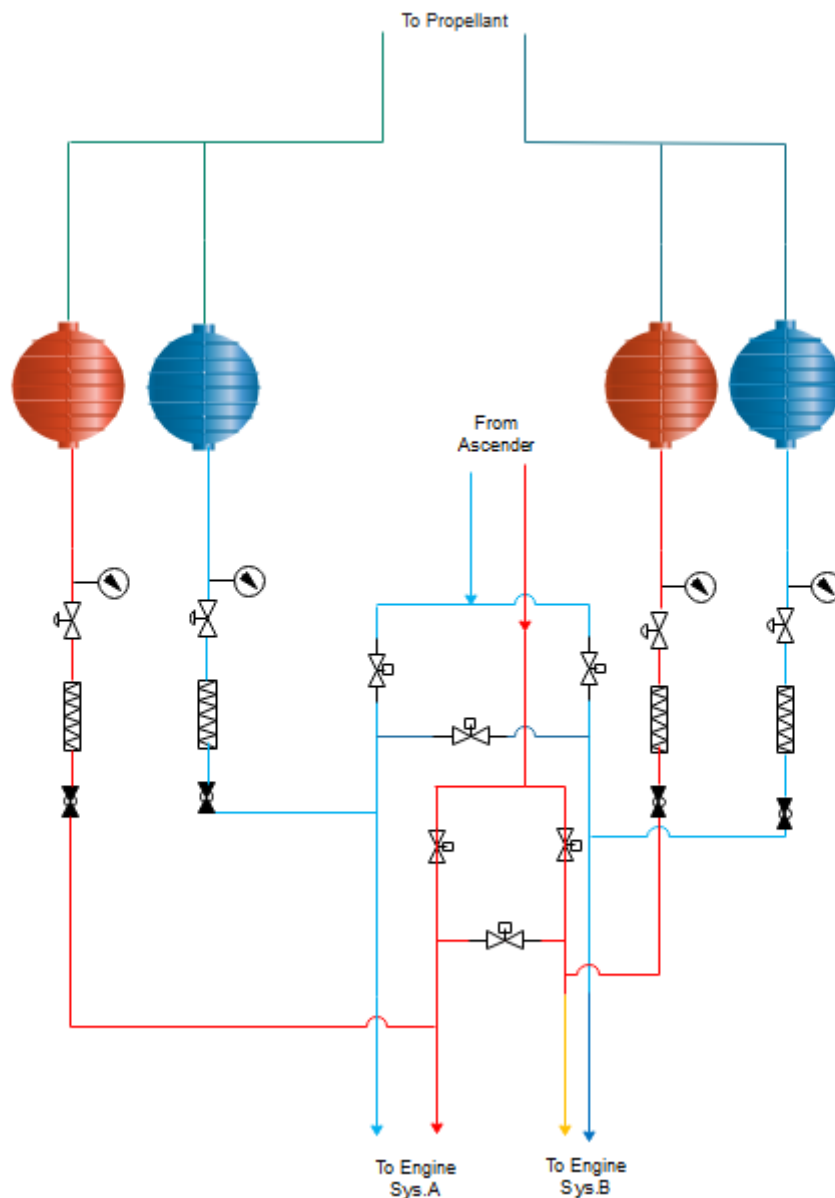


Figure 6.17 RCS propellant storage and feed system

The RCS propellant supply section consists of two pairs of two oxidizer and fuel tanks. Each pair, for redundancy, feed two clusters of four thrusters, associated with system A or B. Once the propellant is pressurized, it flows within main flow lines to the engine assembly entering trim orifices, filters and normally open (NO) shut-off valves. Propellant can be delivered from one system to another through interconnecting lines characterized by normally closed and electrically actuated solenoid valves, in case of undesired damage or in case only one of the two thruster systems is to be used. In addition, it is possible to use pressure

propellant from the ascent stage by activating the solenoid valves on the two lateral flow lines and closing the main shut-off valves.

6.4.3 Reaction control system engine assembly

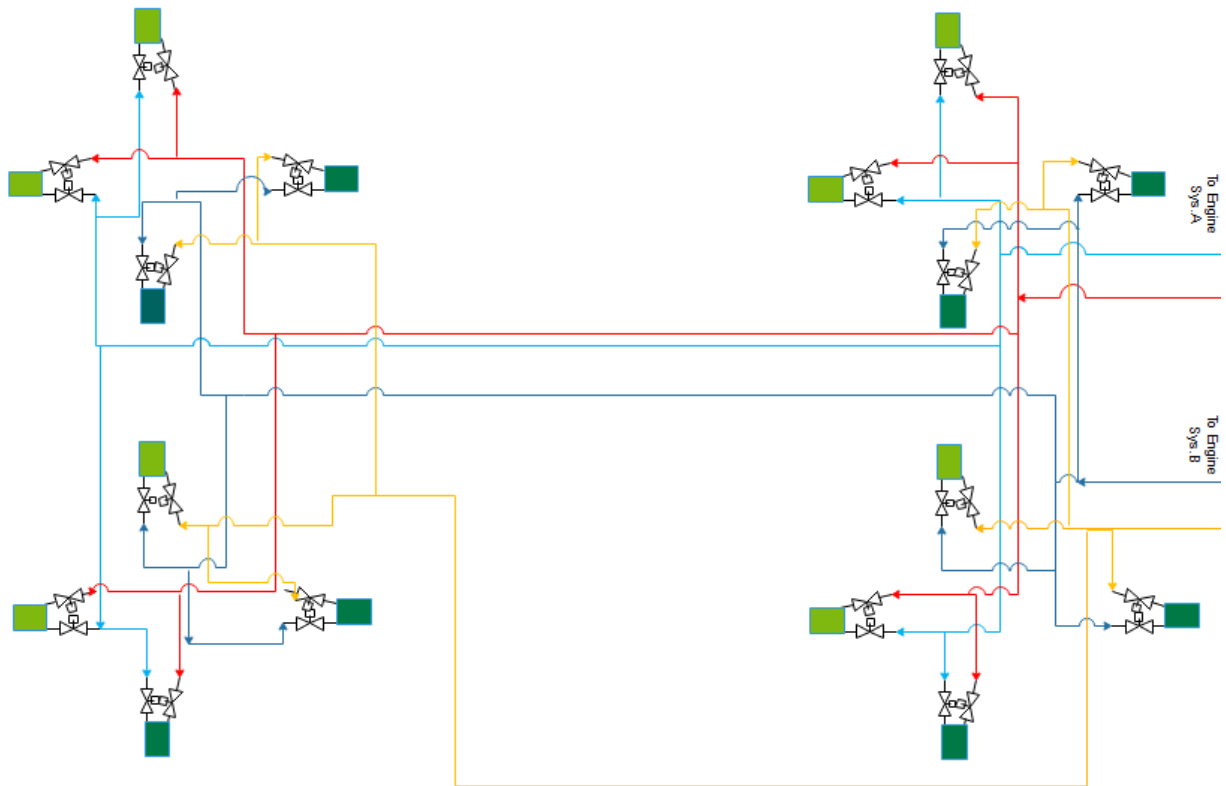


Figure 6.18 RCS engine assembly

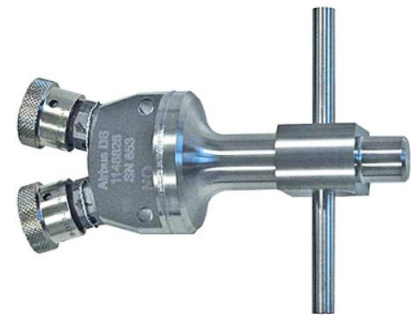
The RCS engine assembly is characterized by four main flow lines leading to the thrust chamber inlet for each of the four thrusters' groups. Each thruster is a radiation-cooled engine that operates in a pulse mode to generate short impulses for fine attitude corrections or in a steady-state mode to produce continuous thrust for major attitude or translation changes. Propellants are prevented from entering the thruster by normally closed solenoid-operated shut-off valves at oxidizer and fuel inlet ports. These valves open when an ignition signal energizes the coil. The propellant then flows through injector into combustion chamber.

6.5 Space market: valves

Space market offers a wide variety of valves with different features in terms of design, weight, material, and operating method. The main used for descent and ascent architectures are presented below, with relative company descriptions:

Table 6.21 ArianeGroup's pyro valve Ref. [25]

PYROTECHINIC VALVE		
Parameter	Value	Unit
Valve Name	Pyrotechnic Valve	
Industry	ArianeGroup	EU
Design	All-welded Ti	
Fluid Compatibility	He, MON, MMH	
Op. Temperature	168-373	K
Response Time	< 7	ms
Mass	0.168	kg
MEOP	31	Mpa
Burst Pressure (NC)	> 160 (pre-firing)	MPa
Burst Pressure (NC)	>124 (post-firing)	MPa
Burst Pressure (NO)	>160 (pre-firing)	MPa
Burst Pressure (NO)	>124 (post-firing)	MPa
Leakage (NC & Internal before firing)	<0.000001	scc/s
Leakage (NC & external b/a firing)	<0.000001	scc/s
Leakage (NO & Internal after firing)	<0.000001	scc/s
Leakage (NO & external b/a firing)	<0.000001	scc/s



Pyrotechnic Valve

Figure 6.19 ArianeGroup pyro valve

In accordance with Ref.[ArianeGroup], such pyro valves are a family of Normally Open and Normally Closed valves designed for spacecraft and launch vehicle propulsion systems where a reliable “one shot” device is needed for the permanent opening or closing of a fluid circuit. Due to their excellent leak tightness capability prior or after firing in combination with low mass and simplicity, these valves represent a state-of-the-art solution to a range of propulsion system’s needs.

Table 6.22 Omnidea-RTG's pressurant filter Ref. [26]

PRESSURANT FILTER

Parameter	Value	Unit
Filter Name	P/N PF1	
Industry	OMNIDEA-RTG	EU
Operating Media	Inert Gases	
MEOP	35	Mpa
Leakage Rate (all welded design)	0	scc/s
Max Flow Rate ($\Delta P=0.1$ Mpa)	< 17	l/min
Filter Mesh Size	2	μm
Filter Size	4.6	cm ²
Mass	0.076	kg
Dimensions	50x30x30	mm
Materials	Stainless Steel	



Figure 6.20 Omnidea-RTG pressurant filter

The Omnidea-RTG qualified and flight-proven pressurant filter is designed for inert gases with a MEOP of 35 Mpa, a slightly higher value than that used in pressure vessel of the current mission. With a stainless-steel body and an all-welded design, this component is suitable for propulsion systems, as it features low weight and zero leakage rate.

Table 6.23 ArianeGroup's fill & drain valves

FILL & DRAIN VALVES (2 FAILURE TOLERANT)

Parameter	Value	Unit
Operating Media	Various Fluids	
Industry	ArianeGroup	EU
Mass	0.09	kg
Total Length	109 ±1	mm
Standard Tube Dimensions (OD)	6.4 ± 0.02	mm
Standard Tube Dimensions (ID)	4.9 ± 0.01	mm
Standard Tube Dimensions (ID) at weld	5.58 ± 0.02	mm
Tube Length	43	mm
Open/Close Cycles	40	cycles
Standard Operating Temperature	243 to 353	K



Ground Half Coupling

Figure 6.21 ArianeGroup ground half coupling



Figure 6.22 fill & drain valve

Burst Pressure	12.4	MPa
Internal Leakage	< 0.000001	scc/s Ghe
External Leakage	< 0.00028	scc/s Ghe

All fill and drain valves are machined from titanium alloy leading to a lightweight unit with 6.4 mm of outlet diameter tube stub which forms a weldable connection to the titanium tubing of the subsystems. The all-welded housing contains a spring supported guided valve poppet equipped with the primary seal. This ensures, in accordance with Ref. [25], that the valve is kept closed in non-actuated conditions, while in flight configuration the valve poppet sealing will be additionally protected and sealed by mounting cap, providing a metal-to-metal seal. For servicing, a dedicated Ground Half Coupling for each fill and drain valve is required.

Table 6.24 MAROTTA's relief valve Ref. [27]

HIGH PRESSURE RELIEF VALVE

Parameter	Value	Unit
Industry	MAROTTA	USA
Valve name	PRV95	
Pressure range	0-68.947	MPa
End Connections	As required	
Cv	0.245 and higher	
ESEOD	31.75	mm
Body Material	Stainless steel	
Trim	Stainless steel	
Seal Material	Fluorocarbon	
Seat Material	Vespel SP-1	



Figure 6.23 MAROTTA relief valve

PRV95 has a pressure-sensing disc on the poppet upstream of the seat that controls the valve position. By placing this control surface in the area of relatively constant fluid density, the PRV95 provides highly stable control throughout its operating range. Moreover, the PRV95 incorporates a unique valve seat that adds to its “no impact” characteristics. The valve seat seals against the outer radius of the poppet, providing a larger, more contamination-tolerant sealing surface than a typical point-contact valve seat.

Table 6.25 Bradford Space's pressure transducer Ref. [28]

STANDARD ACCURACY PRESSURE TRANSDUCER		
Parameter	Value	Unit
Valve Name	SAPT	
Industry	BRADFORD SPACE	EU
Medium Compatibility	MON/MMH/Ghe	
Proof Pressure Factor	2	times o.p
Burst Pressure	125	MPa
Internal/External Leakage (Ghe)	< 0.0001	scc/s
Measurement Accuracy	0.3-0.5 %	
Mass	0.23	kg
Dimension (l x w x h)	126 x 77 x 43.5	mm
Fluidic Interface	Weldable Tube Stub	
Structural Interface	4 bolt M4	
Wetted Materials	Ti-6Al-4V	
Operational Life	18	years
Constant Acceleration	20g	
Power Supply	15 to 28 V	< 300 mW
Output Signal	0.5 to 5	V



Figure 6.24 BRADFORD SPACE pressure transducer

The Standard Accuracy Pressure Transducer (SAPT) is a piezo-resistive based, fully ESA qualified pressure gauging component, both for gaseous or liquid media. The unit consists of a pressure-sensing element and dedicated set of electronics, integrated into one compact design. The fully seal-welded sensor housing construction is optimised to enable one generic design for pressure ranges from 0.1 to 32 MPa, with maximum flexibility for adaptation to customer specific requirements. Wetted parts have demonstrated compatibility with the all typical propellants currently in use in spaceflight, whereas a qualified joint material enables different materials for fluidic interfaces.

Table 6.26 MAROTTA's pressure regulator Ref. [29]

PRESSURE REGULATOR		
Parameter	Value	Unit
Regulator Name	MV400	Electronic Regulator
Industry	MAROTTA	USA
Pressure range	0-68	Mpa
Power Ground	0	VDC
Pressure Command	1-5	VDC
Sys Output Pressure	2-24	milliamps
Line Fluid	334-430	K
ESEOD (max)	0.386	in
Weight	3.6	kg
Regulation Set Point	± 0.1379	MPa
Response Time	<250	milliseconds
Internal Leak Rate	0.001	sccs
Material	Titanium	



Figure 6.25 MAROTTA pressure regulator

Marotta's electronic pressure regulator is suitable for spaceflight, defence, and facility applications. Through a closed loop electronic control system controlling piezo-actuated pilot valves, the regulator constantly measures actual downstream outlet pressure and adjusts to changing inlet conditions. The precise flow control results in accurate outlet pressure insensitive to inlet pressure, flow rate and temperature.

Table 6.27 VACCO's check valve Ref. [30]

CHECK VALVE		
Parameter	Value	Unit
Valve Name	V0D10840-01	
Industry	VACCO	USA
Operating Pressure	0.34-1.723	MPa
Burst Pressure	6.9	MPa
Flow (Ghe)	1.87	scfm
Pressure Drop	0.03	MPa
Internal Leakage	0.0000083	sccs
External Leakage	0.000001	sccs



Figure 6.26 VACCO check valve

Operating Temperature	265.9-322.04	K
Weight	0.17	kg
Construction Material	Ti	
Body and Interface	Stainless Steel	
N	8	
Total Mass	1.36	kg

VACCO Aerospace Products maintains a product line of stainless steel and titanium check valves to meet industry's demand for high reliability, and tight leakage. The low-pressure check valve is a single poppet valve with stainless steel body and interface. The unit integrates VACCO's etched disc technology with an integral inlet filter. The valve is fully flight qualified and holds extensive heritage.

Table 6.28 VACCO's propellant filter Ref. [31]

PROPELLANT FILTER MON3

Parameter	Value	Unit
Valve Name	15228-601	
Industry	VACCO	USA
Operating Pressure	1.7	MPa
Proof Pressure	2.585	MPa
Filtration Micron	25	
Flow Rate (Max Clean)	0.0997	kg/s
Pressure Drop (Max Clean)	0.03447	MPa
Weight	0.2495	kg
N	1	
Total Mass	0.2495	kg

Table 6.29 VACCO's propellant filter

PROPELLANT FILTER MMH

Parameter	Value	Unit
Valve Name	15241-509	
Industry	VACCO	USA
Operating Pressure	1.7	MPa
Proof Pressure	3.447	MPa
Filtration Micron	18	

Flow Rate (Max Clean)	0.0997	kg/s
Pressure Drop (Max Clean)	0.003447	MPa
Weight	0.08618	kg
N	1	
Total Mass	0.0997	kg

Table 6.30 Omnidea-RTG ball valve

BALL LATCH VALVE

Parameter	Value	Unit
Valve Name	BLV	
Industry	OMNIDEA-RTG	EU
Operating Media	MMH/MON	
MEOP	0-35	MPa
Leakage Rate (Intern)	0.000001	scc/s
Leakage Rate (Extern)	0.000001	scc/s
Flow Rate (DP < 0.01MPa)	30	g/s
Flow Rate (DP < 0.2 MPa)	300	g/s
Opening Speed (1526:1 gear)	4	s
Life cycles	1000	cycles
Power supply	28±5 V, 10-30 V for position indicators	
Power Consumption	< 10	W
Mass	0.83	kg
Material	Ti-6Al-4V	
N	8	
Total Mass	6.64	kg

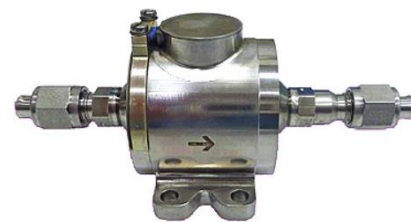


Figure 6.27 Omnidea-RTG ball valve

The motor driven ball valve is stable in open and closed position and include position indication sensors. In addition, is characterized by water hammer dissipation due to slow opening.

Table 6.31 ArianeGroup's solenoid valve

LOW PRESSURE SOLENOID VALVE		
Parameter	Value	Unit
Valve Name	Latch Valve	
Industry	ARIANEGROUP	EU
Tubing Interface	0.25	in
Operating Voltage	22-32	VDC
Response Time	< 30	ms
Coil Resistance	37.5±1.5	Ω
Max Operating Pressure	2.425	Mpa
Internal Leakage Rate (GHe)	< 5	scc/h
Back-Relief Pressure	0.8-1.4	MPa
Flow Rate and Pressure Drop	< 0.015 MPa at 4.5 g/s	
Fluid Compatibility	He,MMH,NTO	
Mass	0.545	kg
N	8	
Total Mass	4.36	kg



Low Pressure Latch Valve

Figure 6.28 ArianeGroup solenoid valve

The ArianeGroup low pressure latching valve is a solenoid-operated, bi-stable valve constructed essentially of stainless steel and qualified to operate with a number of different working media, including hydrazine and its most common derivatives. The component provided by ArianeGroup represents the switchable, fully reliable safety barrier in the propellant flow between tank and thrusters. It is equipped with a back-relief-function protecting the downstream lines and equipment against over-pressure. For switching 2 electromagnetic coils are to be activated to change the status of the valve to open or closed. Switching can be performed by using a non-regulated supply within a range of $22\text{VDC} < 28\text{VDC} \leq 38\text{VDC}$. At room-temperature the low-pressure latch valve can be closed or opened within a switch-time of 30ms while the cycle-time is defined to 50ms. A microswitch is installed for position indication, activated by a pin, which is directly mounted on the component-anchor. The variant with welded interface is identical to the screwed-interface one except for the tubing connection.

7. Thrust chamber

7.1 Thrust chamber fundamentals

In a liquid-bipropellant rocket engine the conversion of the energy of propellant into thrust is based on the following steps:

- The liquid propellant is injected into combustion chamber at a specific mixture ratio and atomized into droplets.
- The droplets are then vaporized by heat transfer from the surrounding gas. The size and velocity of the droplets change continuously during combustion process.
- The vaporized propellants are mixed rapidly and further heated. Combustion will essentially be complete in upstream throat section when all liquid droplets have been vaporized.
- Combustion products are accelerated to sonic condition in the throat, expanded in diverging nozzle section and then ejected externally.

In this chapter the preliminary sizing of the thrust chamber will be analysed. Generally, a thrust chamber is characterized by injector, combustion chamber, ignition devices (for nonhypergolic propellant), expansion nozzle, distribution manifolds and appropriate structures for component mounting and for carrying the thrust forces to the vehicle. It is possible to examine three fundamental subassemblies which are thrust-chamber body (combustion chamber and expansion nozzle), injector, and igniter (where required), as shown in the following figure in accordance with [1]:

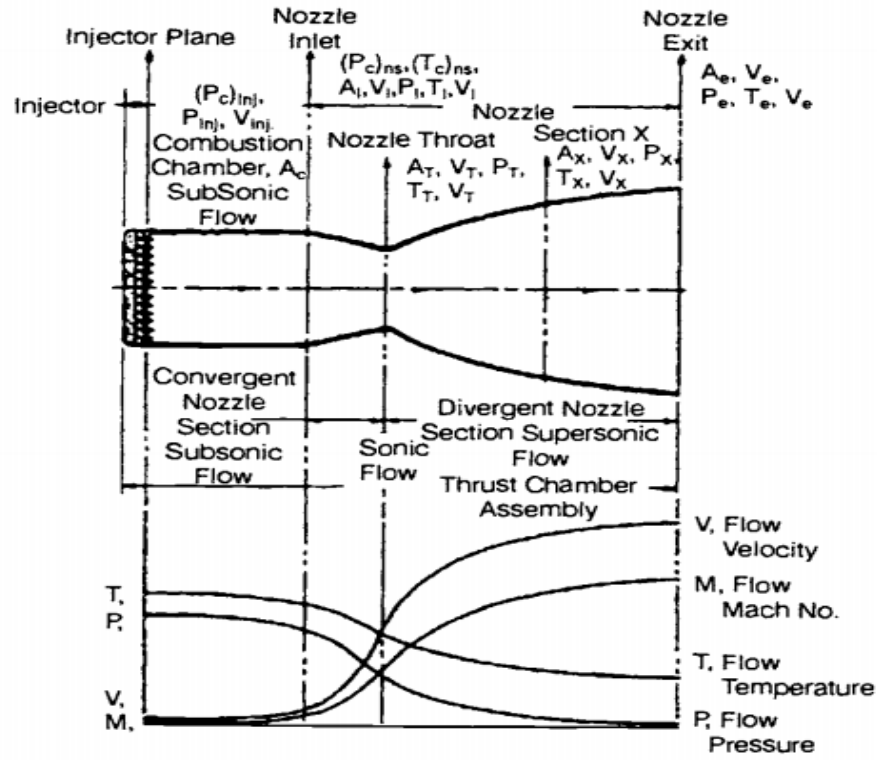


Figure 7.1 Rocket engine main sections

As mentioned in Chap. 3, small chamber cross section relative to the throat area cause pressure losses in chamber. The liquid propellants are injected at the injection plane with a small axial velocity which is assumed to be zero, as seen in previous gas-flow calculations. The heat released in combustion process between injector plane and nozzle inlet increases the specific volume of the gas. To satisfy the conditions of the constant mass flow, the gas must accelerate toward the nozzle inlet with some pressure drop. The gas-flow process within the combustion chamber is not entirely isentropic but rather is a partly irreversible, adiabatic expansion. Even if the total temperature remains constant, the total pressure decreases and this causes permanent energy losses and slight reduction in engine performance, as a function of gas properties and contraction ratio. Therefore, neglecting the flow velocity at the injector-end, the total chamber pressure ratio between this section and the nozzle inlet can be expressed as follows:

$$\frac{P_{c_{inj}}}{P_c^0} = \frac{1 + \gamma M_i^2}{\left(1 + \frac{\gamma - 1}{2} M_i^2\right)^{\frac{\gamma}{\gamma - 1}}} \quad (7.1)$$

where the subscript i indicates the section at the nozzle inlet, as shown in fig. 8.1. The static pressure ratio will be:

$$\frac{P_{c_{inj}}}{P_c} = 1 + \gamma M_i^2 \quad (7.2)$$

For a finite area combustor, the equation (7.2) identifies the performance reduction due to influence of chamber geometry. For the current propellant combination, the trend of the pressure ratio as a function of the contraction ratio defined as the ratio between chamber and throat area, is shown below:

$$\varepsilon_c = \frac{A_c}{A_t} \quad (7.3)$$

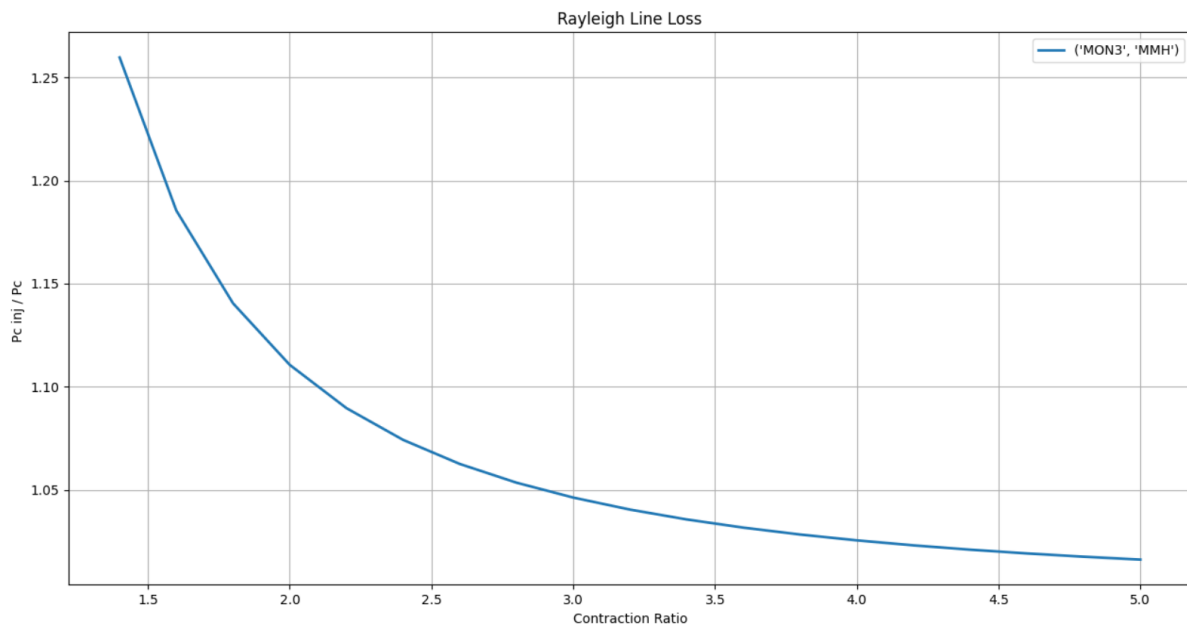


Figure 7.2 Variation of injector-to-nozzle inlet pressure ratio as a function of contraction area ratio

RocketCEA v1.1.24 documentation proposes an approximate equation to estimate the Rayleigh line losses that is essentially dependent on the contraction ratio:

$$\frac{P_{c_{inj}}}{P_c} = 1 + \frac{0.54}{\varepsilon_c^{2.2}} \quad (7.4)$$

The trend is shown below:

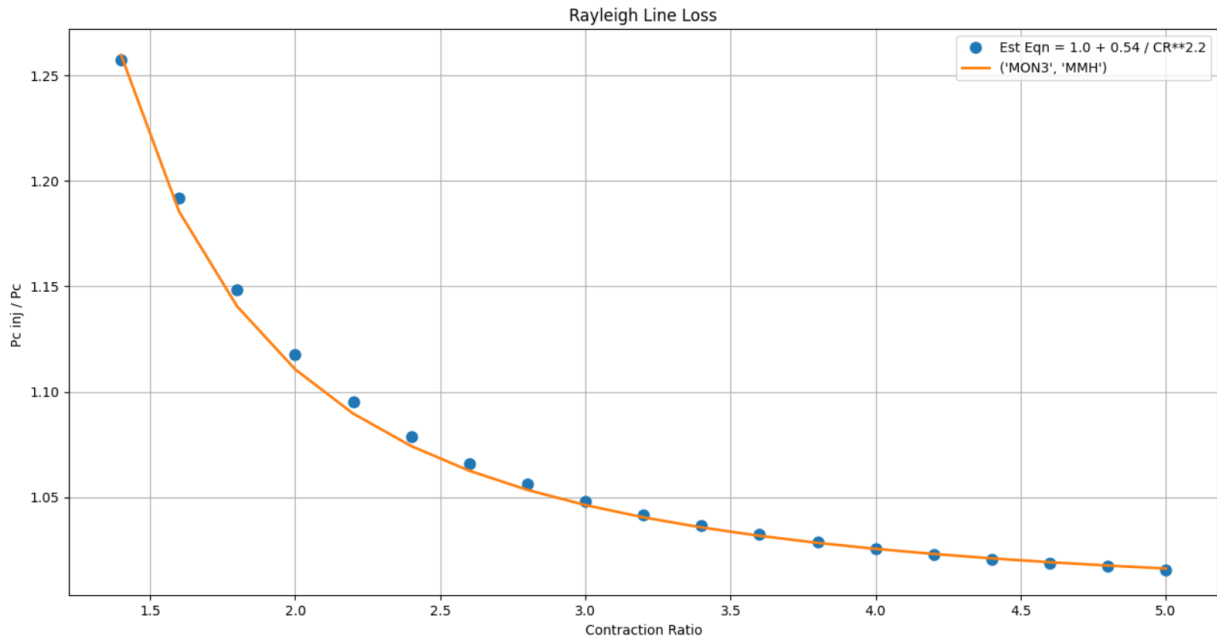


Figure 7.3 Variation of injector-to-nozzle inlet pressure ratio and approximate equation as a function of contraction area ratio

with an excellent correspondence between estimated and actual data.

7.1.1 Thrust chamber body

The thrust chamber body consists of a cylindrical or spherical sections in which the combustion occurs, a section narrowing toward a throat, and a conical or bell-shaped expanding nozzle section through which the combustion gases are expelled. The combustion chamber is essentially a structure that serves to retain the propellant for a proper “stay time”, during which mixing and complete combustion is achieved. The rate of combustion depends generally by the propellant combination, the injected conditions of the propellant, combustion geometry and injector design. The rate-limiting factors are vaporization rates for liquid propellants, mixing time, and the kinetic rates of the reactions. Generally, larger engines with larger injector will produce larger drop sizes, extending the stay time for complete combustion. Combustor volume thus has a definite effect on combustion efficiency. The stay time is defined by the following equation:

$$t_s = \frac{L_c}{v_c} \quad (7.5)$$

where L_c and v_c are the characteristic length and characteristic velocity of propellant travel into the chamber, respectively. The previous equation is modified as follows:

$$t_s = \frac{L_c}{v_c} \left(\frac{A_c \rho_{Bulk}}{A_c \rho_{Bulk}} \right) = \frac{m_c}{\dot{m}_p} \quad (7.6)$$

where A_c is the characteristic chamber area and m_c , the characteristic propellant mass contained into combustion chamber and \dot{m}_p the propellant flow rate. In accordance with equation [c*], it is obtained:

$$t_s = \frac{L_c A_c \rho_{Bulk} c^*}{P_c A_t} = \frac{V_c}{A_t} \frac{1}{RT_c} \frac{c^{*2}}{c^*} \quad (7.7)$$

Using the equation [C* F(RTC)], and defining characteristic chamber length the following ratio:

$$L^* = \frac{V_c}{A_t} \quad (7.8)$$

an expression of stay time is obtained that depends on L^* , c^* and Γ :

$$t_s = \frac{L^*}{c^*} \frac{1}{\Gamma^2} \quad (7.9)$$

However, it is easier to evaluate L^* parameter rather than t_s because the latter is expressed in fractions of seconds. The characteristic chamber length increases as c^* increases until a point for which there is a decrease in engine overall performance due to the following reasons:

- Larger L^* results in higher thrust-chamber volume and weight.
- Larger L^* creates more surface area in need of cooling and may increase thermal losses.
- Larger L^* increases the frictional losses in the combustion chamber, reducing nozzle total pressure and resultant thrust.

A table of maximum and minimum allowable L^* values for a give propellant combination is presented below, in accordance with Ref. [Hubble]:

Propellants	Characteristic Length (L^*)	
	Low (m)	High (m)
Liquid fluorine / hydrazine	0.61	0.71
Liquid fluorine / gaseous H_2	0.56	0.66
Liquid fluorine / liquid H_2	0.64	0.76
Nitric acid / hydrazine	0.76	0.89
N_2O_4 / hydrazine	0.60	0.89
Liquid O_2 / ammonia	0.76	1.02
Liquid O_2 / gaseous H_2	0.56	0.71
Liquid O_2 / liquid H_2	0.76	1.02
Liquid O_2 / RP-1	1.02	1.27
H_2O_2 / RP-1 (including catalyst)	1.52	1.78

Figure 7.4 Characteristic length values for several propellant combination

Moreover, as it noticed from equation (7.6), the stay time is theoretically independent from combustion-chamber geometry. This means that for a given volume, the chamber can assume any shape. In actual design, however, this choice is limited. Long chambers with small contraction ratio results in high pressure losses and space limitation on injector design. Short chamber with high contraction ratio results in reduction of combustion efficiency due to imperfect mixing and combustion of the propellant. In accordance with Ref. [1] the three most common room shapes are represented in the following figure:

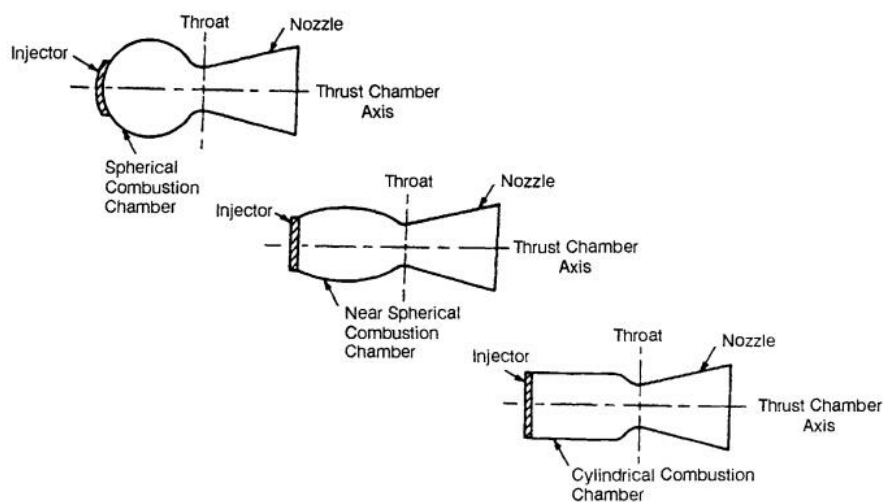


Figure 7.5 Several combustion chamber shapes

Using the same volume, compared to cylindrical shape, a spherical or near-spherical chamber offers the advantage of less cooling surface and weight. A sphere has the lowest surface-to-volume ratio of all the

geometric choice, as mentioned in Chap.5, and for the same material strength and chamber pressure, the minimum wall thickness required for a given pressure load. However, the spherical shape is more difficult to manufacture and has provided poorer performance in other respects. Generally, a good place to start for sizing a new thrust chamber is to evaluate historical data associated with engine previously produced. The throat size and chamber length for example can be derived from experimental data as a function of contraction ratio:

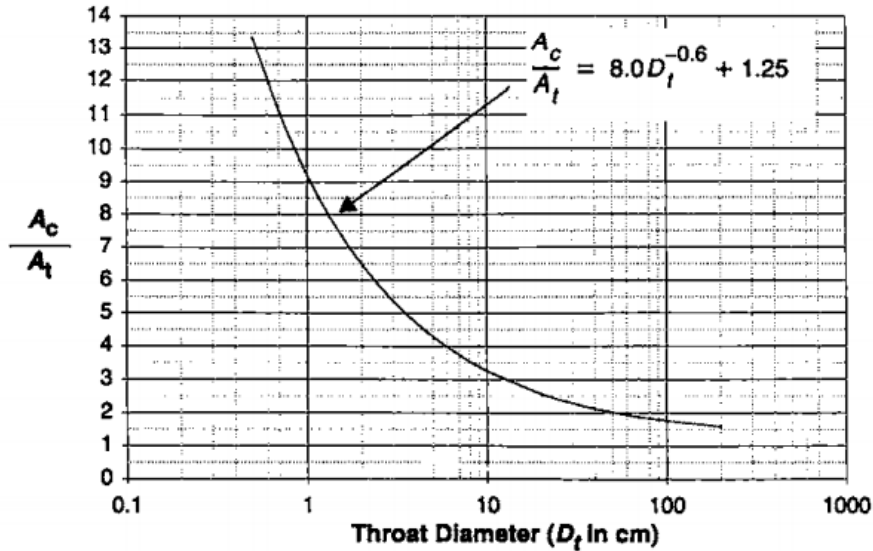


Figure 7.6 Variation of contraction area ratio as a function of throat chamber diameter

but throat dimension, as mentioned, is not the only driving force in chamber sizing. Since the primary purpose of the combustion chamber is to make the propellants react appropriately, the forces which govern and limit these reactions are of fundamental importance, such as the conditions of the injected reactants for proper atomization, the shape of propellant related to chamber volume and stay time, the injector design, and its orifices. Even though the combustion chamber might have scaled proportions approaching sphere, the combustor requires a certain volume to accomplish vaporization and reaction. In accordance with Ref. [1], the suggested guideline tends to maintain the proportions of the combustion neither too long and thin nor too short and fat, but not to force it to a spherical proportion. In the following preliminary design, a cylindrical combustion shape will be considered. Concerning the nozzle, many of these have a convergent-divergent pattern (De Laval nozzle). While within convergent section the velocity is relatively low, any well-rounded and smooth geometry generates minimal energy loss, within the divergent section the velocities are very high. Therefore, it is appropriate to exhibit the following characteristics:

- The flow should be uniform, parallel, and axial at the nozzle exit for maximum momentum vector.
- The flow should manifest minimum separation and turbulence losses within the nozzle.

- The nozzle length should be as short as possible for minimum space envelope, weight, wall friction losses and cooling requirements.
- The nozzle should be easily manufactured.

Any discontinuity in the nozzle wall contour should be avoided to prevent the possibility of shock waves or turbulence losses. Generally, the nozzle can have conical or bell shape. Conical shape allows ease of manufacture and flexibility in converting an existing design to higher or lower expansion ratio without redesign it. The following schematic is applicable:

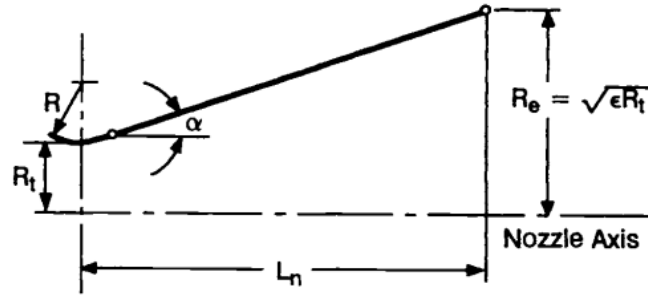


Figure 7.7 Conical nozzle section

where R is the radius of curvature of the throat section, R_t is the radius of the throat, R_e is the nozzle exit radius and α the divergent half-angle with typical value of 15° . In accordance with the previous figure, the length of conical nozzle can be calculated as follows:

$$L_{n\text{conical}} = \frac{1}{\tan(\alpha)} \left(R_t(\sqrt{\epsilon} - 1) + R(\sec(\alpha) - 1) \right) \quad (7.10)$$

Performance losses occur inside the conical nozzle because the exhaust velocity is not perfectly axial. Therefore, it is possible to define divergence efficiency, the parameter:

$$\lambda = \frac{1}{2} (1 + \cos(\alpha)) \quad (7.11)$$

which modifies the momentum thrust component. For an α of 15° , λ will be 0.983. About the bell shape, this configuration results in increased performance with a fast-expansion section in the initial divergent region, and a shorter length. The true bell shape nozzle is obtained by the method of characteristics and is not the subject of this preliminary discussion. For the purposes of this section, Rao's approximate method will be applied. The bell shape is approximated by a parabola. The nozzle contour immediately upstream of the

throat is a circular arc with radius of $1.15R_t$, while the divergent contour is made up of a circular entrance section with a radius of $0.382R_t$ from the throat to the point N , which identifies the beginning of the parabola. The schematization is shown in the following figure:

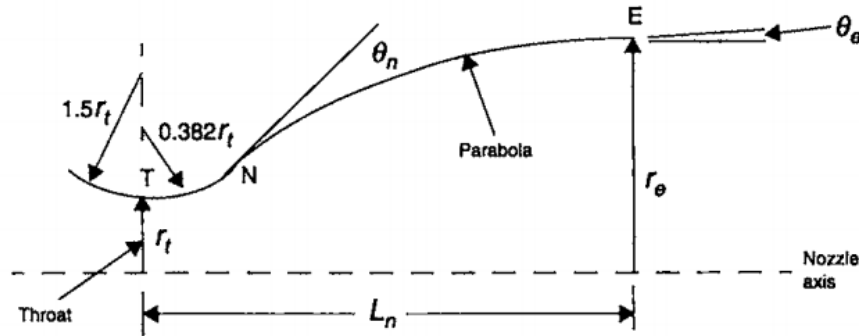


Figure 7.8 Rao nozzle section approximation

and evaluated in detail in the dedicated section. θ_n and θ_e angles are respectively the initial wall angle of the parabola and the nozzle-exit wall angle and depend on the expansion ratio and L_f , the fractional length based on a 15° conical nozzle:

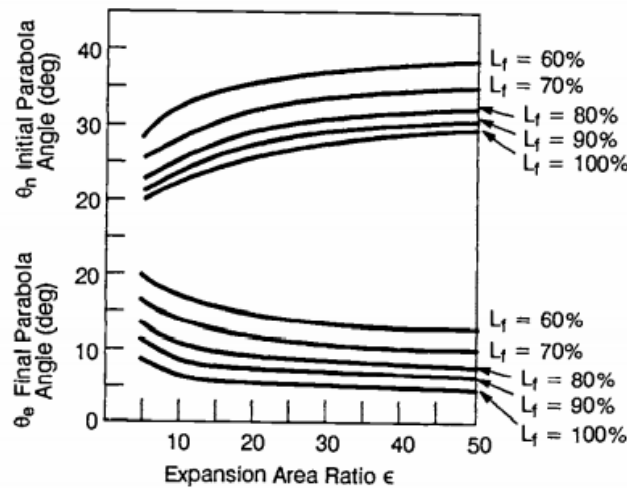


Figure 7.9 Nozzle angle variation as a function of expansion area ratio and bell nozzle

7.1.2 Injector

The functions of injectors are to introduce and meter liquid propellant flows into the combustion chamber, to break up liquid into small droplets (atomization) and to distribute and mix the propellant so the desired mixture ratio will result, with uniform propellant mass flows and composition over the chamber cross section. The two common design approaches for admitting propellants into the combustion chamber are listed below:

- Propellant jets are routed through a multitude of holes on the injector face.
- Propellants are routed through cylindrical injection elements, which are inserted and fastened into the injector face and each element delivers a conically shaped spray of propellants into the combustion chamber.

The first category of injectors is shown in the following figure:

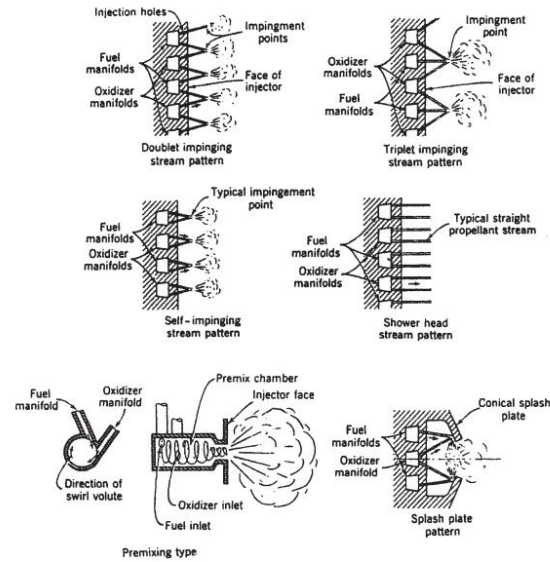


Figure 7.10 Injection design using holes

while the second category is illustrated below:

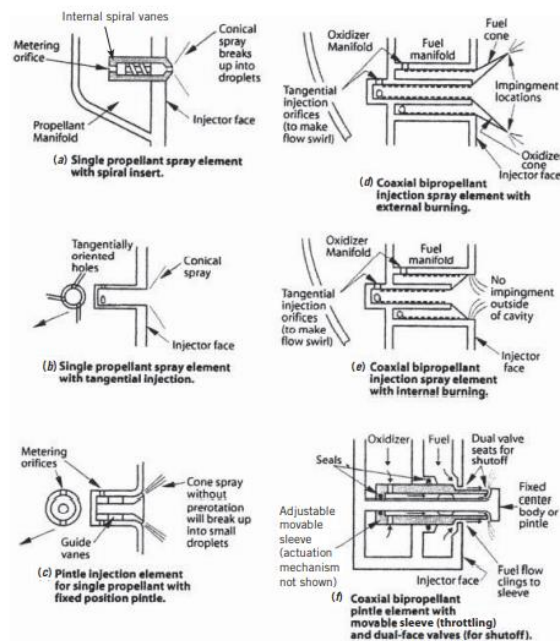


Figure 7.11 Spray Injection elements

The injection patterns on the injector face are related to its internal manifolds or feed passages. These distribute propellant from inlets to injection holes. A large complex manifold volume allows for low passage velocities and proper flow distributions over the chamber cross section. Small manifold volumes permit lighter injector and faster starts. However, higher passage velocities usually cause uneven flows through identical injection holes and thus yield poorer distributions and local composition variations. Generally, doublet impinging-stream-type injectors are used with storable propellant and belong to the first category of injectors mentioned above. For unlike doublet patterns, propellants are injected through separate orifices, then fuel and oxidizer streams impinge upon each other, creating a thin liquid fan and aiding in atomization process. For a like-on-like doublet pattern, two liquid films form a fan which breaks up into droplets. For uneven volume flows, triplet patterns often are more effective. Shower head injector routes the propellants in a direction normal to the injector face, then mixing is achieved through subsequent turbulence and diffusion. Sheet or spray-type injectors produce different types of spray sheets, which intersect and thereby promote mixing, atomization, and subsequent vaporization. By modifying spray internal dimensions, such as size or number of tangential feed holes, the length of internal cylinder, it is possible to change the conical sheet angle, the impingement location of propellants, to affect the mixture ratio and combustion efficiency. By varying sheet widths through and axially injector sleeve, it is possible to throttle propellant flows over a wide thrust range without excessive pressure drop through injector. This configuration was used on the Apollo LMDE. Coaxial hollow post or spray injector work well when one propellant is gasified. This flows at a relatively higher speed with respect to the other propellant that flows at a much lower speed. The differential velocity causes shearing which helps to break up the liquid propellant stream into small droplets. Hydraulic injector characteristics can be accurately evaluated and designed for orifices with any desired injection pressures, velocity, flows and mixture ratio. The thrust-to-effective exhaust velocity ratio provides the flow rate required by the engine. For an injector, assuming incompressible flow, this assumes the following equation:

$$\dot{m} = C_d A \sqrt{2\rho\Delta P} \quad (7.12)$$

where C_d is a discharge coefficient, A the cross-sectional area of orifice, ρ the propellant density and ΔP the pressure drops through the orifices.

7.2 Thrust chamber preliminary design

After the fundamental principles associated with the thrust chamber have been presented, the preliminary design is carried out, which essentially depends on the requirements to be met based on the type of rocket engine considered.

7.2.1 Descender thrust chamber

To perform the preliminary design of the descent-stage rocket engine, it is appropriate to evaluate the thrust required to perform a given manoeuvre. It is desirable to consider a reasonable value of the thrust-to-weight ratio. A comparison is made with the Apollo LMDE. The Apollo descent engine was sized with a thrust-to-weight ratio of 0.3. The equation is the following:

$$\left(\frac{T}{W}\right)_{Earth} = \left(\frac{T}{m_{LEM}g_0}\right)_{Earth} \quad (7.13)$$

To derive this ratio on the moon, the previous equation is modified as follows:

$$\left(\frac{T}{W}\right)_{Moon} = \left(\frac{T}{m_{LEM}g_0}\right)_{Earth} \left(\frac{g_0}{g_{Moon}}\right) \quad (7.14)$$

The Moon's gravitational acceleration is 1.622 m/s², therefore the gravity ratio is about 6, as shown in the following table:

Table 7.1 Gravitational acceleration parameters

Gravitational accelerations		
Parameter	Value	Unit
g0 Earth	9.80665	m/s ²
g Moon	1.622	m/s ²
g0 Earth/ g0 Moon	6.04	

The required thrust is derived from equation (7.13), knowing the total mass of the lander and the thrust-to-weight ratio:

$$T = \left(\frac{T}{W} \right)_{Earth} m_{LEM} g_0$$

Considering an average weight from the tables 4.2, 4.3, 4.4, 4.5 and 4.6 of 15997.54 kg, the required thrust is 47 kN, a very close value to that reported in the literature of 46.7 kN. The Moon's thrust-to-weight ratio will be 1.8138. The current mission is characterized by a lander weight of 44542.72 kg. Using the same thrust-to-weight ratio, the required thrust will be 131.044 kN. Analysing the upper-stage engine table [], it is noted that none of those engines provide such thrust. It is appropriate then to consider a multi-engine configuration. The AJ10-118K would appear to be the most suitable engine, as it has the highest thrust in the pressure-fed category. With three such rocket, a total thrust of 130.2 kN is reached. It follows that the required thrust-to-weight ratio will be slightly less than 0.3 and equal to 0.29806, a reasonable result. Since the descent manoeuvre additionally requires a throttled rocket engine, as will be seen in detail in the dedicated section, the minimum thrust required is also analysed. The minimum thrust is 75% of the lander weight on the moon, assuming that in descent phase it is reduced by half. Under this assumption, considering the Apollo LMDE the minimum thrust required in that phase is 9.73 kN. The current mission then requires a thrust of 27.01 kN. The throttling ratio is defined as the following equation:

$$TR = \frac{T_{max}}{T_{min}} \quad (7.15)$$

With these estimates it is noted that a TR greater than or equal to 4.799 is required for the Apollo mission, while a value greater than or equal to 4.82 is required for the current mission. While the actual LEM data, due to uncertainties, report that the choice made was a throttling range of 10:1, for the current mission a range of 5:1 can reasonably be assumed. The data derived from the various assumptions are summarized in the following table:

Table 7.2 Descender engine preliminary requirements

Descender Requirements		
Parameter	Value	Unit
Vacuum Thrust (x1)	43.4	kN
g0 Earth	9.80665	m/s ²
g Moon	1.622	m/s ²
g0 Earth/ g0 Moon	6.04	
T/W (Lander)	0.298	wrt Earth

T/W (Lander)	1.8	wrt Moon
TR	5	

Thrust and throttling ratio are some of the input parameters to be entered into RPA software. To evaluate rocket engine performance and the correspondent geometry for a finite area combustor it is appropriate to calculate the contraction ratio. The initial parameters required are the expansion ratio and the nozzle-exit diameter. The latter is obtained from the table 4.1. With an ε of 65 and a D_e of 1.53 m the following equation are applicable:

$$A_e = \frac{\pi D_e^2}{4} \quad (7.16)$$

$$A_t = \frac{\pi D_t^2}{4} \quad (7.17)$$

$$D_t = \sqrt{\frac{4A_e}{\pi\varepsilon}} \quad (7.18)$$

where D_t and D_e are respectively the throat and exit diameter, A_t the throat area and A_e the exit area. The expression (7.18) is derived from the relation (3.3). The calculated values are shown in the following table:

Table 7.3 Descender throat and outlet section engine requirements

Throat and exit section design requirements		
Parameter	Value	Unit
De	1.53	
Ae	1.83	m2
At	0.028	m2
Dt	0.189	m

The contraction ratio is evaluated by the graph in figure 7.6, characterized by the following equation:

$$\varepsilon_c = 8D_t^{-0.6} + 1.25 \quad (7.19)$$

The estimated value is 2.618. The input parameters for the descent engine to be inserted within RPA are summarized in the following table:

Table 7.4 Descender RPA input parameters

Descender input parameters		
Parameter	Value	Unit
Vacuum Thrust	43.4	kN
ϵ_C	2.618	
ϵ_E	65	
Chamber Pressure	0.896	MPa
Oxidizer	MON3	
Fuel	MMH	
MR	1.65	
TR	5	

The design of engine geometry is based on the following assumptions:

- The combustion chamber has cylindrical shape with a conical convergent nozzle- inlet section.
- The nozzle shape is based on Rao's approximations.

The schematization of the cylindrical section and the converging section of conical shape are shown in detail in the following figure:

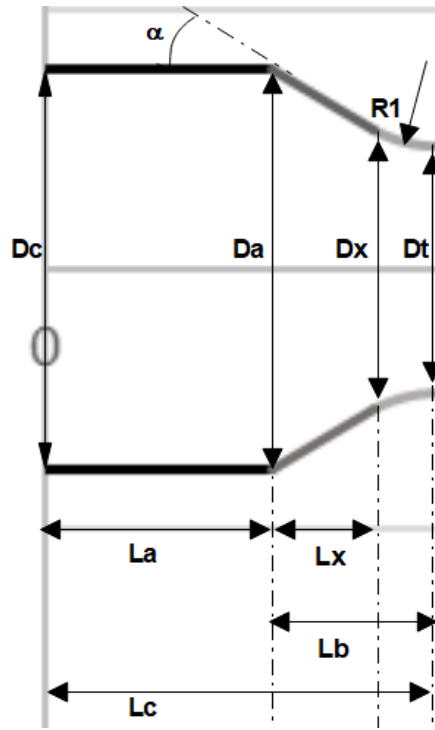


Figure 7.12 Combustion chamber section

As the actual data on the engine geometries are generally hard to collect, it is desirable to estimate them. In accordance with tables 7.3 and 4.1, the outer diameter, the expansion ratio, and the overall length of the AJ10-118K are known. In addition, according to Ref. [1], the half-angle α of the nozzle convergent cone section can range from 20° to 45° . To estimate the sections shown in the figure, the following equations based on geometric considerations are used:

$$L_x = \frac{D_c - D_x}{2 \tan(\alpha)} \quad (7.20)$$

where:

$$D_x = D_t + 2R_1(1 - \cos(\alpha)) \quad (7.21)$$

$$D_c = \sqrt{\epsilon} D_t \quad (7.22)$$

$$R_1 = 1.5R_t \quad (7.23)$$

The length L_b will be:

$$L_b = L_x + R_1 \sin(\alpha) \quad (7.24)$$

From the equation (7.8), imposing a reasonable value of the characteristic length according to the propellant combination used, it is possible to derive the chamber volume as follows:

$$V_c = L^* A_t$$

Since the chamber is the sum of a cylinder and a frustrum of cone, it is possible to rewrite the previous equation as follows:

$$V_c = \frac{\pi D_c^2}{4} L_a + \frac{\pi L_b}{3} (R_c^2 + R_t^2 + R_c R_t) \quad (7.25)$$

It is possible to calculate the length L_a from the previous equation:

$$L_a = \frac{4}{\pi D_c^2} \left[V_c - \frac{\pi}{3} L_b (R_c^2 + R_t^2 + R_c R_t) \right] \quad (7.26)$$

and finally, the chamber length:

$$L_c = L_a + L_b \quad (7.27)$$

The calculated values are summarized in the following table:

Table 7.5 Descender combustion chamber main design parameters

Descender: combustion chamber		
Parameter	Value	Unit
α	20	deg
L^*	0.825	m
V_c	0.02	m ³
A_c	0.07	m ²
D_c	0.3	m
R_1	0.14	m
L_a	0.19	m
L_x	0.13	m
L_b	0.18	m
L_c	0.37	m

The nozzle section is analyzed below. The schematization follows the Fig. 7.8. The next figure shows a zoom of the initial section of the divergent:

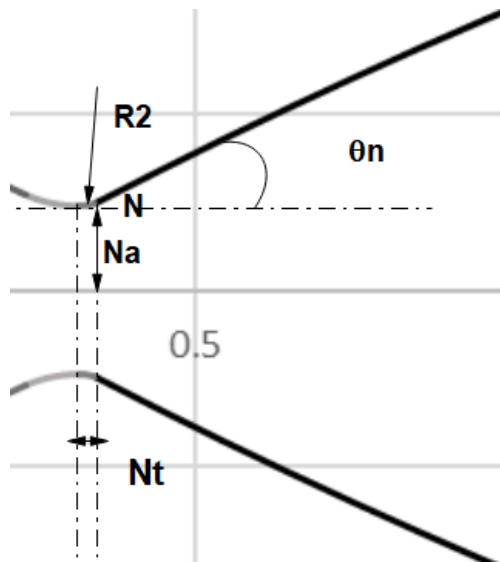


Figure 7.13 Nozzle section

The circular section before the divergent is characterized by the following relationships:

$$N_t = R_2 \sin(\theta_N) \quad (7.28)$$

$$N_a = R_t + R_2(1 - \cos(\theta_N)) \quad (7.29)$$

$$R_2 = 0.382R_t \quad (7.30)$$

The length of the divergent section is calculated from the bell-nozzle percentage and the length of the conical nozzle, the latter calculated from equation (7.10). The relationship is the following:

$$L_n = L_{n_{conical}} L_f \quad (7.31)$$

The length of the overall engine will be:

$$L_{engine} = L_c + L_n \quad (7.32)$$

The following mathematical treatment is performed to represent the parabola that best approximates the bell shape. The tangent lines at points N and E are defined by the following relationships:

$$y - y_N = (x - x_N) \tan(\theta_N) \quad (7.33)$$

$$y - y_E = (x - x_E) \tan(\theta_E) \quad (7.34)$$

The intersection of the two tangents will define a point M of coordinates:

$$x_M = \frac{y_E - x_E \tan(\theta_N) - y_N + x_N \tan(\theta_N)}{\tan(\theta_N) - \tan(\theta_E)} \quad (7.35)$$

$$y_M = y_N + \tan(\theta_N) (x_M - x_N) \quad (7.36)$$

By introducing a sliding parameter K , it is possible to find the coordinates of a point P moving from N to M , and of a point P' moving from M to E such that:

- For $K = 0$, $P = N$ and $P' = M$.
- For $K = 1$, $P = M$ and $P' = E$.

The coordinates of points P and P' are:

$$x_P = x_N + K(x_M - x_N) \quad (7.37)$$

$$y_P = y_N + K(y_M - y_N) \quad (7.38)$$

The line through points P and P' is:

$$y - y_P = \tan(\theta) (x - x_P) \quad (7.39)$$

where:

$$\tan(\theta) = \frac{y_{P'} - y_P}{x_{P'} - x_P} \quad (7.40)$$

θ is a generic angle ranging between θ_N and θ_E . By introducing the coefficients D_N and D_E , it is possible to express the parameter K as a function of θ :

$$D_N = (x_M - x_N)(\tan(\theta_N) - \tan(\theta)) \quad (7.41)$$

$$D_E = (x_E - x_M)(\tan(\theta_E) - \tan(\theta)) \quad (7.42)$$

$$K = \frac{D_N}{D_N - D_E} \quad (7.43)$$

The straight-line bundle is defined as a function of the generic angle θ , as follows:

$$y - y_N = \tan(\theta) (x - x_N) + KD_N \quad (7.44)$$

$$F(\theta, x, y) = y - y_N - \tan(\theta) (x - x_N) - KD_N = 0 \quad (7.45)$$

Every point of the parabola must belong to the straight-line bundle $F(\theta, x, y) = 0$. Consequently, the total derivative of F as a function of θ must also be zero for each value of the sliding parameter, since F assumes a constant value here:

$$\begin{cases} F(\theta, x, y) = 0 \\ \frac{dF}{d\theta} = \frac{\partial F}{\partial x} \left(\frac{dx}{d\theta} \right) + \frac{\partial F}{\partial y} \left(\frac{dy}{d\theta} \right) + \frac{\partial F}{\partial \theta} \end{cases} \quad (7.46)$$

In particular, F assumes zero value along the parabola, so the gradient of the function is at every point orthogonal to the tangent of the parabola, which is inclined by the angle θ given by:

$$\tan(\theta) = \frac{dy}{dx}$$

$$\begin{cases} \frac{\partial F}{\partial x} = - \left(\frac{dy}{d\theta} \right) \\ \frac{\partial F}{\partial y} = \left(\frac{dx}{d\theta} \right) \end{cases} \quad (7.47)$$

Substituting into the system [] and solving, the parametric equation of the parabola as a function of the sliding parameter is obtained:

$$\begin{cases} y = y_N + \tan(\theta) (x - x_N) + KD_N \\ x = x_N + K(2 - K)(x_M - x_N) + K^2(x_E - x_M) \end{cases} \quad (7.48)$$

In accordance with fig. 7.9, the calculated parameters for the descender and engine geometry are presented below:

Table 7.6 Descender nozzle section main design parameters

Descender: nozzle section		
Parameter	Value	Unit
Rt	0.09	m
R2	0.03	m
θ_n	27.5	deg
θ_e	9.8	deg
Lf	0.8	m
L conical	2.5	m
L engine	2.4	m

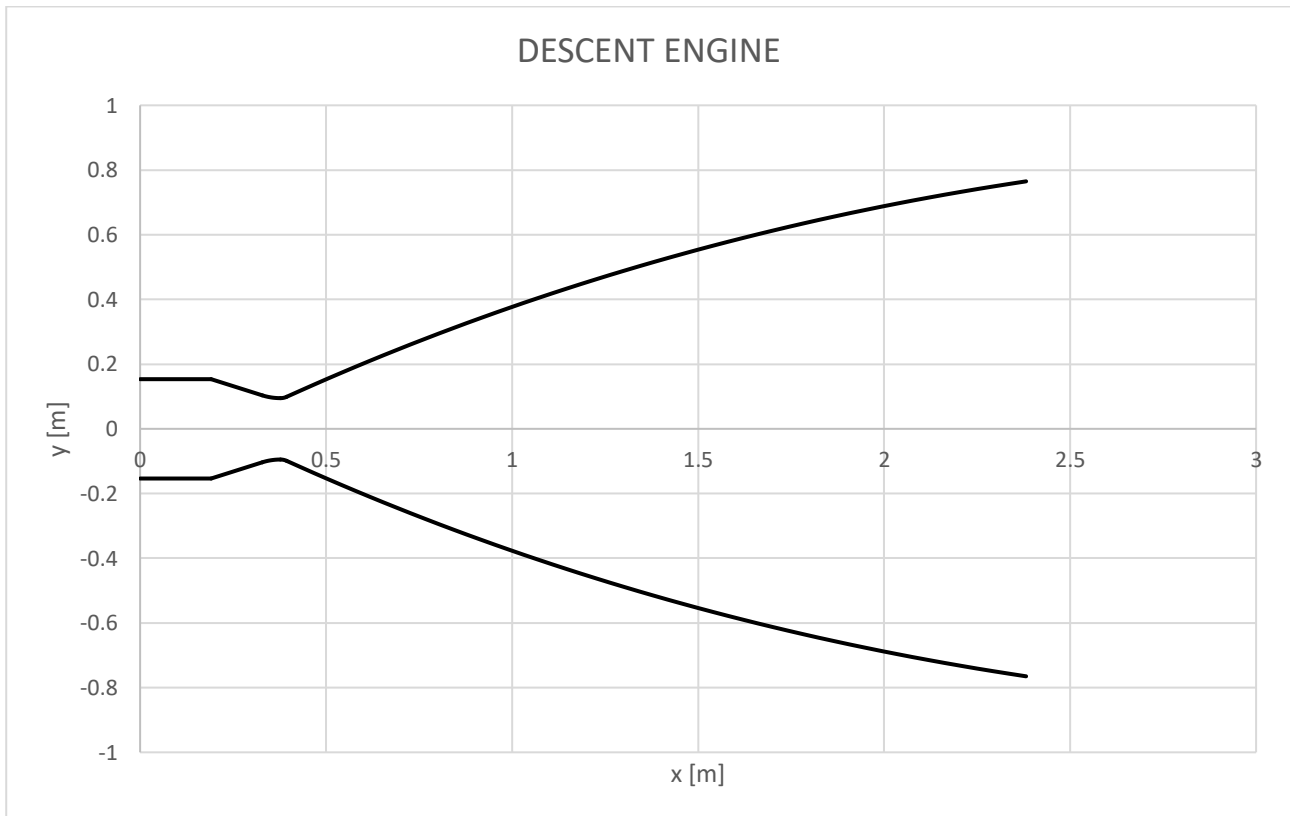


Figure 7.14 Descent engine sketch

The engine length is slightly smaller than the reference [6], but this depends on the input parameters such as the outer diameter, which varies between values of 1.5 and 1.7. By entering the input parameters into the RPA software, it is possible to calculate the thermodynamic properties of the flow at the various engine stations, as well as the overall performance (theoretical and corrected)

Table 7.7 Descender thermodynamic properties

Descender: thermodynamic properties

Parameter	Injector	N. inlet	N. throat	N. exit	Unit
Pressure	0.896	0.8429	0.4972	0.0008	MPa
Temperature	3051.0056	3037.7166	2851.8236	881.8059	K
Enthalpy	325.1797	286.2394	-343.8666	-4779.37	kJ/kg
Entropy	12.7263	12.7384	12.7384	12.7384	kJ/(kg·K)
Internal energy	-917.484	-950.5351	-1494.6312	-5129.2436	kJ/kg
Specific heat (p=const)	4.5494	4.5315	3.8573	1.98	kJ/(kg·K)
Specific heat (V=const)	3.887	3.8723	3.2879	1.5832	kJ/(kg·K)
Gamma	1.1704	1.1702	1.1732	1.2506	
Isentropic exponent	1.1543	1.1543	1.1628	1.2506	
Gas constant	0.4073	0.4071	0.4035	0.3968	kJ/(kg·K)
Molecular weight (M)	20.4138	20.4217	20.6049	20.9554	
Molecular weight (MW)	0.0204	0.0204	0.0206	0.021	
Density	0.721	0.6815	0.432	0.0024	kg/m ³
Sonic velocity	1197.6435	1194.8258	1156.7521	661.4837	m/s
Velocity	0	279.0712	1156.7521	3195.1682	m/s
Mach number	0	0.2336	1	4.8303	
Area ratio	2.6182	2.6182	1	65	
Mass flux	190.2001	190.2001	499.7712	7.692	kg/(m ² ·s)
Mass flux (relative)	0.0002	0.0002	0	0	kg/(N·s)
Viscosity	0.0001	0.0001	0.0001	0	kg/(m·s)
Conductivity, frozen	0.3289	0.3275	0.3078	0.1128	W/(m·K)

Specific heat (p=const), frozen	2.158	2.157	2.14	1.727	kJ/(kg·K)
Prandtl number, frozen	0.624	0.6243	0.6308	0.6124	
Conductivity, effective	1.031	1.025	0.8186	nan	W/(m·K)
Specific heat (p=const), effective	4.549	4.531	3.857	1.727	kJ/(kg·K)
Prandtl number, effective	0.4195	0.4192	0.4277	nan	

Table 7.8 Descender RPA theoretical performance

Descender theoretical performance			
Parameter	Optimum expansion	Vacuum	Unit
c*	1740.45	-	m/s
c	3195.17	3304.67	m/s
lsp	325.82	336.98	s
Cf	1.8358	1.8987	

Table 7.9 Descender RPA estimated performance

Descender estimated performance			
Parameter	Optimum expansion	Vacuum	Unit
c*	1690.67	-	m/s
c	3028.62	3138.12	m/s
lsp	308.83	320	s
Cf	1.7914	1.8561	

The estimated efficiencies are listed below:

Table 7.10 Descender estimated efficiencies

Efficiencies	
Parameter	Value
η^*	0.9714

η_{CF}	0.9776
η_V	0.94964064

It is noted that the η^* efficiency is slightly smaller than that used in Chap.4. This is caused by the choice of specific impulse approximated to 320 s. Fixed the η_{CF} efficiency, estimated by the program based on the input data provided, the engine geometry and the losses associated with multi-phase flow, transition effects and separation due to over-expansion, the η^* value adapted to the specific impulse chosen, is obtained using the following scaled relationship:

$$\eta_2^* = \frac{I_{sp\eta_2^*}}{I_{sp\eta_1^*}} \eta_1^*$$

where η_1^* is equal to 0.975 and the $I_{sp\eta_1^*}$ is equal to 321.20 s.

7.2.2 Throttling

The term “throttling” is commonly used to describe a varying thrust profile or thrust modulation in a liquid rocket engine. This nomenclature is used primarily because one of the most common methods of thrust control in a liquid rocket engine is from regulation of propellant flow rates by control valves. While throttling a liquid rocket engine is a critical requirement during a lunar descent, there are many other applications for throttleable liquid rocket engines. Generally, the continually changing thrust reduces the amount of propellants required for a mission, thus reducing the mass of the vehicle. From thrust equation (3.2), it is noted that there are only a few physical parameters that can be varied to change the thrust of a single engine, including the propellant types or compositions, the propellant flow rates, the nozzle exit area, and the nozzle throat area. The propellants and nozzle exit area are difficult to control or vary due to physical restrictions, while the nozzle throat area is difficult to vary if the heat fluxes are high. Consequently, varying the propellant flow rates is found to be the simplest recourse to varying thrust. As will be seen in the next sections this is achieved through the use of venturi valves working in conjunction with a pintle injector. RPA provides the required performance trend as the throttling ratio changes, as is shown below:

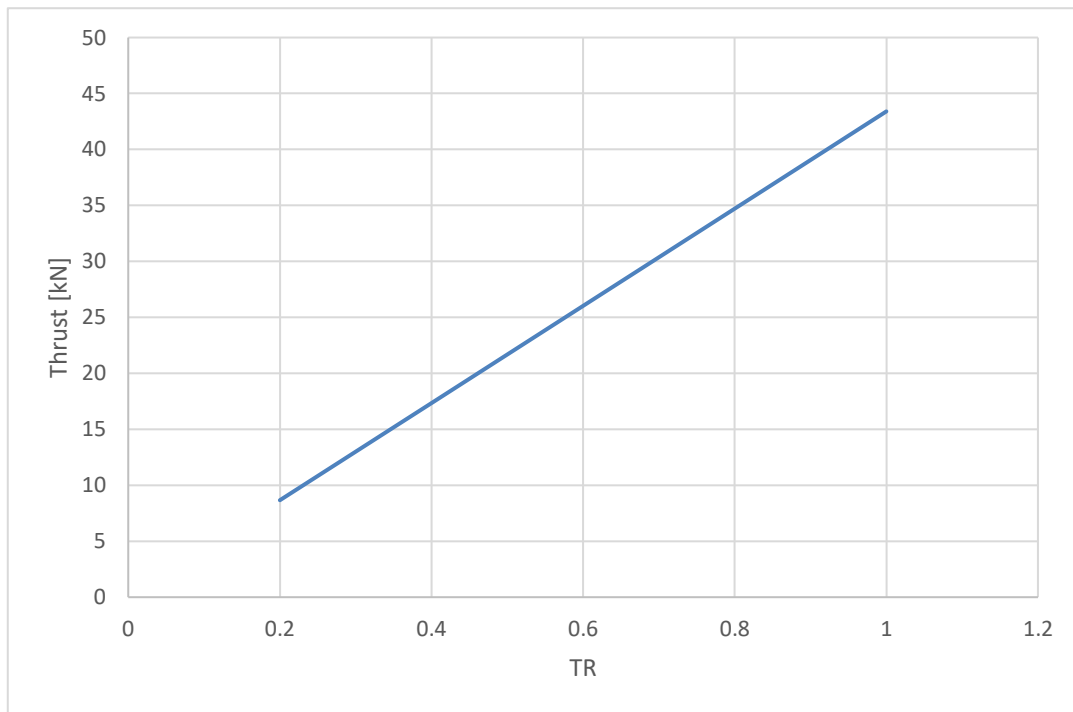


Figure 7.15 Thrust variation as a function of throttling ratio

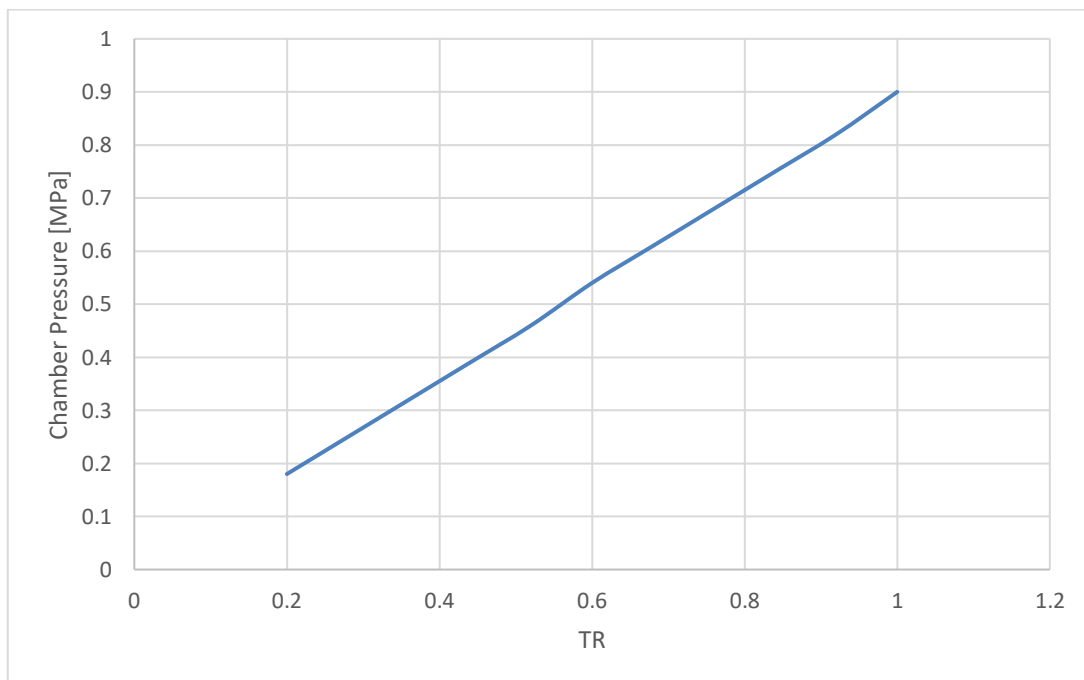


Figure 7.16 Chamber pressure variation as a function of throttling ratio

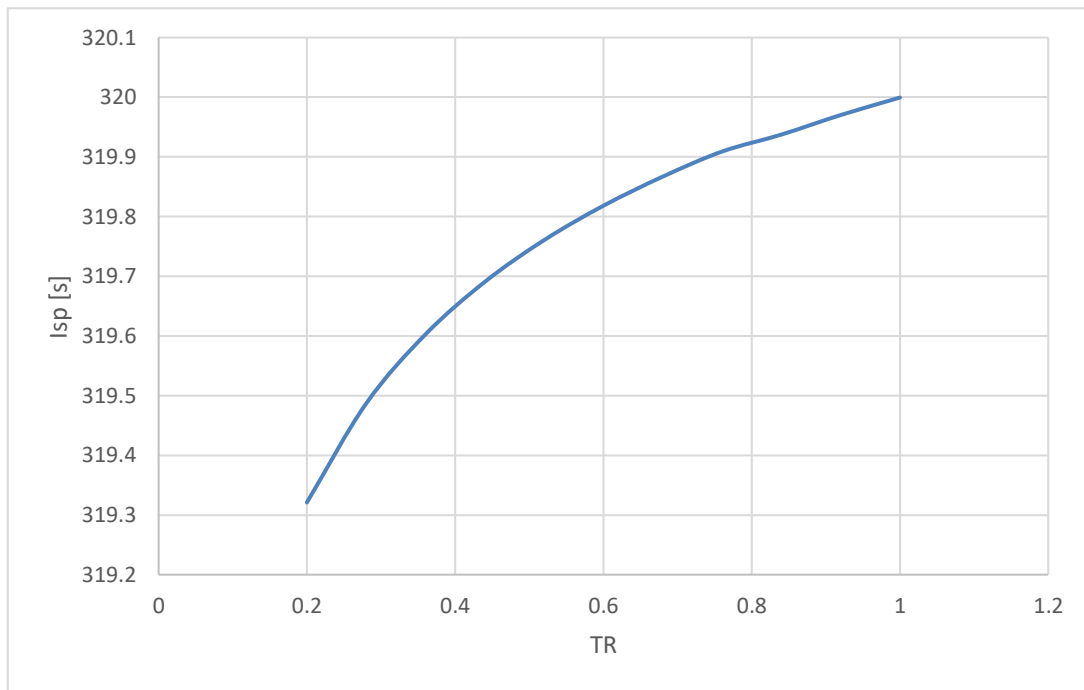


Figure 7.16 Specific impulse variation as a function of throttling ratio

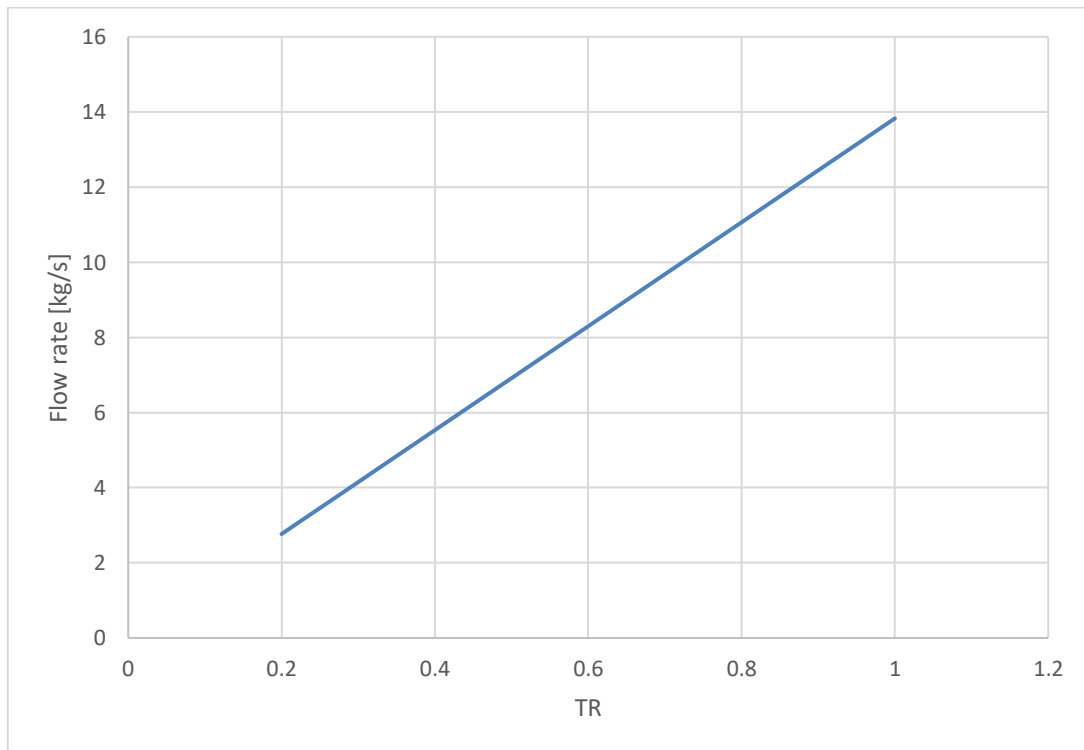


Figure 7.17 Flow rate variation as a function of throttling ratio

7.2.3 Descender pintle injector

The following section presents a general overview of the pintle injector and the main parameters on which it depends most. Therefore, advanced sizing of this component is not required in this preliminary study. A pintle injector is a representative area control method mostly used for high-throttling requirements. As basic concept, one propellant is fed through outer injector flow passages into circumferential annulus, formed between the injector outer wall and the injector body, which meters the flow into the combustion chamber. This propellant exits the injector as an axially flowing annular sheet that arrives at the impingement point with a circumferentially uniform velocity profile. The other propellant enters the injector body via a separate centrally located passage and flows axially through a central pintle sleeve toward the injector, where is turned to uniform radial flow by the pintle's tip internal contoured surface. Generally, this propellant is metered into combustion chamber by passing through a continuous gap between cylindrical sleeve and pintle tip, or slots and holes of certain geometry machined into the end of the sleeve which may be integral with the tip, or a combination of the above two designs. Thus, the pintle injector can meter the central propellant as a continuous radial sheet, a series of radially flowing "spokes", or a combination of both. A schematic, from Ref. [32] is shown below:

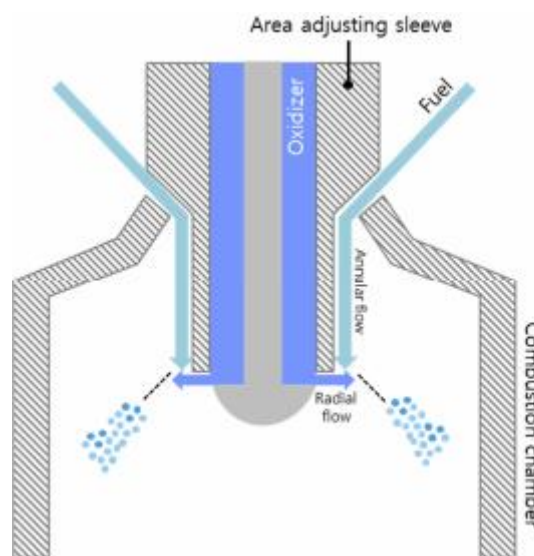


Figure 7.18 Pintle injector section

The propellant flow rate is regulated by using the movable sleeve, whose axial motion adjust the injector orifices size. Pintle injectors enjoy several advantages over other types of liquid-liquid injectors. First, the design is inherently simpler in the sense that only a single injector element is required. This issue is somewhat

misleading in that the “single element” can have multiple radial holes, but in any case, pintle engines have inherently lower number of injection sites than the face-type injectors. The second characteristic is combustion stability, as the pintle injector has recirculation zones around the injector. Because the recirculation zone at the centre of the combustion chamber acts as a deflector and mixer for unburned droplets, it has a positive effect on combustion stability and performance. The third attractive feature of the pintle injector involves its throttleability. By using the movable sleeve, the flow areas in both the annulus and the holes/ slots can be adjusted to provide deep throttling and/or face shutoff of the propellant flows. Throttling ratios of 10-20:1 have been demonstrated with hypergolic propellants using this capability. The most important variables of a pintle injector are listed below. Total momentum ratio (TMR) is defined as the ratio of the momentum of the oxidizer to the fuel and is a measure of the inherent propellant energy available for mixing and atomization:

$$TMR = \frac{F_{ox}}{F_{fu}} = \frac{\dot{m}_{ox} v_{ox}}{\dot{m}_{fu} v_{fu}} = MR \left(\frac{v_{xo}}{v_{fu}} \right) \quad (7.49)$$

The maximum in performance, in accordance with Refs. [33], [34], is obtained when individual droplets of mixed constituents meet at design mixture ratio. The proper areas for fuel and oxidizer depend on orifices geometry. For a slotted orifice configuration, the following model can be used:

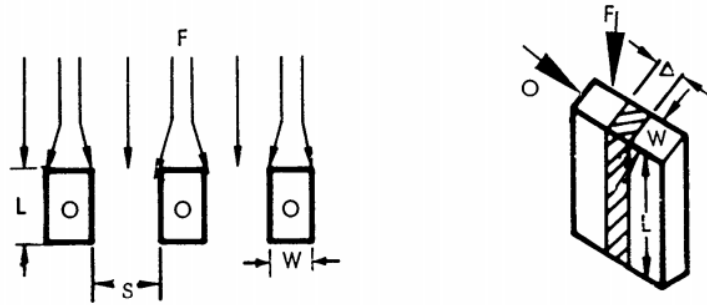


Figure 7.19 Pintle injector slotted orifice section

$$F_f = \rho_f v_f^2 t_f [W + 2LC] \quad (7.50)$$

where t_f is the thickness of the annular propellant sheet, L is the slot height and W the slot width. The parameter C is a cross influence term to account for the side interaction of fuel acting on the oxidizer. Based on single reflective interaction between elements, for a fuel particle a first approximation to C is given:

$$C = \left(\frac{L}{v_f}\right) \left(\frac{a}{S}\right) \left[1 - \left(\frac{NS}{\pi d_p}\right)\right] \quad (7.51)$$

where N is the slot number, S the spacing between two adjacent orifices and d_p is the pintle tip diameter. C can be seen as the ratio of time of flight of fuel to the dispersion of the reactants. The parameter a is a measure of the velocity of a disturbance of propellant, and ranges between 183 m/s and 244 m/s. The oxidizer force on fuel is given by:

$$F_{ox} = \rho_{ox} v_{ox}^2 WL \quad (7.52)$$

Therefore, the equation [] can be rewritten as follows:

$$TMR = \frac{\rho_{ox} v_{ox}^2 WL}{\rho_f v_f^2 t_f [W + 2LC]} \quad (7.53)$$

For circular orifices, the fuel force on the oxidizer is:

$$F_f = \rho_f v_f^2 t_f d \quad (7.54)$$

and the force of the oxidizer on the fuel is:

$$F_{ox} = \frac{\rho_{ox} v_{ox}^2 \pi d^2}{4} \quad (7.55)$$

The total momentum ratio will be:

$$TMR = \frac{\rho_{ox} v_{ox}^2 \pi d}{4 \rho_f v_f^2 t_f} \quad (7.56)$$

The geometric layout of the pintle injectors include some relevant parameters. The schematic is as follows:

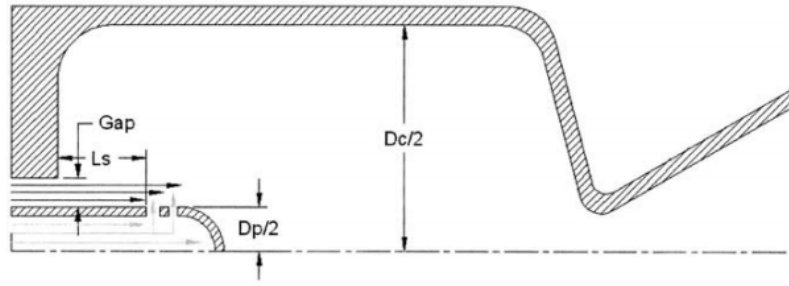


Figure 7.20 Pintle injector main design parameters

The blockage factor is defined as the ratio of the total hole or slot circumferential length divided by the circumference of the pintle:

$$BF = \frac{NW}{\pi d_p} \quad (7.57)$$

for slotted orifices. In some pintle designs, a group of secondary orifices may be arranged adjacent to the primary holes/slots. In this case, the equation is modified as follows:

$$BF = \frac{N_{po}W_{po} + N_{so}W_{so}}{\pi d_p} \quad (7.58)$$

where the subscript po indicates the primary orifices and so the secondary ones, as shown in the following figure:

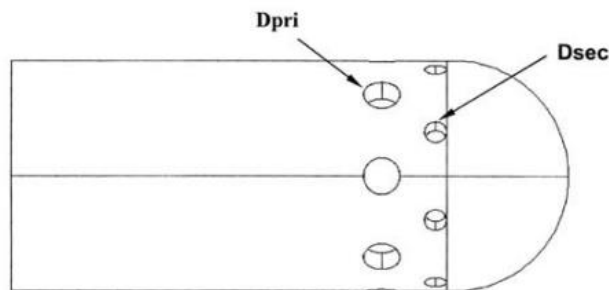


Figure 7.21 Pintle section with primary and secondary circular orifices

For a circular orifice, the blockage factor is:

$$BF = \frac{Nd}{\pi d_p} \quad (7.59)$$

Another important parameter is, as mentioned above, the pintle diameter. This must be chosen in such way that the pintle-to-chamber diameter ratio must provide sufficient radial reaction time and stability, the resultant fuel sheet thickness at the design pressure drops and the resulting pintle circumference length available for locating the oxidizer injection orifices. Typical pintle-to-chamber diameter ratio values ranges between 3 and 5, while the Apollo LMDE employed a value of 3.3. Finally, the skip distance is defined as the length required for the annular sheet to travel to impinge the radial streams of propellants. Typical value of the skip distance-to-pintle diameter ratio is about 1 for good combustion efficiency. The following estimated data can be taken as a starting point for sizing pintle injector with circular orifices for such a propellant combination:

Table 7.11 Descender pintle injector preliminary design

Pintle injector		
Paramter	Value	Unit
Dp/Dc	3.5	
Dp	0.08	m
Ls/Dp	1	
Ls	0.08	m
Δp	0.26	MPa
Flow rate (Full thrust)	13.82	kg/s
Flow rate (Min.thrust)	2.76	kg/s
Ox. Flow rate (Full thrust)	8.61	kg/s
Fu. Flow rate (Full thrust)	5.21	kg/s
Ox. Flow rate (Min thrust)	1.72	kg/s
Fu. Flow rate (Min thrust)	1.04	kg/s
Discharge Coefficient	0.7	
A fuel (Full Thrust)	0.0003	m ²
A fuel (Min. Thrust)	6.8E-05	m ²

V fuel design	17.36	m/s
TMR	1	
A oxidizer (Full Thrust)	0.0005	m2
A oxidizer (Min. Thrust)	0.0001	m2
V oxidizer design	10.52	m/s
N orifices	10	
d orifices	0.026	m
BF	97.8	%
t sheet	0.0127	m

7.2.4 Descender cavitating venturi flow control valves

The main function of flow control valves (FCV) is to obtain a constant value of the Mixture-Ratio over the entire throttling range, appropriately controlling the propellant flow rate. Variable area cavitating venturi (CV) are used in the Apollo LMDE. Through this approach the cavitation phenomenon is properly exploited, providing a hydraulic decoupling between the propellant flow control function (associated to FCVs) and the injection function (associated to the injector), allowing the optimization of the single mechanical components. To explain this concept in detail, the design of the FCV is first evaluated. A cross-section of LMDE flow control valve is shown below from Ref. [35]:

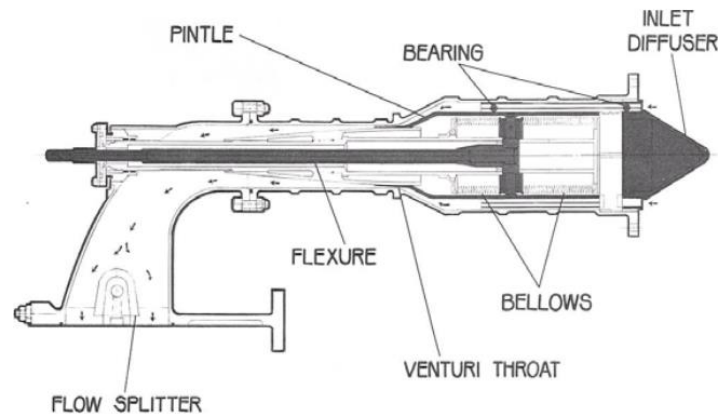


Figure 7.22 Cavitating venturi flow control valve section

The valve pintle is driven by a shaft positioned in the middle (flexure) while the flow control area is comparable to the space between the main body of the valve and the pintle contour. The following picture shows the valve pressure drop, i.e., the pressure difference between the inlet and the throat section,

expressed as a function of thrust (which is approximately proportional to the propellant flow rate) as the positioning of the pintle varies. It is noted that:

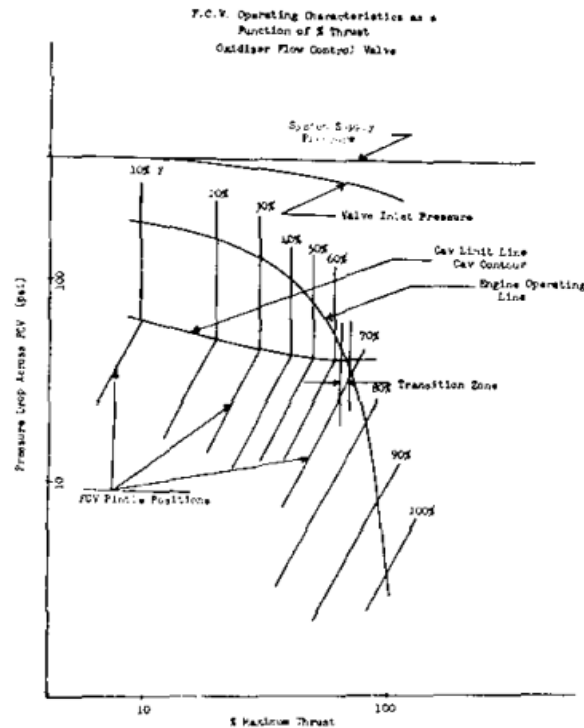


Figure 7.23 Variation of pressure drop across venturi valve as a function of thrust level

at fixed pintle position and therefore fixed throat area, the increase of thrust (and therefore of flow rate) imposes an increase of pressure drop across the control valve until the cavitation phenomenon occurs. From that point on, a further increase in pressure drop does not affect the flow rate, which remains constant. In other words, as long as the pressure drop remains above the cavitation limit, identified in the figure as the “Cavitation Line” curve, the propellant flow is not altered by the pressure variations that occur in the combustion chamber and in the injector manifold, but is determined only by the throat area (and therefore by the relative position of the pintle) and by the difference between the inlet and throat pressures. Physically, Bernoulli's principle for incompressible fluids applies. As the pressure downstream of the valve decreases and thus as the pressure drop increases, the total pressure losses are minimized by the expansion of the fluid in the throat. In other words, as the pressure drop increases, the total pressure of the fluid will change in terms of kinetic energy and static pressure. In the following figure it can be seen that:

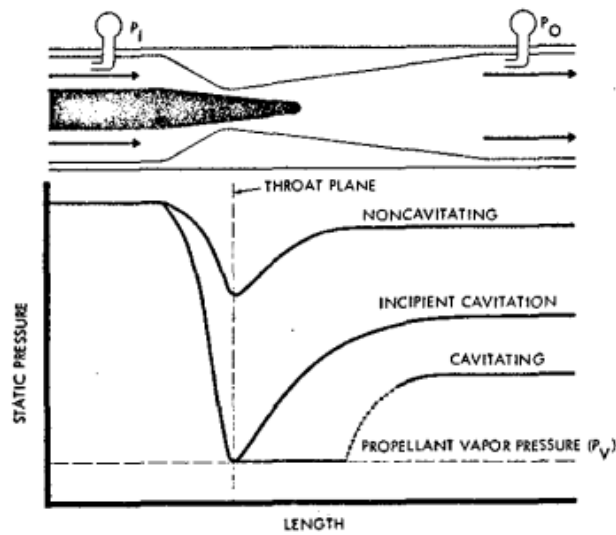


Figure 1. Typical Pressure Profile Through a Cavitating Venturi Valve

Figure 7.24 Pressure evolution inside the valve

in correspondence of a given value of pressure drop, in the throat section (in which the expansion is maximum) a minimum value of the static pressure equal to that of the vapour pressure of the fluid is reached. This is the point of incipient cavitation. A further decrease in downstream pressure will cause the formation of vapor zones within the fluid (cavitation), but not a change in flow rate. As the pressure drop increases then, these zones tend to expand and collapse due to the subsequent recovery of pressure in the divergent, which tends to raise the value again above that of the fluid vapor pressure (recovery region). This means that the cavitation phenomenon effectively eliminates the dependence of the fluid on the pressure downstream of the valve so that the flow rate will depend only on upstream conditions and throat setting. For deep throttling applications, as in the case of Apollo LMDE, the flow rate can be varied linearly as a function of the pintle stroke:

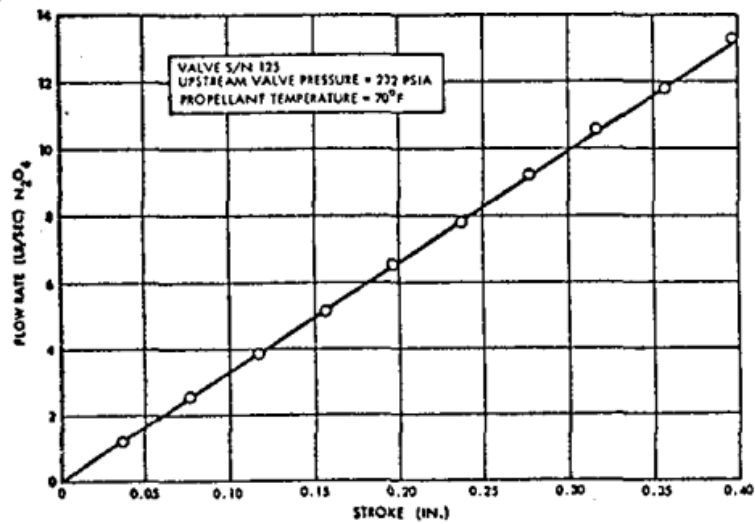


Figure 7.25 Apollo oxidizer evolution as a function of pintle stroke

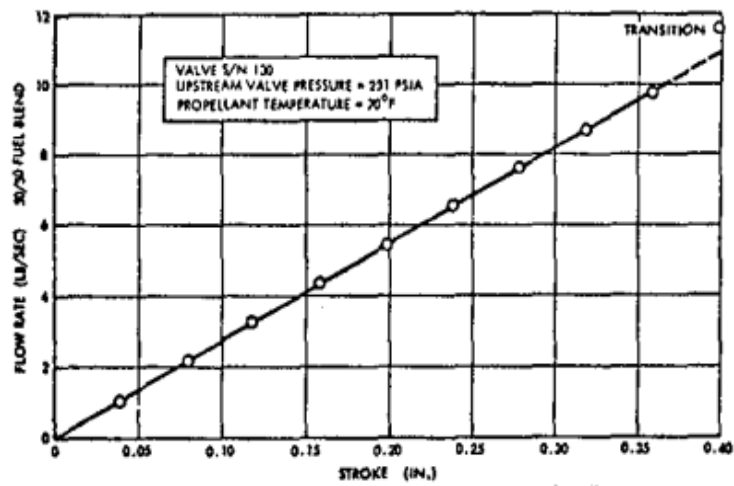


Figure 7.26 Apollo fuel evolution as a function of pintle stroke

In accordance with Ref. [35], in order to preliminary size such a valve, a conical pintle contour could be selected, as it is very close to the paraboloid shape theoretically required to provide a linear relationship between pintle stroke and flow in the throttling region. The schematic is as follows:

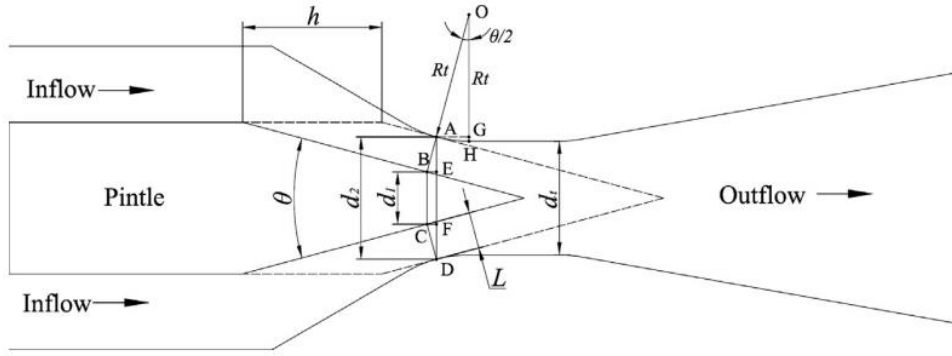


Figure 7.27 Conical-shaped cavitating venturi flow control valve

The venturi is commonly composed of a converging section, a cylindrical throat section and a diverging section. In accordance with Ref. [36], when the downstream pressure is less than 85–90% of upstream pressure, the flow may cavitate at the throat, and the mass flow rate through the venturi becomes independent of the downstream pressure. As shown in fig. 7.27, the flow control area is equal to the side area of the truncated cone ABCD and it can be expressed as:

$$A = \frac{\pi L(d_1 + d_2)}{2} \quad (7.60)$$

where, according to the symbology listed in figure:

$$L = h \operatorname{sen} \left(\frac{\theta}{2} \right) \quad (7.61)$$

$$d_2 = d_t + 2GH \quad (7.62)$$

$$d_1 = d_2 - AE - DF \quad (7.63)$$

$$GH = R_t - R_t \cos \left(\frac{\theta}{2} \right) \quad (7.64)$$

$$AE = DF = L \cos \left(\frac{\theta}{2} \right) \quad (7.65)$$

Combining equations (7.62) and (7.64), it is possible to write:

$$d_2 = d_t + 2R_t \left[1 - \cos\left(\frac{\theta}{2}\right) \right] \quad (7.66)$$

Combining equations (7.61), (7.63), (7.65), and (7.62), the following equation is valid:

$$d_1 = d_t + 2R_t \left[1 - \cos\left(\frac{\theta}{2}\right) \right] - 2h \sin\left(\frac{\theta}{2}\right) \cos\left(\frac{\theta}{2}\right) \quad (7.67)$$

where θ is the pintle angle, d_t is the throat diameter, R_t is the rounding radius at the throat and h is the pintle stroke. Two coefficients are defined below:

$$a = \pi \sin\left(\frac{\theta}{2}\right) \left[d_t + 2R_t \left(1 - \cos\left(\frac{\theta}{2}\right) \right) \right] \quad (7.68)$$

$$b = \pi \sin^2\left(\frac{\theta}{2}\right) \cos\left(\frac{\theta}{2}\right) \quad (7.69)$$

The flow control area can be rewritten as a function of the pintle stroke:

$$A = ah - bh^2 \quad (7.70)$$

The flow rate equation [] can be modified as follows:

$$\dot{m} = C_D (ah - bh^2) \sqrt{2\rho(P_{inlet} - P_v)} \quad (7.71)$$

where P_v is the propellant vapor pressure. The overwritten equation depends on a term that varies linearly with the pintle stroke and a nonlinear term. As θ decreases, the nonlinearity becomes negligible. The design parameters are summarized below:

Table 7.12 Descender cavitating venturi preliminary design

Cavitating venturi design		
Parameter	Value	Unit
MMH Vapor Pressure	0.005	MPa
MON3 Vapor Pressure	0.1	MPa
MEOP	1.59	MPa
Maximum Stroke	0.02	m
Pintle Half-Angle	5	deg
Rt	0.07	m
dt	0.05	m
At oxidizer (Full Thrust)	0.0001	m ²
At fuel (Full Thrust)	0.0001	m ²
Discharge Coefficient	0.7	

The flow rate trend as a function of pintle stroke is shown below:

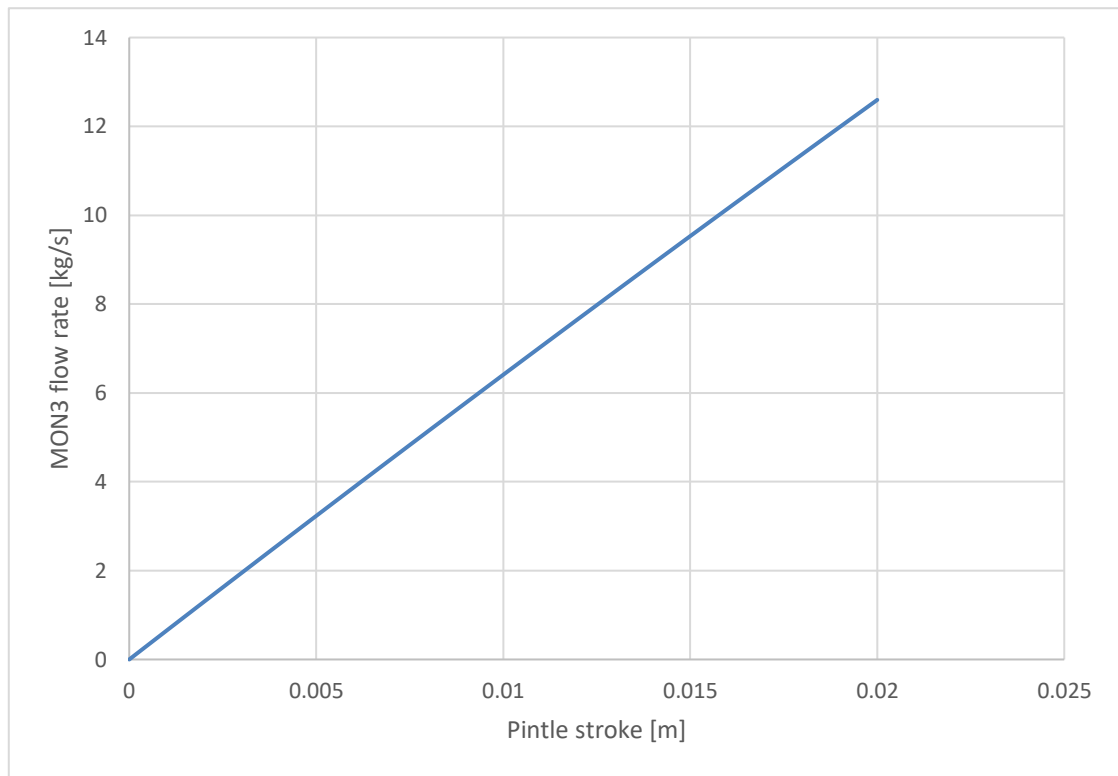


Figure 7.28 MON3 flow rate distribution as a function of pintle stroke

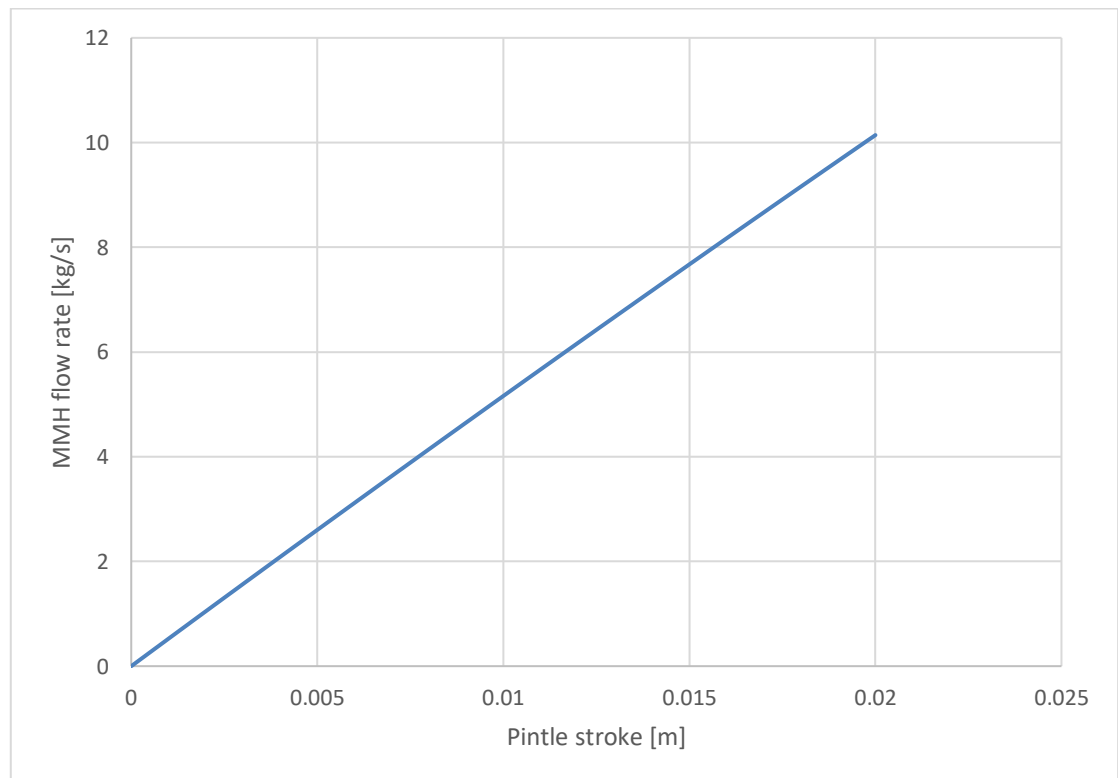


Figure 7.29 MMH flow rate distribution as a function of pintle stroke

The trend as θ varies is illustrated as follows:

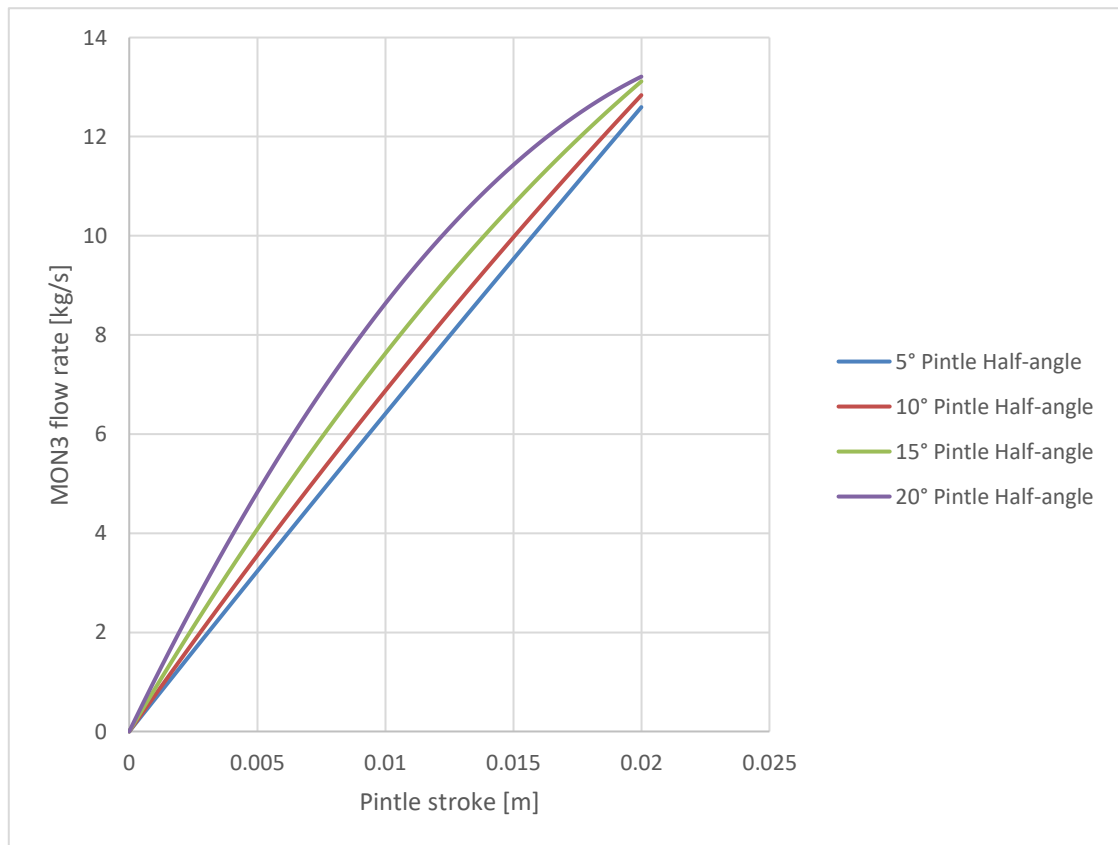


Figure 7.30 MON3 flow rate distribution as a function of pintle stroke and pintle half-angle

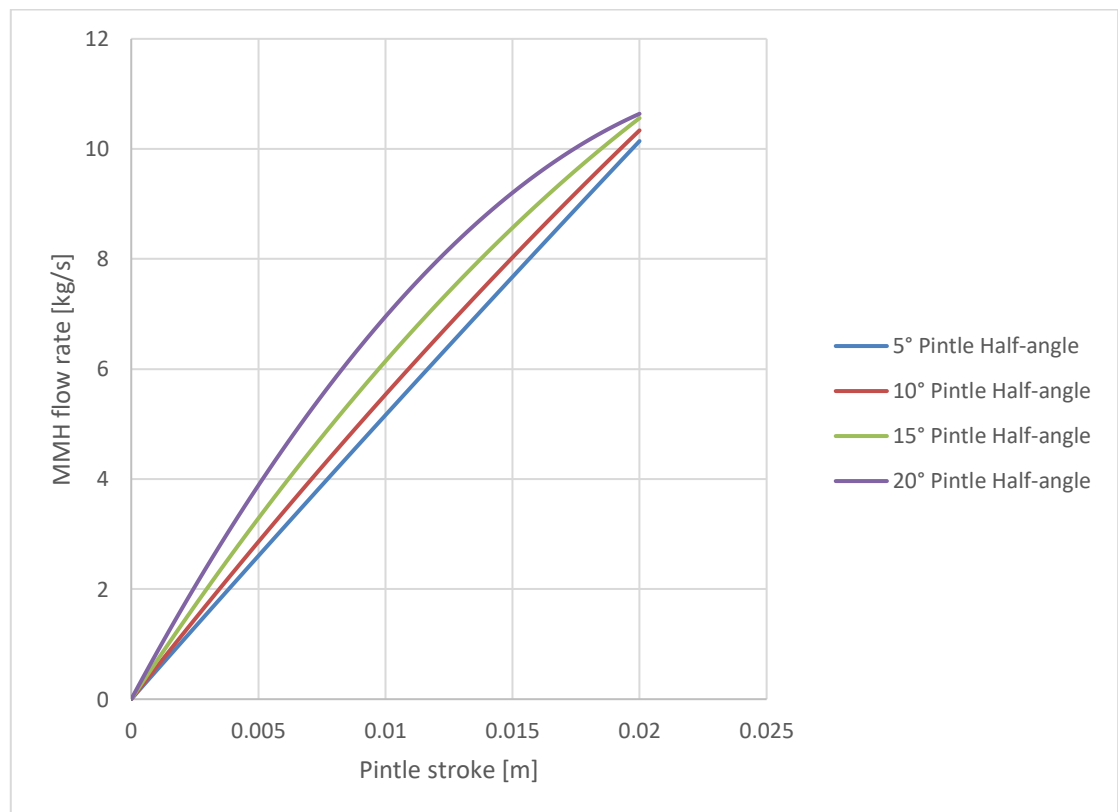


Figure 7.31 MMH flow rate distribution as a function of pintle stroke and pintle half-angle

7.2.5 Ascender thrust chamber

To perform the preliminary design of the ascent-stage rocket engine it is appropriate, as in the case of the descender, to evaluate the thrust-to-weight ratios and compare them with those of the Apollo mission. The Apollo Lunar Module Ascent Engine (LMAE) was sized with a thrust-to-weight ratio of 0.35. From tables 4.2, 4.3, 4.4, 4.5 and 4.6, considering an average value of 4651.59 kg, the required LMAE thrust is 15.965 kN, a value consistent with that found in the literature of 16 kN. It can be seen from Table [], that the current mission is characterized by an overall ascent stage weight of 14219.05 kg. With this value, using the same thrust-to-weight ratio as the apollo mission, the required thrust will be 48.804 kN. Analysing the upper-stage engine table 4.1, it is noted that none of those engines provide such thrust. It is appropriate then to consider a multi-engine configuration. The Aestus (L7) would appear to be the most suitable engine, for compatibility with the specific impulse chosen. With two engines, the total thrust will be 55 kN, and the corresponding thrust-to-weight ratio of 0.3944. The data are summarized in the following table:

Table 7.13 Ascender engine preliminary requirements

Ascender requirements		
Parameter	Value	Unit
Ascender Thrust (x1)	27.5	kN
g0 Earth	9.80665	m/s ²
g Moon	1.622	m/s ²
g0 Earth/ g0 Moon	6.04	
T/W (Ascender)	0.39	wrt earth
T/W (Ascender)	2.38	wrt moon

Using the following input data:

Table 7.14 Ascender RPA input parameters

Ascender input parameters		
Parameter	Value	Unit
Vacuum Thrust	27.5	kN
ϵ_C	2.902310	
ϵ_E	84	
Chamber Pressure	1.1	MPa

Oxidizer	MON3
Fuel	MMH
MR	1.65

The estimated engine shape is as follows:

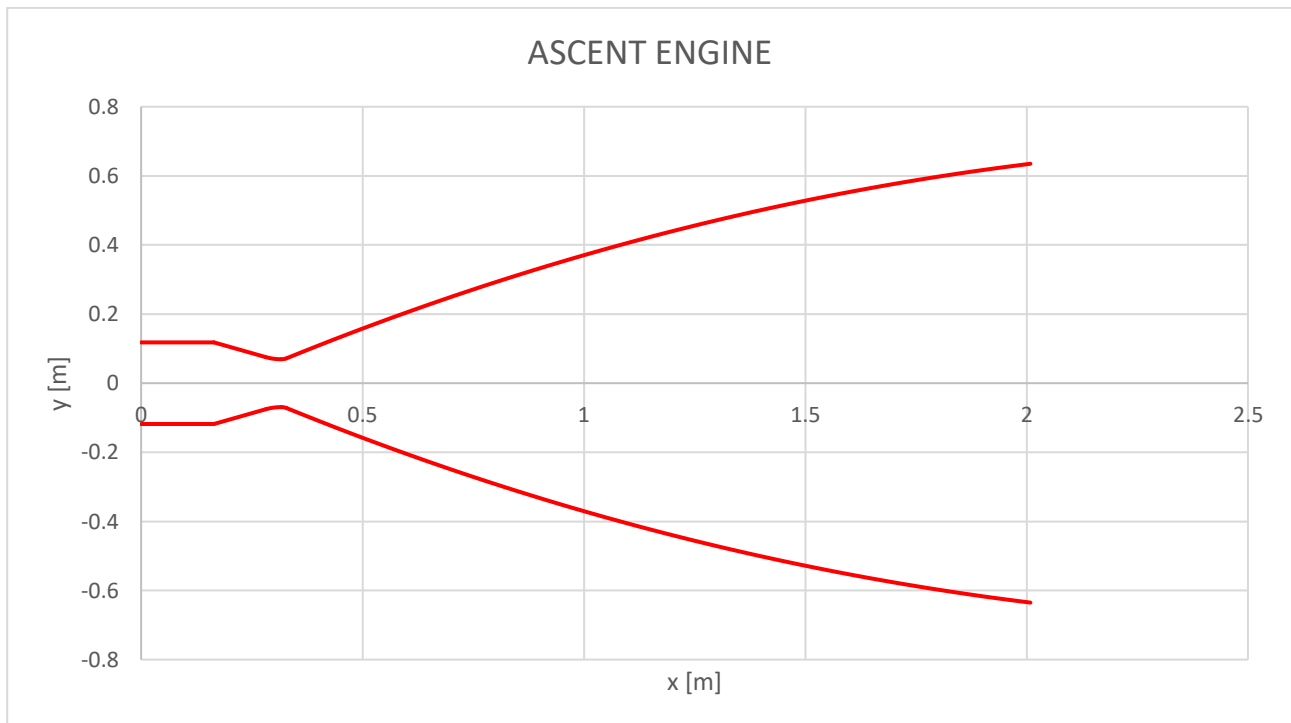


Figure 7.32 Ascent engine sketch

with relative tabulated values of combustion chamber and nozzle section:

Table 7.15 Ascender combustion chamber main design parameters

Ascender: combustion chamber		
Parameter	Value	Unit
α	20	deg
L^*	0.76	m
V_c	0.01	m ³
A_c	0.04	m ²
D_c	0.23	m
R_1	0.1	m
La	0.16	m

Lx	0.12	m
Lb	0.15	m
Lc	0.32	m

Table 7.16 Ascender nozzle section main design parameters

Ascender: nozzle section		
Parameter	Value	Unit
Rt	0.07	m
R2	0.026	m
θ_n	27.5	deg
θ_e	9	deg
Lf	0.8	
L conical	2.114	m
L engine	2.01	m

By entering the input parameters into the RPA software, it is possible to calculate the thermodynamic properties of the flow at the various engine stations, as well as the overall performance (theoretical and corrected):

Table 7.17 Ascender thermodynamic properties

Ascender: thermodynamic properties					
Parameter	Injector	N. inlet	N. throat	N. exit	Unit
Temperature	3066.7485	3055.8229	2862.7999	822.9861	K
Enthalpy	325.1797	293.6137	-347.2271	-4895.7246	kJ/kg
Entropy	12.6429	12.6527	12.6527	12.6527	kJ/(kg·K)
Internal energy	-922.1834	-948.9338	-1501.1562	-5222.2593	kJ/kg
Specific heat (p=const)	4.4013	4.3875	3.7323	1.9749	kJ/(kg·K)
Specific heat (V=const)	3.7562	3.7448	3.1761	1.5781	kJ/(kg·K)
Gamma	1.1717	1.1716	1.1751	1.2515	
Isentropic exponent	1.1564	1.1565	1.1654	1.2515	
Gas constant	0.4067	0.4066	0.4031	0.3968	kJ/(kg·K)
Molecular weight (M)	20.4418	20.448	20.6275	20.9555	
Molecular weight (MW)	0.0204	0.0204	0.0206	0.021	

Density	0.8819	0.8425	0.5314	0.0023	kg/m ³
Sonic velocity	1201.0404	1198.7433	1159.6555	639.2563	m/s
Velocity	0	251.2611	1159.6555	3231.3788	m/s
Mach number	0	0.2096	1	5.0549	
Area ratio	2.9023	2.9023	1	84	
Mass flux	211.6798	211.6798	616.1842	7.3328	kg/(m ² ·s)
Mass flux (relative)	0.0002	0.0002	0	0	kg/(N·s)
Viscosity	0.0001	0.0001	0.0001	0	kg/(m·s)
Conductivity, frozen	0.3299	0.3288	0.3085	0.1076	W/(m·K)
Specific heat (p=const), frozen	2.159	2.158	2.14	1.708	kJ/(kg·K)
Prandtl number, frozen	0.6246	0.6249	0.6314	0.6038	
Conductivity, effective	0.9911	0.986	0.7839	0.1076	W/(m·K)
Specific heat (p=const), effective	4.401	4.387	3.732	1.708	kJ/(kg·K)
Prandtl number, effective	0.4239	0.4237	0.4333	0.6038	

Table 7.18 Ascender RPA theoretical performance

Ascender theoretical performance			
Parameter	Optimum expansion	Vacuum	Unit
c*	1740.49	-	m/s
c	3231.38	3332.43	m/s
lsp	329.51	339.81	s
Cf	1.8545	1.9125	

Table 7.19 Ascender RPA estimated performance

Ascender estimated performance			
Parameter	Optimum expansion	Vacuum	Unit
c*	1678.42	-	m/s
c	3037.07	3138.12	m/s
lsp	309.7	320	s
Cf	1.8095	1.8697	

The efficiencies are summarized below:

Table 7.20 Ascender estimated efficiencies

Efficiencies	
Parameter	Value
η^*	0.9632
η_{CF}	0.9776
η_v	0.9417

7.2.6 Ascender injector

The ascent stage does not have the need to throttle the rocket engine, so it will be a fixed area injector. As mentioned above, generally doublet impinging-stream-type injector are used with storable propellant. For unlike doublet patterns, oxidizer and fuel are injected through separate orifices and then their streams impinge upon each other, creating a liquid fan and aiding in atomization. The preliminary design is shown below. Once the flow rate of oxidizer and fuel has been calculated, dependent on the mixture ratio used, it is possible to write, for the fuel:

$$\dot{m}_f = \frac{\pi}{4} N_f d_f^2 v_f \quad (7.72)$$

where N_f and d_f are respectively the number and the diameter of fuel-injector orifices, v_f is the fuel velocity through orifices. From equation (7.12), it is possible to modify the previous equation as follows:

$$\dot{m}_f = \frac{\pi}{2\sqrt{2}} C_d N_f d_f^2 \sqrt{\rho_f \Delta P_f} \quad (7.73)$$

ΔP_f is the pressure drop through injector orifices. Imposing a value of $0.2P_c$, it is possible to obtain:

$$d_f = \sqrt{\frac{2\sqrt{2}\dot{m}_f}{\pi C_d N_f \sqrt{\rho_f \Delta P_f}}} \quad (7.74)$$

The fuel velocity is calculated by the following equation:

$$v_f = \frac{4\dot{m}_f}{\pi\rho_f N_f d_f^2} \quad (7.75)$$

For the oxidizer, the equality condition for momentum is imposed:

$$\rho_f v_f^2 \frac{\pi}{4} d_f^2 = \rho_{ox} v_{ox}^2 \frac{\pi}{4} d_{ox}^2 \quad (7.76)$$

The following two equations are used to determine the problem in the two unknowns N_{ox} and d_{ox} :

$$N_{ox} d_{ox}^2 v_{ox} = \frac{4\dot{m}_{ox}}{\pi\rho_{ox}} \quad (7.77)$$

$$N_{ox} d_{ox}^2 = \frac{2\sqrt{2}\dot{m}_{ox}}{\pi C_d \sqrt{\rho_{ox} \Delta P_{ox}}} \quad (7.78)$$

By dividing the first equation by the second, it is possible to derive v_{ox} . The oxidizer velocity allows to determine d_{ox} from the equation (7.77). The results are summarized in the following table:

Table 7.21 Ascender unlike doublet injector preliminary design

Fixed-area injector		
PARAMETER	VALUE	UNIT
Cd	0.8	
N fuel orifices	100	
Δp	0.22	MPa
d fuel	0.0016	m
v fuel	17.95	m/s
v oxidizer	14.01	m/s
d oxidizer	0.0013	m
N oxidizer orifices	200	

7.2.7 Reaction control system thrust chamber

The RCS system, unlike the descent and ascent stages of the lunar lander, covers a very small portion of the overall weight of the structure, which can therefore be neglected. The geometry of the thrust chamber will be ideally analysed, based on the engines presented in the following table, in accordance with Ref. [6]:

Engine	Manuf.	Application	Vac. Thrust [N]	Life Span [s]	Cycle Life [cycles]	Spec. Impulse [s]	Propellant	Mixture Ratio [-]	Engine Mass [kg]	Chamber Pressure [bar]	Expansion Ratio [-]
S4	DASA	RCS	4,0	-	-	285	MON/MMH	-	0,29	4	-
R-2B	Marquardt	RCS	4,5	>6000	>1.200	280	NTO/Hydrazine	1,65	0,43	-	-
RS-45	Rocketdyne	RCS	4,5	-	-	300	NTO/MMH	1,6	0,73	4,8	175
S10/1	DASA	RCS	10,0	50000	>300.000	287	MON/MMH	1,64	0,35	10	90
R-6C	Marquardt	RCS	22,0	60000	>300.000	290	NTO/MMH	1,6	0,67	6,8	100
Leros 20	ARC	RCS	22,0	20000	>300.000	296	NTO/MMH	1,65	0,73	9	180
RS-43	Rocketdyne	RCS	22,2	-	-	284	NTO/MMH	1,6	0,62	6,9	150
R-43	Marquardt	RCS	67,0	13500	-	290	NTO/Hydrazine	1,6	-	-	-
R-1E	Marquardt	Orbit adjust/RCS	110	82000	>30.000	280	NTO/MMH	1,65	4,26	-	100
RS-25	Rocketdyne		111	10000	-	285	NTO/MMH	1,6	0,96	6,9	40
S400/1	DASA	Kick motor/RCS	400	15000	30.000	303	MON/MMH	1,64	2,8	7,2	102
RS-42	Rocketdyne		445	-	-	229 ¹	NTO/MMH	1,6	2,32	9,7	150
Leros 1	ARC	Kick motor	467	20000	-	314	MON/Hydrazine	0,8	4,2	6,2	150
R-4D	Marquardt	Kick motor/RCS	490	40000	>20.000	309	NTO/MMH	1,65	3,76	6,9	164
R-42	Marquardt	Orbit adjust	890	21000	-	303	MON/MMH	1,65	4,54	-	-
RS-21	Rocketdyne	Deep space	1330	900	-	294	NTO/MMH	1,52	8,39	8	60
RS-14	Rocketdyne		1401,2	-	-	287,8	NTO/MMH	1,6	8,8	8,5	30
RS-28	Rocketdyne		2670	-	-	220 ¹	NTO/MMH	1,63	12,7	13,8	40
S3K	DASA		3500	-	-	352	MON/MMH	1,6-2,1	14,5	9-12	125
R-40B	Marquardt	Orbit adjust	4000	25000	>50.000	303	NTO/MMH	1,65	13,6	10,5	160
RS-41	Rocketdyne		11100	2000	-	312	NTO/MMH	1,63	68,95	13,2	260

Figure 7.33 Several attitude and control engines

The Apollo lunar module used a configuration of sixteen 490 kN thrusters. Therefore, the R-4D engine manufactured by Marquardt will be considered. Using the following input data:

Table 7.22 RCS preliminary requirements

RCS input parameters		
Parameter	Value	Unit
Vacuum Thrust	490	N
ϵ_C	6.25	
ϵ_E	164	
Chamber Pressure	0.69	MPa
Oxidizer	MON3	
Fuel	MMH	
MR	1.65	

The estimated engine shape is as follows:

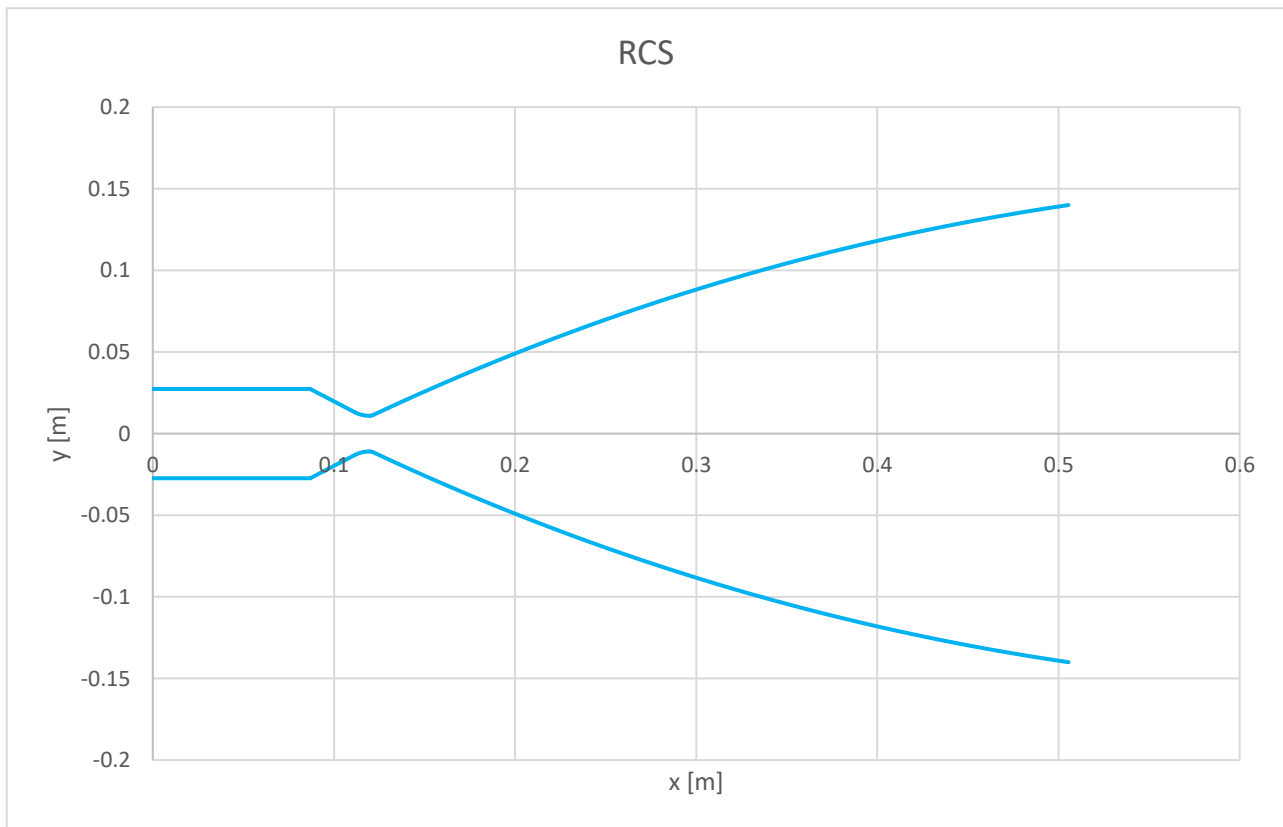


Figure 7.34 RCS engine sketch

with relative tabulated values of combustion chamber and nozzle section:

Table 7.23 RCS combustion chamber main design parameters

RCS: combustion chamber		
Parameter	Value	Unit
α	30	deg
L^*	0.65	
V_c	0.0002	m ³
A_c	0.002	m ²
D_c	0.05	m
R_1	0.016	m
L_a	0.08	m
L_x	0.02	m
L_b	0.03	m
L_c	0.12	m

Table 7.24 RCS nozzle section main design parameters

RCS: nozzle section		
Parameter	Value	Unit
Rt	0.01	m
R2	0.004	m
θ_n	27.5	deg
θ_e	9.25	deg
Lf	0.8	
L conical	0.48	m
L engine	0.5	m

By entering the input parameters into the RPA software, it is possible to calculate the thermodynamic properties of the flow at the various engine stations, as well as the overall performance (theoretical and corrected):

Table 7.25 RCS thermodynamic properties

RCS: thermodynamic properties					
Parameter	Injector	Nozzle Inlet	N. throat	N. exit	Unit
Pressure	0.69	0.6828	0.3928	0.0002	MPa
Temperature	3030.456	3028.246	2838.95	691.9112	K
Enthalpy	325.1797	318.6576	-340.007	-5151.26	kJ/kg
Entropy	12.8328	12.835	12.835	12.835	kJ/(kg·K)
Internal energy	-911.327	-916.866	-1487.05	-5425.77	kJ/kg
Specific heat (p=const)	4.7472	4.7443	4.0061	1.918	kJ/(kg·K)
Specific heat (V=const)	4.0617	4.0593	3.4211	1.5195	kJ/(kg·K)
Gamma	1.1688	1.1687	1.171	1.2623	
Isentropic exponent	1.1515	1.1515	1.1598	1.2621	
Gas constant	0.408	0.408	0.404	0.3967	kJ/(kg·K)
Molecular weight (M)	20.3773	20.3786	20.5785	20.9568	
Molecular weight (MW)	0.0204	0.0204	0.0206	0.021	

Density	0.558	0.5526	0.3424	0.0007	kg/m ³
Sonic velocity	1193.26	1192.786	1153.418	588.6066	m/s
Velocity	0	114.2116	1153.418	3309.513	m/s
Mach number	0	0.0958	1	5.6226	
Area ratio	6.2532	6.2532	1	164	
Mass flux	63.1171	63.1171	394.9399	2.407	kg/(m ² ·s)
Mass flux (relative)	0.0001	0.0001	0	0	kg/(N·s)
Viscosity	0.0001	0.0001	0.0001	0	kg/(m·s)
Conductivity, frozen	0.3275	0.3273	0.307	0.0954	W/(m·K)
Specific heat (p=const), frozen	2.156	2.156	2.138	1.664	kJ/(kg·K)
Prandtl number, frozen	0.6232	0.6233	0.6302	0.583	
Conductivity, effective	1.085	1.084	0.8596	0.0954	W/(m·K)
Specific heat (p=const), effective	4.747	4.744	4.006	nan	kJ/(kg·K)
Prandtl number, effective	0.4142	0.4141	0.4216	nan	

Table 7.26 RCS RPA theoretical performance

RCS theoretical performance			
Parameter	Optimum expansion	Vacuum	Unit
c*	1737.99	-	m/s
c	3309.51	3392.46	m/s
Isp	337.48	345.93	s
Cf	1.9042	1.9519	

Table 7.27 RCS RPA estimated performance

RCS estimated performance			
Parameter	Optimum expansion	Vacuum	Unit
c^*	1668.48	-	m/s
c	3101.61	3184.56	m/s
I_{sp}	316.28	324.73	s
Cf	1.8590	1.9087	

The efficiencies are summarized below:

Table 7.28 RCS estimated efficiencies

Efficiencies	
Parameter	value
η^*	0.9600
η_{CF}	0.9778
η_v	0.9387

It is noted that the specific impulse is oversized, due to the lack of information on efficiencies related to attitude control systems. In any case, for practical purposes this value does not affect the overall weight of the structure which, as mentioned above, is negligible with respect to the ascent and descent stages.

7.2.8 Reaction control system injector

RCS system injector is based on the same principle as the ascent engine. The following table summarizes the estimated values:

Table 7.29 RCS unlike doublet injector preliminary design

Fixed-area injector		
Parameter	Value	Unit
Cd	0.8	
N fuel orifices	50	
ΔP	0.138	
D fuel	0.0003	
v fuel	14.21	

v oxidizer	11.09
D oxidizer	0.00027
N oxidizer orifices	100

8. Conclusions and future works

The purpose of this discussion was to provide preliminary requirements for lunar descent and ascent engines for a mission planning different from the Apollo mission. Higher ΔV 's relative to the dry masses analysed, as noted, require higher propellant masses, implying a significantly higher overall weight of the structure. This results in a high thrust demand to compensate for the weight involved and a continuous throttling to allow a soft landing for all descent conditions. Preliminary mass analysis, however, provides approximate and sometimes overestimated values of individual subsystems. The true propellant and volume values required in fact could vary significantly from those presented in this discussion. The use of hypergolic propellants such as MON3 and MMH is a good compromise as they provide a high specific impulse which implies a reduction of mass requirements, and a fast engine response, especially in the most critical phases of the mission. In addition, as storable propellants, they are stable over high temperature and pressure ranges and can be stored for long periods of time, satisfying the long-term mission planning requirement. The choice of a different number of engines implies in addition an increase of the overall dimensions if interfaced with the lander structure. This is because the clustered configuration requires a certain safety distance between each engine, due to the exhaust of hot gases that can damage the adjacent nozzles. Again, the descender must also be thrust vectored, so in addition to the nozzles, actuators must be mounted along the pitch and yaw axes. This implies an increase in the base diameter of the structure which among other things will have to fit within the requirements of the launcher that will have to carry the stage to the Gateway. The overall dimensions associated with the tanks and their assembly will also have to be taken into account as it strongly depends on the shape of the lander structure under consideration. The ascender, a fixed thrust engine, depends instead essentially on the payload carried (pressurized cabin and crew), which in turn depends on the amount of personnel to accomplish the mission and the time spent on the moon. An increase in these parameters implies an overall increase in the weight of the payload and thus of the ascent stage, which in turn implies an increase in the requirements of the descender, and thus of the lander. It will result in an iterative process, that step by step will have to limit for each subsystem weights and dimensions and provide the performance required to accomplish the mission in an efficient and safe way. It is also appropriate to evaluate the stability of the chosen configurations and to limit the moments of inertia created by the arrangement of engines and tanks making the lander shape as symmetrical as possible. In addition, the thrust profile of the descender should be investigated, and the impact velocity achieved through the use of the chosen engines evaluated, while ascent stage should satisfy all mission requirements, performing correctly manoeuvres such as ascent from the lunar surface, docking and rendezvous with a two-engine configuration.

Bibliography

- [1] Dieter K. Huzel and David H. Huang MODERN ENGINEERING FOR DESIGN OF LIQUID-PROPELLANT ROCKET ENGINES.
- [2] George P. Sutton and Oscar Biblarz ROCKET PROPULSION ELEMENTS.
- [3] Assessment of MON-25/MMH Propellant System for Deep-Space Engines
<https://ntrs.nasa.gov/api/citations/20190033304/downloads/20190033304.pdf>
- [4] RocketCEA Documentation Release v1.1.24
<https://rocketcea.readthedocs.io/en/latest/pdf/>
- [5] Rocket Propulsion Analysis v.2.3 https://www.rocket-propulsion.com/downloads/2/docs/RPA_2_User_Manual.pdf
- [6] Modern Liquid Propellant Rocket Engines, 2000 Outlook. Doi: [10.13140/2.1.4640.0003](https://doi.org/10.13140/2.1.4640.0003)
- [7] Ronald W. Humble, Gary N. Henry and Wiley J. Larson SPACE PROPULSION ANALYSIS AND DESIGN.
- [8] Wilfried Hofstetter Extensible Modular Landing Systems for Human Moon and Mars Exploration.
Master Thesis (Diplomarbeit) written at the MASSACHUSETTS INSTITUTE OF TECHNOLOGY
- [9] Joseph G. Gavin, JR. The Apollo Lunar Module: A Retrospective.
- [10] Apollo Lunar Module QUICK REFERENCE DATA
https://www.hq.nasa.gov/alsj/LM04_Lunar_Module_pplV1-17.pdf
- [11] Spacecraft Mass Estimation, Relationships, and Engine Data. NASA Contract Number NAS 9-1 7878
EEI Report #87-171 April 6, 1988.
- [12] Kir Latyshev, Nicola Garzaniti, Edward Crawley and Alessandro Golkar Lunar human landing system
architecture tradespace modelling. <https://doi.org/10.1016/j.actaastro.2021.01.015>
- [13] F.Daghia, E.Baranger, D.-T.Tran, P.Picho A hierarchy of models for the design of composite
pressure vessels. <https://doi.org/10.1016/j.compstruct.2019.111809>
- [14] <https://www.infinitecomposites.com/composite-pressure-vessel-resources>
- [15] <https://www.torayca.com/en/download/pdf/torayca.pdf>
- [16] Somnath Chattopadhyay PRESSURE VESSEL DESIGN AND PRACTICE
- [17] <https://www.cobhammissionsystems.com/composite-pressure-solutions/composite-cylinders/composite-cylinders-catalog/docview/>
- [18] https://www.ihl.co.jp/ia/en/products/space/tanks/i/Tank_lineup.pdf
- [19] <https://www.mt-aerospace.de/tanks-produkte.html>
- [20] <https://www.infinitecomposites.com/downloads>
- [21] <https://www.space-propulsion.com/spacecraft-propulsion/bipropellant-tanks/index.html>

- [22] W. Tam and D. Jaeckle The Evolution of a Family of Propellant Tanks Containing Propellant Management Devices
https://www.researchgate.net/publication/306078461_The_Evolution_of_a_Family_of_Propellant_Tanks_Containing_Propellant_Management_Devices
- [23] <https://keyengco.com/wp-content/uploads/2020/02/Data-Sheet-1260000.pdf>
- [24] Apollo RCS QUICK REFERENCE DATA
https://www.hq.nasa.gov/alsj/LM10_Reaction_Control_ppRC1-12.pdf
- [25] <https://www.space-propulsion.com/spacecraft-propulsion/valves/index.html>
- [26] http://www.omnidea-rtg.de/site/images/stories/Downloads/Omnidea-RTG_Catalogue_Feb2016.pdf
- [27] <https://marotta.com/products/flow-controls/pressure-controls/relief-valves/>
- [28] https://static1.squarespace.com/static/603ed12be884730013401d7a/t/6054f46fbaf06f76bbaba605/1616180337738/be_datasheet_sapt_2019oct.pdf
- [29] <https://marotta.com/products/flow-controls/pressure-controls/pressure-regulators-reducers/>
- [30] https://www.vacco.com/images/uploads/pdfs/check_valves.pdf
- [31] https://www.vacco.com/images/uploads/pdfs/VACCO_Filtration_Catalog_042121_FINAL_with_bookmarks_web.pdf
- [32] Suji Lee, Daehwan Kim, Jaye Koo and Youngbin Yoon Spray characteristics of a pintle injector based on annular orifice area <https://doi.org/10.1016/j.actaastro.2019.11.008>
- [33] W. A. Carter and G. S. Bell DEVELOPMENT AND DEMONSTRATION OF A to N₂O₄/N₂H₄ INJECTOR
- [34] Brunno Barreto Vasques Development of a Rocket Engine Injection System with Throttling Capability Based on the LO₂/LCH₄ Propellant Combination
<https://mediatum.ub.tum.de/doc/1432797/1432797.pdf>
- [35] D. W. Harvey THROTTLING VENTURI VALVES FOR LIQUID ROCKET ENGINES
<https://doi.org/10.2514/6.1970-703>
- [36] Hui Tian, Peng Zeng n , Nanjia Yu, Guobiao Cai Application of variable area cavitating venturi as a dynamic flow controller <https://doi.org/10.1016/j.flowmeasinst.2014.05.012>



**Politecnico
di Torino**